Dynamic Programming Revisited for Aircraft Flight Trajectory Optimization

原田, 明徳

https://doi.org/10.15017/1654886

出版情報：九州大学, 2015, 博士（工学）, 課程博士
バージョン：

Academic Year 2015 DISSERTATION

Dynamic Programming Revisited for Aircraft Flight Trajectory Optimization

Akinori Harada

Graduate School of Engineering
Kyushu University
744, Motooka, Fukuoka, Japan, 819-0395

A Dissertation Submitted in Partial Fulfillment of the Requirements for the Degree of Doctor of Philosophy

January 2016

Acknowledgment

I would like to express my sincerest appreciations for Professor Yoshikazu Miyazawa, who has supervised and supported my work since I started my research in 2010. I'm obliged to the thesis committee consisting of Professor Hiroyuki Kajiwara of the Department of Marine Systems Engineering and Professor Shinji Hokamoto and Associate Professor Shin'ichiro Higashino of the Department of Aeronautics and Astronautics for review of my work and a lot of precious comments.

This work would not have been completed without the productive discussions with the members of the Flight Dynamics Laboratory. Assistant Professor Shuji Nagasaki gave me valuable advice from the viewpoint of actual requirements in the general society.

This work was supported by Japan Society for the Promotion of Science KAKENHI Grant Numbers 14J05104. I would like to thank Research Fellowship for Young Scientists which supported my research life for two years since 2014.

Finally, my deepest gratitude goes to my parents, Mrs. Kumi Harada and Mr. Toshiaki Harada, who have understood my further study in the Ph.D course and supported it mentally. I would like to convey my highest possible appreciation to my grandmother, Mrs. Misue Ushijima, who had gone in 2014. If you would not have encouraged me since I was a child, I could not continue my effort to reach the top of the education. I will never stop my step. I apologize for my powerlessness for you, but please warmly watch me and my family from the sky.

January 27th, 2016

Contents

List of Figures

List of Tables

Nomenclature

Symbols

A	:	system matrix of the continuous time system equation
B	:	system matrix of the continuous time system equation
C	:	constraints, coefficient
D	:	drag
F	:	thrust, integrand in functional
H	:	altitude, Hamiltonian
I	:	functional, identity matrix
J	:	objective function
L	:	Lagrangian, lift
M	:	Mach number
N	:	number of division of independent variable
P	:	solution of Riccati equation
Q	:	weight matrix for state variable
R	:	weight matrix for control variable, set of real numbers, radius of the Earth, gas constant
S	:	wing area
T	:	thrust, temperature
V	:	velocity
a	:	time adjustment parameter, speed of sound
b	:	lapse rate
c	:	thrust specific fuel consumption
f	:	function vector, fuel flow
g	:	gravity acceleration
k	:	induced drag coefficient
m	:	dimension of control variable, mass of aircraft
n	:	dimension of state variable, number of elements
p	:	pressure
r	:	weight matrix for control variable, dimension of constraints
t	:	time
u	:	control variable
x	:	state variable, downrange
γ	:	flight path climb angle
δ	:	variation

η	:	cross range angle, thrust specific fuel consumption
θ	:	longitude
λ	:	Lagrangian's multiplier, adjoint
μ	:	fuel flow
ν	:	adjoint
ξ	:	down range angle
ρ	:	air density
ϕ	:	latitude, objective function at terminal
ψ	:	constraint function at terminal, flight path heading angle

Subscripts

0	:	initial, above sea level
1	:	at tropopause
$D0$	:	parasite drag
EAS	:	equivalent airspeed
ES	:	Earth speed
GS	:	ground speed
IAS	:	indicated airspeed
V	:	vertical
TAS	:	true airspeed
d	:	discrete
eq	:	equality
f	:	final
i, j	:	element numbers for vector and matrix
$ineq$	:	inequality
k	:	number for time stage
max	:	maximum
min	:	minimum
MO	:	maximum operating
opt	:	optimal

Superscripts

$\circ$	:	optimal
*	:	mark for the extended objective function

Chapter. 1

Introduction

1.1 Background

The practical utilization of optimal control has been widely demanded by the society and expected to resolve a number of challenges. The establishment of trajectory optimization technology for the practical use is desired in the various research field of aeronautical and astronautical engineering. Researchers and engineers who design guidance and control system aspire for an easy to handle numerical optimization method that provides an accurate solution in a short amount of time. Nevertheless, most conventional optimal control theory usually requires special skills in formulating with the design conditions and computing the requisite quantities. Additionally, solving optimal control problems requires large amounts of engineering resources to select the optimization tools, prepare data such as models and objective function, and set adjustable parameters in each tool.

Looking at our daily life, we notice that it is supported by the highly-developed and complicated engineering system which is built on the accurate sensing technology and the advanced information processing technology. A flood of data called “big data” is produced every day in those systems. The optimization technology will play a significant role to extract the beneficial new findings, laws and phenomena from the big data which we can say “a gold mine”. The basic technology used in the big data analysis is intimately related with the optimal control in finding an optimal solution under an arbitrary objective function. The increasing amount of memory and processing speed of recent computers encourage that the optimization technology is widely used in our daily life and the society founded upon the big data.

The optimal control is a theory that aims at finding an optimal control time history which minimizes or maximizes the objective function defined with the design conditions and requirements in a time-variant dynamic system. The optimal control method is roughly classified into two categories, indirect method and direct method. The calculus of variations has been established by early studies and is categorized as the indirect method which was mainly used in the optimal control field several decades ago. Euler-Lagrange differential equations derived from the variational principle and Pontryagin’s maximum principle are solved as

two-point boundary value problem. Although this method can give an exact solution, some special techniques are required to solve the two-point boundary value problem and it's extremely tough to get the solution for a highly non-linear problem. Furthermore, it's difficult and time-consuming to implement a new formulation and parameter adjustments for every change of design conditions. On the other hand, direct methods, in which a finite number of parameters constitute the trajectory and are solved as a parameter optimization problem, include Evolutionary Algorithm, Pseudospectral method and collocation method. Especially, from a practical application perspective, gradient based method available with generalized optimization tools has been expected as a versatile optimization method. This method discretizes the objective problem into finite parameters and finds the solution using the Non Linear Programming (NLP) optimizer. The gradient based method has great capability of solving the high-dimensional problem with a short amount of computational time. The direct methods have become widely and actively used with the assistance of processing capability of highly-sophisticated recent computers, though these methods don't always work perfectly because the good convergence performance cannot be guaranteed by the iterative calculation if the complicated models and inequality constraints are added.

Therefore, a more easy to handle numerical optimization method is necessary to introduce an optimal solution which satisfies researchers' and engineers' demands during a defined period for the research and development. This research focuses on dynamic programming as a promising numerical optimization method and demonstrates its applicability and feasibility into the optimal control problems through practical application examples in the aerospace engineering field. Dynamic programming (DP) is firstly proposed by Richard E. Bellman in the 1950s [1]. DP is an optimization theory based on the Hamilton-Jacobi-Bellman (HJB) partial differential equation and classified into the direct method because the objective system is represented by the quantized grid points of state variables and solved as the combinatorial optimization problem for those points. This method has many favorable advantages over the other methods. The most conclusive one is that DP can provide a global optimum. The calculation algorithm determined by the principle of optimality guarantees the global optimality and does not include any iterative calculations for the convergence. Thus, the computational process is decisive and the calculation time may be estimated in advance because it depends only on the number of state variables and their grid points. Additionally, inequality constraints may easily be added to the state variables and their functions. Rather, inequality constraints are suitable for limiting the search space. It's not the serious matter either to apply the inequality constraints on the control variables. Furthermore, the discrete form of the HJB optimality conditions makes the programming code comparatively simple and easy to be understood.

Conversely, DP has two major disadvantages which generally limit its practical usage in engineering applications. One is quote-unquote "Curse of dimensionality" as designated by Bellman himself. This is the problem such that computational time and memory increase explosively with the number of state variables and number of their divisions. The other is the "Menace of the expanding grid" which was named by Rein Luus [2]. This problem, which is also called as the dimensional difference problem in this thesis, is caused

by the difference between the number of state variables and the number of control variables. If the number of control variables is the same as that of state variables, DP optimization may be easily implemented; otherwise, a dimensional difference problem inevitably arises. Regarding the "Curse of dimensionality", this insuperability has prevented dynamic programming from being used in the practical applications [3]. Some possible strategies were invented in the previous literature. The branch-and-bound algorithm was proposed by Alekseev and Morin [4, 5] in 1976. This algorithm works to remove the paths which cannot be a part of optimal solution. The differential dynamic programming introduced in 1966 by Mayne [6] is also effective to reduce the total amount of calculation. This approach was published by Jacobson and Mayne in 1970 [7]. Concerning the dimensional difference problem, iterative dynamic programming method was invented by Rein Luus [2]; however, this method is hard to be accepted as a desirable one for the engineers who must implement the optimal control to the practical objectives because the method uses the quantized grid points to calculate the objective function value tolerating the error occurred between those points and a feasible state point. In this manner, some methods were proposed to resolve the "Curse of dimensionality" and the "Menace of the expanding grid"; however, the DP's capability still remains not fully used.

The two bottlenecks, the "Curse of dimensionality" and the "Menace of the expanding grid", have interfered dynamic programming which has many favorable advantages over the other methods from being widely utilized in the optimal control field. In the meanwhile, the computational capability of recent miniaturized computers has been rapidly increasing with the high-performance processors and large-scale parallel computation technology. The DP's scope of application to the practical usage is expected to be enlarged by those trends in modern computers. Therefore, the restrictions of DP should be identified to obtain clarity about its suitability for further applications.

1.2 Research objectives

The main objective of this thesis is to demonstrate the potential and versatility of dynamic programming by exploring its scope of application to the practical optimal control problems using proposed numerical methods to overcome the two drawbacks of dynamic programming.

To establish a versatile and more easy to handle optimal control method for the researchers and engineers, some conditions are required, i.e. providing an optimal solution accurate enough to be applied to the practical usages with a reasonable computational time, enduring many analyses with various design conditions, and unnecessity of trial-and-error analyses. In spite of having many favorable advantages to satisfy those demands, dynamic programming has been limited by the two major challenging drawbacks as represented by the "Curse of dimensionality" and the "Menace of the expanding grid". This thesis quantitatively clarifies the limit of DP's potential and evaluates its applicability to the practical problems.

Two novel methods, Moving Search space Dynamic Programming (MS-DP) and Piecewise Linear Approximation Dynamic Programming (PLA-DP) were invented to alleviate the major drawbacks of dynamic

programming by the author's research group [8, 9]. The MS-DP method enormously contributed to solve a large-scale optimization problem. In this method, the optimization calculation is performed by a basic concept of gradient based method. A partial search space is set around an arbitrary initial guess and the optimal solution is searched by shifting the space toward a direction such that the objective function value gets smaller. The name of the method is originated in the search space shifting process. Any research to reduce calculation amount by the same method has not been found in the trajectory optimization research. The PLA-DP method which was established on the long-term accumulation represented by the two methods, Augmented Control Variable (ACV) and Least-error Grid point Selection (LGS) proposed in the previous literatures [10, 11, 12], is promising approach to resolve the "Menace of the expanding grid". Although a similar calculation to approximate the objective function value was invented by Luus [13], how to obtain the optimal trajectory by using the optimal path information stored in grid points was not proposed in his research. The PLA-DP method can be expected to resolve the "Menace of the expanding grid" which has prevented dynamic programming from being used in various engineering problems over a long duration. The applications of these methods to practical problems are introduced and their versatility is objectively investigated from engineering perspectives in this thesis. As the first application, dynamic programming is applied to an optimal trajectory design of JAXA's next generation Supersonic Transport (SST) to analyze its operational feasibility. Normal DP algorithm can be easily applied to this problem because it does not include difficulties arising from above mentioned drawbacks. As the second application, an usability of flight trajectory optimization tool developed using dynamic programming is introduced in Air Traffic Management (ATM) research. The potential benefits of current Japanese airspace, which are the key issues to consider the Japanese ideal ATM system, are quantitatively evaluated in the application example by using the optimization tool and the passenger aircraft's actual position data recorded by Secondary Surveillance Radar (SSR). Multiple aircraft must be analyzed in terms of operational efficiency; therefore, the proposed MS-DP method works quite effectively to save the computational time taken in the large-scale optimization analysis for multiple aircraft in the example. The third example is passenger aircraft's reference trajectory design problem. To design a smooth optimal trajectory by considering an additional state variable, "Menace of the expanding grid" arises in the defined optimal control problem. The difficulty is resolved by the proposed PLA-DP method and its validity and availability are demonstrated numerically.

1.3 Dissertation overview

This thesis consists of seven chapters. The foundation of the optimal control methods are stated in chapters 2 and 3. The two novel methods proposed to resolve the drawbacks of dynamic programming are explained in detail and the practical application results of those methods are demonstrated in chapters 5 and 6. The contents of each chapter are described below.

In chapter 2, the general optimal control problem is stated at the first section. As a representative indirect

method, the basic concept of calculus of variations is introduced by formulating the Euler-Lagrange differential equation from the variational principle. A detailed formulation of the equation is shown with four categories at the terminal conditions.

In chapter 3, dynamic programming which is highlighted in this thesis as a promising optimization method is presented with its historical background. A fundamental principle is stated to introduce the Hamilton-Jacobi-Bellman equation which is a core equation in optimal control theory. How to design an optimal trajectory by dynamic programming is explained by a basic combinatorial optimization algorithm. Characteristics of dynamic programming are listed with its advantages and disadvantages from an engineering perspective. The reasons why it is significant and meaningful to overcome the two drawbacks of the method in the trajectory optimization research field are described.

In chapter 4, as a fist application, a trajectory optimization analysis is implemented to reveal an operational feasibility of JAXA's supersonic transport. The optimization is limited to longitudinal variables without considering aircraft dynamics. This application example does not include the two drawbacks; thus, the normal combinatorial optimization algorithm can be easily applied to the optimal trajectory design problem with actual aerodynamic and engine model given in a tabular data form.

In chapter 5, an application of the fast computation algorithm named as MS-DP is proposed to optimize the flights of multiple aircraft in terms of their operational efficiency. A trajectory optimization tool is developed by the MS-DP method and is utilized to evaluate potential benefits of current Japanese airspace. The amount of calculation is extremely large because all the flights inbound to Tokyo International Airport must be analyzed for one day and each flight is optimized with regard to three state variables which strongly influence on the objective function value. The MS-DP greatly exerted the power to analyze a huge number of actual flights as well as to reveal the potential benefits by using the outstanding advantages of dynamic programming.

In chapter 6, an application result of PLA-DP method to a fuel minimal trajectory generation problem is presented with the aim of designing a practically preferable reference trajectory. Flight path climb angle rate is considered in the longitudinal dynamic model to obtain a smooth optimal trajectory. The dimensional difference problem arising from different number of the state and control variables is resolved by the PLA-DP method. It is indicated that unfavorable oscillation occurred on the trajectory obtained by a conventional optimization approach is suppressed by an appropriate problem formulation and the newly-proposed PLA-DP method.

In chapter 7, the usefulness of the proposed methods is described with the new findings gained in the three practical application examples. It is stated that the scope of application of dynamic programming in the flight trajectory optimization has been extended than before by demonstrating the versatility and applicability of those methods in the practical applications.

This thesis consists of the previously published journals and proceedings listed in the following.

1. Harada, A., Matsuda, H. and Miyazawa, Y.: "Dynamic Programming Trajectory Optimization by Piecewise Linear Approximation", Proceedings of the AIAA Guidance, Navigation, and Control Conference, AIAA-2015-1075, Kissimmee, Florida, 2015.

2. Harada, A., Kozuka, T., Miyazawa, Y., Wickramasinghe, N.K., Brown, M. and Fukuda, Y.: "Quantitative Operational Flight Efficiency Analysis of Passenger Aircraft Scheduled Flight", in Japanese, *JSASS Kouku-Uchu Gijutu (Aerospace Technology)*, Vol. 14, pp. 171-178, 2015.

3. Harada, A., Miyazawa, Y., Ueno, A. and Watanabe, Y.: "Trajectory Optimization Analysis by Dynamic Programming for Operational Feasibility Study of Supersonic Transport," Proceedings of the Asia-Pacific International Symposium on Aerospace Technology (APISAT) 2014, Shanghai, 2014.

4. Harada, A., Miyamoto, Y., Miyazawa, Y. and Funabiki, K.: "Accuracy Evaluation of an Aircraft Performance Model with Airliner Flight Data," *Transactions of JSASS Aerospace Technology Japan*, Vol. 11, pp. 79-85, 2013.

Chapter. 2

Optimal Control

2.1 Statement of optimal control problem

The general optimal control problem (OCP) is defined from the mathematical and engineering aspects. In the differential equation system which includes the variable $u_1, u_2, \cdots, u_m$,

$$\frac{dx_i}{dt} = f_i(x_1, x_2, \cdots, x_n, u_1, u_2, \cdots, u_m) \tag{2.1}$$

$$x_i(t_0) = x_{i0}, \qquad (i = 1, 2, \cdots, n) \tag{2.2}$$

the problem which derives a series of the variable $u_i = u_i(t)$ such that minimizes a functional of $u(t)$

$$J[\boldsymbol{u}] = \int_{t_0}^{t_1} f(x_1, x_2, \cdots, x_n, u_1, u_2, \cdots, u_m) dt \tag{2.3}$$

over the time interval $t_0 \leq t \leq t_1$ is generally called as the optimal control problem. In the engineering, Eq.(2.1) is called as the dynamical system equation or the state equation. $\boldsymbol{x}$ and $\boldsymbol{u}$ are respectively the state variable (or the states) and the control variable (or the inputs) which denote the state and input of the system. The functional J is called the objective function or the Optimal Return Function (ORF).

These mathematical expressions are extended from an engineering perspective. The state variable values do not have to be fixed at the initial and final point. Additionally, the objective function may include a not-integrated term with regard to the initial or/and final state conditions and time. Furthermore, the equality or/and inequality constraints in terms of state variables or/and control variables may be added. The typical optimal control problem is formulated below.

Let us assume that the state equation of a system is given as follows.

$$\dot{\boldsymbol{x}} = \boldsymbol{f}(\boldsymbol{x}, \boldsymbol{u}, t) \tag{2.4}$$

Note that, the time t is defined as an independent variable which monotonously varies independent on the other variables. The state variable $\boldsymbol{x}$ and control variable $\boldsymbol{u}$ are the time-variant quantities which belong to

real vectors, $\mathbb{R}^n$ and $\mathbb{R}^m$, respectively. $\boldsymbol{f}$ is a n-dimensional vector function, i.e., $\boldsymbol{f} \in \mathbb{R}^n$.

$$\boldsymbol{x}^{\mathrm{T}}(t) = (x_1(t), x_2(t), ..., x_n(t)) \tag{2.5}$$

$$\boldsymbol{u}^{\mathrm{T}}(t) = (u_1(t), u_2(t), ..., u_m(t)) \tag{2.6}$$

$$\boldsymbol{f}^{\mathrm{T}} = (f_1, f_2, ..., f_n) \tag{2.7}$$

Therefore, the optimal control problem is defined as finding a time history of optimal control input $\boldsymbol{u}(t)$ such that minimizes the objective function

$$J[\boldsymbol{u}] = \int_{t_0}^{t_f} \mathscr{L}(\boldsymbol{x}, \boldsymbol{u}, t)dt + \phi[\boldsymbol{x}(t_f), t_f] \tag{2.8}$$

over the object time interval

$$t_0 \leq t \leq t_f \tag{2.9}$$

subject to the state equation Eq. (2.4). Note that, the second term of Eq. (2.8) is the evaluation amount at the terminal time and $\mathscr{L}$ is the Lagrangian of the system. This formulation has been led according to the reference [14].

2.2 Indirect method - Calculus of variations

This section introduces a methodology to get an optimal solution with the calculus of variations which is classified as an indirect method. A series of getting the optimal solution from the variational principle is described analytically.

2.2.1 Derivation of Euler's equation

The function which satisfies the boundary conditions or the continuity conditions is called the admissible function. The variational problem is defined as deriving the unique stationary function within this admissible function such that minimizes or maximizes a given functional. Here, regarding a general variational problem, a process to gain the Euler's equation from the optimality necessary condition is introduced. After the Euler's equation is led, it is presented that the stationary function derived by solving the Euler's equation as the two-point boundary value problem is the solution of the variational problem.

Now, here is a simple curve line which connects two points. An admissible function $y = y(x)$ is defined with the independent variable x and the following boundary condition (2.10).

$$y(x_0) = y_0, \qquad y(x_1) = y_1 \tag{2.10}$$

Let us consider to get the stationary function $y = y(x)$ for a given functional I

$$I(y) = \int_{x_0}^{x_1} F(x, y, \dot{y})dx \tag{2.11}$$

under the boundary condition.

At first, an admissible function $y = \tilde{y}(x)$ close to the function $y = y(x)$ is assumed. This function $\tilde{y}(x)$ is described with a small perturbation parameter ε and an arbitrary function $\eta(x)$ which is continuous and differentiable in the interval $x_0 \leq x \leq x_1$.

$$\tilde{y}(x) = y(x) + \varepsilon\eta(x) = y(x) + \delta y \tag{2.12}$$

$\eta(x)$ satisfies the following condition.

$$\eta(x_0) = 0, \quad \eta(x_1) = 0 \tag{2.13}$$

The δy in Eq. (2.12) is called the variation which means the gap of the admissible function from the solution. If the amount of change of the functional $I(y)$ by the variation is expressed as δI, it is described below.

$$\begin{aligned}
\delta I &= I(\tilde{y}) - I(y) \\
&= I(y(x) + \varepsilon\eta(x)) - I(y) \\
&= \int_{x_0}^{x_1} F(x, y + \varepsilon\eta, \dot{y} + \varepsilon\dot{\eta})dx - \int_{x_0}^{x_1} F(x, y, \dot{y})dx
\end{aligned}$$

This equation is rewritten by applying the Taylor expansion.

$$\delta I = \int_{x_0}^{x_1} (\frac{\partial F}{\partial y}\varepsilon\eta + \frac{\partial F}{\partial \dot{y}}\varepsilon\dot{\eta})dx + \frac{1}{2}\int_{x_0}^{x_1} (\frac{\partial F}{\partial y}\varepsilon\eta + \frac{\partial F}{\partial \dot{y}}\varepsilon\dot{\eta})^2 dx + \cdots \tag{2.14}$$

The first and second term of Eq. (2.14) is called the first variation and the second variation respectively. The stationary condition of the functional I is determined by the first derivation because ε can be regarded as a negligible parameter.

$$\delta I = 0 \tag{2.15}$$

Therefore, the following relationship should be established.

$$\begin{aligned}
\delta I &= \int_{x_0}^{x_1} \left(\frac{\partial F}{\partial y}\varepsilon\eta + \frac{\partial F}{\partial \dot{y}}\varepsilon\dot{\eta} \right) dx \\
&= \left[\varepsilon\eta \frac{\partial F}{\partial \dot{y}} \right]_{x_0}^{x_1} + \int_{x_0}^{x_1} \left\{ \frac{\partial F}{\partial y} - \frac{d}{dx}\left(\frac{\partial F}{\partial \dot{y}} \right) \right\} \varepsilon\eta dx = 0
\end{aligned} \tag{2.16}$$

The first term of Eq. (2.16) is zero from Eq. (2.13). Thus, the necessary and sufficient condition for Eq. (2.16) is expressed as Eq. (2.17).

$$\frac{\partial F}{\partial y} - \frac{d}{dx}\left(\frac{\partial F}{\partial \dot{y}} \right) = 0 \tag{2.17}$$

This equation is so-called the Euler's equation. Hence, the stationary function $y(x)$ may be introduced by solving Eq. (2.17) under the boundary condition denoted by Eq. (2.10).

2.2.2 Transversality condition

Let us consider the case that the initial point is fixed at $(x_0,\, y_0)$ and the terminal can move from the point $(x_1,\, y_1)$ to the point $(x_1 + dx_1, y_1 + dy(x_1))$. In such a case, the objective functional is given with a term to evaluate the terminal condition.

$$I(y) = \int_{x_0}^{x_1} F(x,\, y,\, \dot{y})dx + \phi[x_1,\, y_1] \tag{2.18}$$

The initial point is fixed.

$$y(x_0) = y_0 \tag{2.19}$$

The relationship of each quantity at the terminal is illustrated in the Fig. 2.1.

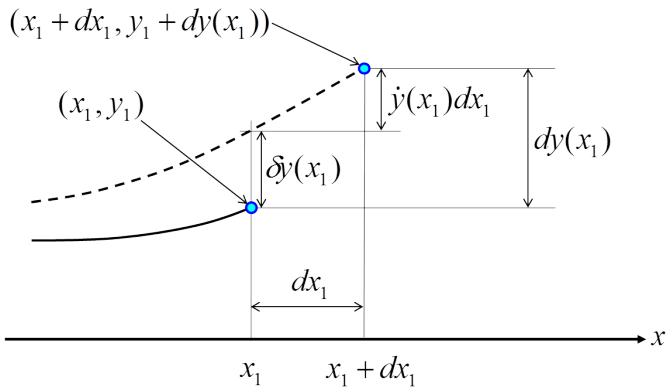

Fig.2.1 Relationships among dx_1, $dy(x_1)$ and $\delta y(x_1)$

The first variation of the functional is denoted by the following equation with considering the amount of change dx_1, $dy(x_1)$ at the terminal and neglecting the higher order term of the small quantity.

$$
\begin{aligned}
\delta I = & \left[\frac{\partial \phi}{\partial x}\right]_{x=x_1} dx_1 + \left[\frac{\partial \phi}{\partial y}\right]_{y=y_1} dy(x_1) \\
& + \left[\frac{\partial F}{\partial \dot{y}}\delta y\right]_{x_0}^{x_1} + \int_{x_0}^{x_1} \left\{\frac{\partial F}{\partial y} - \frac{d}{dx}\left(\frac{\partial F}{\partial \dot{y}}\right)\right\} \delta y dx \\
& + \int_{x_1}^{x_1+dx_1} F(x,\, y+\delta y,\, \dot{y}+\delta \dot{y}) dx \\
\cong & \left[\frac{\partial \phi}{\partial x}\right]_{x=x_1} dx_1 + \left[\frac{\partial \phi}{\partial y}\right]_{y=y_1} dy(x_1) \\
& + \left[\frac{\partial F}{\partial \dot{y}}\delta y\right]_{x_0}^{x_1} + \int_{x_0}^{x_1} \left\{\frac{\partial F}{\partial y} - \frac{d}{dx}\left(\frac{\partial F}{\partial \dot{y}}\right)\right\} \delta y dx \\
& + [F]_{x=x_1} dx_1
\end{aligned}
$$

The following relationship is obvious from the Fig. 2.1 at the terminal.

$$
\delta y(x_1) = dy(x_1) - \dot{y}(x_1) dx_1 \tag{2.20}
$$

$\delta y(x_1)$ is deleted by substituting this equation into Eq. (2.20)

$$
\begin{aligned}
\delta I = & \left[F - \frac{\partial F}{\partial \dot{y}}\dot{y} + \frac{\partial \phi}{\partial x}\right]_{x=x_1} dx_1 + \left[\frac{\partial F}{\partial \dot{y}} + \frac{\partial \phi}{\partial y}\right]_{x=x_1} dy(x_1) \\
& - \left[\frac{\partial F}{\partial \dot{y}}\right]_{x=x_0} \delta y(x_0) + \int_{x_0}^{x_1} \left\{\frac{\partial F}{\partial y} - \frac{d}{dx}\left(\frac{\partial F}{\partial \dot{y}}\right)\right\} \delta y dx
\end{aligned} \tag{2.21}
$$

$\delta y(x_0)$ is zero from Eq. (2.19). The stationary condition is given by Eq. (2.15) and the following three formulae are led by the necessary condition.

$$
\frac{\partial F}{\partial y} - \frac{d}{dx}\left(\frac{\partial F}{\partial \dot{y}}\right) = 0 \tag{2.22a}
$$

$$
\left[F - \frac{\partial F}{\partial \dot{y}}\dot{y} + \frac{\partial \phi}{\partial x}\right]_{x=x_1} = 0 \tag{2.22b}
$$

$$
\left[\frac{\partial F}{\partial \dot{y}} + \frac{\partial \phi}{\partial y}\right]_{x=x_1} = 0 \tag{2.22c}
$$

Eq. (2.22a) is the same as the Euler's equation in the former both fixed case. Eqs. (2.22b) and (2.22c), i.e. the condition that only the stationary function should satisfy, is spontaneously led by the stationary condition of the functional. These are called the natural boundary condition a part of the transversality condition. If the unknown quantity x_1 is deleted by Eq. (2.22b), Eqs. (2.19) and (2.22c) constitute the two-point boundary value problem.

2.2.3 Euler-Lagrange differential equation

Most of the engineering optimal control problems can be formulated as the variational problem which includes collateral conditions. The optimal control problem can be categorized into following four types by

the terminal conditions.

1. Terminal time fixed, terminal states free
2. Terminal time fixed, terminal states constrained
3. Terminal time free, terminal states free
4. Terminal time free, terminal states constrained

The objective function denoted by Eq. (2.8) belongs to the third case.

$$J(\boldsymbol{u}) = \int_{t_0}^{t_f} \mathscr{L}(\boldsymbol{x}, \boldsymbol{u}, t)dt + \phi[\boldsymbol{x}(t_f),\, t_f] \tag{2.8}$$

The second term of this objective function, an algebraic vector term, indicates the terminal condition. This section, at first, introduces the formulation under the terminal time fixed and terminal states constrained condition and thereafter, the formulation under the other cases is considered. The optimal control problem under the terminal free condition is defined again. Regarding the state variable $\boldsymbol{x}$, the control variable $\boldsymbol{u}$ and the function $\boldsymbol{f}$, each variable belongs to the real numbers; $\boldsymbol{x} \in \mathbb{R}^n$, $\boldsymbol{u} \in \mathbb{R}^m$ and $\boldsymbol{f} \in \mathbb{R}^n$. In the dynamic system with the following state equation,

$$\dot{\boldsymbol{x}} = \boldsymbol{f}(\boldsymbol{x}, \boldsymbol{u}, t) \tag{2.23}$$

the initial state is fixed at the initial time.

$$\boldsymbol{x}(t_0) = \boldsymbol{x}_0 \tag{2.24}$$

And the q states are fixed at the terminal.

$$x_i(t_f) = x_{if}, \qquad i = 1, 2, \cdots, q \tag{2.25}$$

This condition can be generally expressed with the q dimensional vector function.

$$\boldsymbol{\psi}\left[\boldsymbol{x}(t_f),\, t_f\right] = \begin{pmatrix} x_1(t_f) - x_{1f} \\ x_2(t_f) - x_{2f} \\ \vdots \\ x_q(t_f) - x_{qf} \end{pmatrix} = \boldsymbol{0} \tag{2.26}$$

The optimal control problem is defined as designing the control input such that minimizes the following objective function under those boundary conditions,

$$J(\boldsymbol{u}) = \int_{t_0}^{t_f} \mathscr{L}(\boldsymbol{x}, \boldsymbol{u}, t)dt + \phi[\boldsymbol{x}(t_f),\, t_f] \tag{2.27}$$

This objective function is extended with the Lagrange's multiplier $\boldsymbol{\lambda}(t)$ and $\boldsymbol{\nu}^{\mathrm{T}} = (\nu_1, \nu_2, \cdots, \nu_q)$. $\boldsymbol{\nu}$, the Lagrange's multiplier vector, is introduced to consider the terminal conditions.

$$J^*(\boldsymbol{x}, \boldsymbol{u}, \boldsymbol{\lambda}, \boldsymbol{\nu}) = \phi[\boldsymbol{x}, \boldsymbol{\nu}^{\mathrm{T}}\boldsymbol{\psi}]_{t=t_f} + \int_{t_0}^{t_f} \left[\mathscr{L}(\boldsymbol{x}, \boldsymbol{u}, t) + \boldsymbol{\lambda}^{\mathrm{T}}(t)\left\{\boldsymbol{f}(\boldsymbol{x}, \boldsymbol{u}, t) - \frac{d\boldsymbol{x}}{dt}\right\}\right] dt \tag{2.28}$$

Now, the Hamiltonian is given as the following.

$$\mathscr{H}(\boldsymbol{x},\boldsymbol{u},\boldsymbol{\lambda},t) = \mathscr{L}(\boldsymbol{x},\boldsymbol{u},t) + \boldsymbol{\lambda}^{\mathrm{T}}(t)\boldsymbol{f}(\boldsymbol{x},\boldsymbol{u},t) \tag{2.29}$$

Eq. (2.28) can be rewritten with this Hamiltonian.

$$J^*(\boldsymbol{x},\boldsymbol{u},\boldsymbol{\lambda},\boldsymbol{\nu}) = \left[\phi + \boldsymbol{\nu}^{\mathrm{T}}\boldsymbol{\psi}\right]_{t=t_f} + \int_{t_0}^{t_f}\left[\mathscr{H}(\boldsymbol{x},\boldsymbol{u},\boldsymbol{\lambda},t) - \boldsymbol{\lambda}^{\mathrm{T}}(t)\frac{d\boldsymbol{x}}{dt}\right]dt \tag{2.30}$$

The first derivation of this extended objective function is

$$\begin{aligned}\delta J^* = &\left[\frac{\partial}{\partial \boldsymbol{x}}\left(\phi + \boldsymbol{\nu}^{\mathrm{T}}\boldsymbol{\psi}\right)\right]_{t=t_f} d\boldsymbol{x}(t_f) + \left[\frac{\partial}{\partial t}\left(\phi + \boldsymbol{\nu}^{\mathrm{T}}\boldsymbol{\psi}\right)\right]_{t=t_f} dt_f \\ &+ \left[\mathscr{H} - \boldsymbol{\lambda}^{\mathrm{T}}\frac{d\boldsymbol{x}}{dt}\right]_{t=t_f} dt_f + \int_{t_0}^{t_f}\left[\frac{\partial \mathscr{H}}{\partial \boldsymbol{x}}\delta\boldsymbol{x} - \boldsymbol{\lambda}^{\mathrm{T}}\delta\dot{\boldsymbol{x}}\right. \\ &\left. + \frac{\partial \mathscr{H}}{\partial \boldsymbol{u}}\delta\boldsymbol{u} + \left(\frac{\partial \mathscr{H}}{\partial \boldsymbol{\lambda}^{\mathrm{T}}} - \frac{d\boldsymbol{x}}{dt}\right)\delta\boldsymbol{\lambda}^{\mathrm{T}}\right]dt\end{aligned} \tag{2.31}$$

and it becomes Eq. (2.32) by applying the partial integral to the term, $\boldsymbol{\lambda}^{\mathrm{T}}\delta\dot{\boldsymbol{x}}$

$$\begin{aligned}\delta J^* = &\left[\frac{\partial \phi}{\partial t} + \boldsymbol{\nu}^{\mathrm{T}}\frac{\partial \boldsymbol{\psi}}{\partial t} + \mathscr{H} - \boldsymbol{\lambda}^{\mathrm{T}}\frac{d\boldsymbol{x}}{dt}\right]_{t=t_f} dt_f + \left[\frac{\partial \phi}{\partial \boldsymbol{x}} + \boldsymbol{\nu}^{\mathrm{T}}\frac{\partial \boldsymbol{\psi}}{\partial \boldsymbol{x}}\right]_{t=t_f} d\boldsymbol{x}(t_f) \\ &+ \left[\boldsymbol{\lambda}^{\mathrm{T}}\right]_{t=t_0}\delta\boldsymbol{x}(t_0) - \left[\boldsymbol{\lambda}^{\mathrm{T}}\right]_{t=t_f}\delta\boldsymbol{x}(t_f) \\ &+ \int_{t_0}^{t_f}\left[\left(\frac{\partial \mathscr{H}}{\partial \boldsymbol{x}} + \frac{d\boldsymbol{\lambda}^{\mathrm{T}}}{dt}\right)\delta\boldsymbol{x}\right. \\ &\left. + \frac{\partial \mathscr{H}}{\partial \boldsymbol{u}}\delta\boldsymbol{u} + \left(\frac{\partial \mathscr{H}}{\partial \boldsymbol{\lambda}^{\mathrm{T}}} - \frac{d\boldsymbol{x}}{dt}\right)\delta\boldsymbol{\lambda}^{\mathrm{T}}\right]dt\end{aligned} \tag{2.32}$$

The following relationship is established at the terminal as illustrated in Fig. 2.1.

$$\delta\boldsymbol{x}(t_f) = d\boldsymbol{x}(t_f) - \dot{\boldsymbol{x}}(t_f)dt_f \tag{2.33}$$

The extended objective function is expressed as Eq. (2.34) by deleting $\delta\boldsymbol{x}(t_f)$.

$$\begin{aligned}\delta J^* = &\left[\frac{\partial \phi}{\partial t} + \boldsymbol{\nu}^{\mathrm{T}}\frac{\partial \boldsymbol{\psi}}{\partial t} + \mathscr{H}\right]_{t=t_f} dt_f + \left[\frac{\partial \phi}{\partial \boldsymbol{x}} + \boldsymbol{\nu}^{\mathrm{T}}\frac{\partial \boldsymbol{\psi}}{\partial \boldsymbol{x}} - \boldsymbol{\lambda}^{\mathrm{T}}\right]_{t=t_f} d\boldsymbol{x}(t_f) \\ &+ \left[\boldsymbol{\lambda}^{\mathrm{T}}\right]_{t=t_0}\delta\boldsymbol{x}(t_0) \\ &+ \int_{t_0}^{t_f}\left[\left(\frac{\partial \mathscr{H}}{\partial \boldsymbol{x}} + \frac{d\boldsymbol{\lambda}^{\mathrm{T}}}{dt}\right)\delta\boldsymbol{x}\right. \\ &\left. + \frac{\partial \mathscr{H}}{\partial \boldsymbol{u}}\delta\boldsymbol{u} + \left(\frac{\partial \mathscr{H}}{\partial \boldsymbol{\lambda}^{\mathrm{T}}} - \frac{d\boldsymbol{x}}{dt}\right)\delta\boldsymbol{\lambda}^{\mathrm{T}}\right]dt\end{aligned} \tag{2.34}$$

As $\delta \boldsymbol{x}(t_0)$ is obviously zero from Eq. (2.24), the optimality necessary condition is given by the five formulae below.

$$\frac{d\boldsymbol{\lambda}}{dt} = -\left(\frac{\partial \mathscr{H}}{\partial \boldsymbol{x}}\right)^{\mathrm{T}} \tag{2.35}$$

$$\frac{\partial \mathscr{H}}{\partial \boldsymbol{u}} = 0 \tag{2.36}$$

$$\frac{d\boldsymbol{x}}{dt} = \frac{\partial \mathscr{H}}{\partial \boldsymbol{\lambda}^{\mathrm{T}}} = \boldsymbol{f} \tag{2.37}$$

$$\boldsymbol{\lambda}^{\mathrm{T}}(t_f) = \left[\frac{\partial \phi}{\partial \boldsymbol{x}} + \boldsymbol{\nu}^{\mathrm{T}} \frac{\partial \boldsymbol{\psi}}{\partial \boldsymbol{x}}\right]_{t=t_f} \tag{2.38}$$

$$\left[\mathscr{H} + \frac{\partial \phi}{\partial t} + \boldsymbol{\nu}^{\mathrm{T}} \frac{\partial \boldsymbol{\psi}}{\partial t}\right]_{t=t_f} = 0 \tag{2.39}$$

Eqs. (2.35), (2.36) and (2.37) are the Euler-Lagrange differential equations. The variational problem with the collateral conditions such as the differential equation is come down to solving the Euler-Lagrange differential equations. Eq. (2.35) is the adjoint equation, the Eq. (2.36) is the optimality condition with regard to the control inputs, Eq. (2.37) is the system equation, Eq. (2.38) is the terminal condition of the adjoint variable and Eq. (2.39) is the condition arising from the free terminal time. If the control $\boldsymbol{u}$ derived from Eq. (2.36) is substituted into Eqs. (2.35) and (2.37), they constitute the simultaneous first-order differential equations in terms of the state variable vector $\boldsymbol{x}$ and the adjoint variable vector $\boldsymbol{\lambda}$. Although the integral constants are produced from $2n$ equations, they can be decided uniquely because the n boundary conditions are given at the initial point and terminal point respectively. The multiplier $\boldsymbol{\nu}$ can be determined by Eq. (2.26).

If the terminal states are constrained, the second term of the objective function (2.27), $\phi[\boldsymbol{x}(t_f),\, t_f]$ doesn't need to be considered; thereby, only the integral term should be evaluated. Therefore, Eqs. (2.38) and (2.39) are reduced to the following equations.

$$\boldsymbol{\lambda}^{\mathrm{T}}(t_f) = \left[\boldsymbol{\nu}^{\mathrm{T}} \frac{\partial \boldsymbol{\psi}}{\partial \boldsymbol{x}}\right]_{t=t_f} \tag{2.40}$$

$$\left[\mathscr{H} + \boldsymbol{\nu}^{\mathrm{T}} \frac{\partial \boldsymbol{\psi}}{\partial t}\right]_{t=t_f} = 0 \tag{2.41}$$

Eq. (2.25) is the special case of

$$\boldsymbol{\psi} = \begin{bmatrix} x_1(t) - x_{1f} \\ x_2(t) - x_{2f} \\ \vdots \\ x_q(t) - x_{qf} \end{bmatrix} \tag{2.42}$$

The Jacobian of this vector is described as the $q \times n$ matrix.

$$\frac{\partial \boldsymbol{\psi}}{\partial \boldsymbol{x}} = \begin{bmatrix} 1 & 0 & 0 & \cdots & 0 & 0 & 0 & \cdots & 0 \\ 0 & 1 & 0 & \cdots & 0 & 0 & 0 & \cdots & 0 \\ 0 & 0 & 1 & \cdots & 0 & 0 & 0 & \cdots & 0 \\ \vdots & \vdots & \vdots & \ddots & \vdots & \vdots & \vdots & \ddots & \vdots \\ 0 & 0 & 0 & \cdots & 1 & 0 & 0 & \cdots & 0 \end{bmatrix}, \quad \frac{\partial \boldsymbol{\psi}}{\partial \boldsymbol{x}} \in \mathbb{R}^{q \times n} \tag{2.43}$$

Thus, Eq. (2.38) is expressed as follows.

$$\boldsymbol{\lambda_j}(\boldsymbol{t_f}) = \begin{cases} \boldsymbol{\nu}_j, & j = 1, 2, \cdots, q \\ \left[\frac{\partial \phi}{\partial x_j}\right]_{t=t_f}, & j = q+1, q+2, \cdots, n \end{cases} \tag{2.44}$$

The q multipliers are determined by Eq. (2.25).

All the optimality necessary conditions corresponding the former four categories are listed in the following. It is clear that the formulation for the fourth case, i.e. “the terminal time free and terminal states constrained case”, includes the other case.

1. Terminal time fixed, terminal states free

Adjoint equation	$\dfrac{d\boldsymbol{\lambda}}{dt} = -\left(\dfrac{\partial \mathscr{H}}{\partial \boldsymbol{x}}\right)^{\mathrm{T}}$
System equation	$\dfrac{d\boldsymbol{x}}{dt} = \dfrac{\partial \mathscr{H}}{\partial \boldsymbol{\lambda}^{\mathrm{T}}} = \boldsymbol{f}$
Optimality condition for control	$\dfrac{\partial \mathscr{H}}{\partial \boldsymbol{u}} = 0$
Terminal condition for adjoint	$\boldsymbol{\lambda}^{\mathrm{T}}(t_f) = \left[\dfrac{\partial \phi}{\partial \boldsymbol{x}}\right]_{t=t_f}$

2. Terminal time fixed, terminal states constrained

Adjoint equation	$\dfrac{d\boldsymbol{\lambda}}{dt} = -\left(\dfrac{\partial \mathscr{H}}{\partial \boldsymbol{x}}\right)^{\mathrm{T}}$
System equation	$\dfrac{d\boldsymbol{x}}{dt} = \dfrac{\partial \mathscr{H}}{\partial \boldsymbol{\lambda}^{\mathrm{T}}} = \boldsymbol{f}$
Optimality condition for control	$\dfrac{\partial \mathscr{H}}{\partial \boldsymbol{u}} = 0$
Terminal condition for adjoint	$\boldsymbol{\lambda}^{\mathrm{T}}(t_f) = \left[\dfrac{\partial \phi}{\partial \boldsymbol{x}} + \boldsymbol{\nu}^{\mathrm{T}}\dfrac{\partial \psi}{\partial \boldsymbol{x}}\right]_{t=t_f}$

3. Terminal time free, terminal states free

Adjoint equation	$\dfrac{d\boldsymbol{\lambda}}{dt} = -\left(\dfrac{\partial \mathscr{H}}{\partial \boldsymbol{x}}\right)^{\mathrm{T}}$
System equation	$\dfrac{d\boldsymbol{x}}{dt} = \dfrac{\partial \mathscr{H}}{\partial \boldsymbol{\lambda}^{\mathrm{T}}} = \boldsymbol{f}$
Optimality condition for control	$\dfrac{\partial \mathscr{H}}{\partial \boldsymbol{u}} = 0$
Terminal condition for adjoint	$\boldsymbol{\lambda}^{\mathrm{T}}(t_f) = \left[\dfrac{\partial \phi}{\partial \boldsymbol{x}}\right]_{t=t_f}$
Terminal condition by the unknown time	$\left[\mathscr{H} + \dfrac{\partial \phi}{\partial \boldsymbol{t}}\right]_{t=t_f} = 0$

4. Terminal time free. terminal states constrained

Adjoint equation	$\dfrac{d\boldsymbol{\lambda}}{dt} = -\left(\dfrac{\partial \mathscr{H}}{\partial \boldsymbol{x}}\right)^{\mathrm{T}}$
System equation	$\dfrac{d\boldsymbol{x}}{dt} = \dfrac{\partial \mathscr{H}}{\partial \boldsymbol{\lambda}^{\mathrm{T}}} = \boldsymbol{f}$
Optimality condition for control	$\dfrac{\partial \mathscr{H}}{\partial \boldsymbol{u}} = 0$
Terminal condition for adjoint	$\boldsymbol{\lambda}^{\mathrm{T}}(t_f) = \left[\dfrac{\partial \phi}{\partial \boldsymbol{x}} + \boldsymbol{\nu}^{\mathrm{T}}\dfrac{\partial \psi}{\partial \boldsymbol{x}}\right]_{t=t_f}$
Terminal condition by the unknown time	$\left[\mathscr{H} + \dfrac{\partial \phi}{\partial \boldsymbol{t}} + \boldsymbol{\nu}^{\mathrm{T}}\dfrac{\partial \psi}{\partial t}\right]_{t=t_f} = 0$

Chapter. 3

Dynamic Programming

3.1 Historical background

Dynamic Programming (DP), first proposed by Richard E. Bellman in the 1950s, is an optimization theory based on the Hamilton-Jacobi-Bellman (HJB) partial differential equation. DP is classified as a direct method because the state of the system is expressed by finite discretized grid points and solved as combinatorial optimization problem for those grid points. DP has been widely used in economics represented by operations research, informatics, and control engineering due to its many great advantages over other methods. One major well-known advantage is guarantee of the global optimality. The computational algorithm based on the principle of optimality works to provide a global optimum under a certain calculation grid settings and does not contain any iterative calculations for the convergence. Therefore, the computational time can be estimated in advance because it depends only on the number of state variables and number of grid points in the state space. While DP has such a great advantage to guarantee the global optimality and it seems to be theoretically applied to many practical problems, DP has been considered to require enormous amounts of calculation and fail at providing accurate solutions due to its fatal drawbacks. Those potential drawbacks arising from the requirement of large computational load and the algorithm itself have limited its further development and acceptance in the aerospace engineering field since 1970s onward. Nevertheless, the rapid increase of capability in recent computers with high-performance processors and parallel processing technology, as well as continual decrease of hardware costs, have encouraged the revival of DP in many practical engineering problems.

This thesis aims to extend the scope of application of dynamic programming with the belief that the outstanding advantages of DP will encourage its revival in the practical usage. This chapter introduces the calculation algorithm and the engineering characteristics of dynamic programming after leading the Hamilton-Jacobi-Bellman (HJB) differential equation with the fundamental concept of DP which is called the principle of optimality.

3.2 The principle of optimality

The Principle of Optimality

An optimal policy has the property that whatever the initial state and the initial decision are, the remaining decisions must constitute an optimal policy with regard to the state resulting from the first decision. (by Richard E. Bellman)

This principle of optimality advocated by Richard E. Bellman in 1950s describes what the optimality is and how it can be defined in a system where the future state is completely or stochastically determined by the current state.

The optimal policy, in other words, the optimal control or optimal input at an arbitrary point of time depends only on the current state at the time point resulting from the first decision and does not depend on the previous state nor the previous decision. Additionally, it may be described that the optimal policy must optimize the trajectory from an arbitrary time point to the terminal point. The principle of optimality is explained with a simple formula and illustration as follows.

Let us consider to design a control system such that minimizes an objective function denoted by

$$J = \int_{t_0}^{t_f} \mathscr{L}(\boldsymbol{x}, \boldsymbol{u}, t)\mathrm{d}t \tag{3.1}$$

in terms of a time-variant dynamic system,

$$\frac{d\boldsymbol{x}}{dt} = \boldsymbol{f}(\boldsymbol{x}, \boldsymbol{u}, t), \qquad \boldsymbol{x}(t_0) = \boldsymbol{x}_0 \tag{3.2}$$

Note that, the state variable and the control variable belong to real vectors, $\mathbb{R}^n$ and $\mathbb{R}^m$ respectively and the initial state $\boldsymbol{x}_0$ is given. The optimal trajectory over the time interval of $t_0 \leq t \leq t_f$ in the n dimensional space is presented by a solid line in Fig. 3.1. Now, a state $x(t_1)$ at the time $t = t_1,\ t_1 \in [t_0,\ t_f]$ on the trajectory is assumed. The trajectory is divided into two parts from $x(t_0)$ to $x(t_1)$ and from $x(t_1)$ to $x(t_f)$. Each part is called the former part and the latter part. The objective function divided into two parts at the point $x(t_1)$ is described as the following.

$$J = \int_{t_0}^{t_1} \mathscr{L}(\boldsymbol{x}, \boldsymbol{u}, t)dt + \int_{t_1}^{t_f} \mathscr{L}(\boldsymbol{x}, \boldsymbol{u}, t)dt \tag{3.3}$$

The trajectory of latter part can be regarded as an independent trajectory which has the initial state $x(t_1)$ and that becomes the optimal trajectory if the second term of Eq. (3.3) takes a minimal value. This means that if the state at the time $t = t_1$ takes the value of $x(t_1)$, the optimal trajectory is determined uniquely whatever the previous decision were made in the former part to reach the state $x(t_1)$.

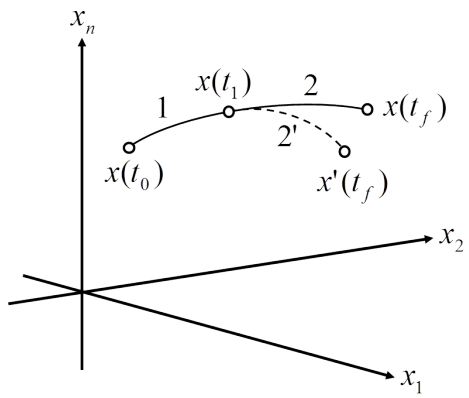

Fig.3.1 An optimal trajectory in the n dimensional space

3.3 Hamilton-Jacobi-Bellman equation

In this section, the Hamilton-Jacobi-Bellman equation is introduced to prove that it is led by the principle of optimality which is a fundamental principle of dynamic programming. An optimization problem such that minimizing the objective function described by the following formula,

$$J = \int_{t_0}^{t_f} \mathscr{L}[\boldsymbol{x}(\tau), \boldsymbol{u}(\tau), \tau] d\tau + \phi[x(t_f), t_f] \tag{3.4}$$

subject to the system equation

$$\dot{\boldsymbol{x}} = \boldsymbol{f}(\boldsymbol{x}, \boldsymbol{u}, t) \tag{3.5}$$

defined with the initial condition

$$\boldsymbol{x}(t_0) = \boldsymbol{x}_0 \tag{3.6}$$

is considered. Note that, the state variable and the control variable $\boldsymbol{x}$ and $\boldsymbol{u}$ belong to the real vectors, $\mathbb{R}^n$ and $\mathbb{R}^m$ respectively. The second term of Eq. (3.4) is the terminal state condition at the time t_f.

Now, a general problem which starts from an initial arbitrary time $t \in [t_0, t_f]$ is assumed at first.

$$J = \int_{t}^{t_f} \mathscr{L}(\boldsymbol{x}, \boldsymbol{u}, \tau) d\tau + \phi[\boldsymbol{x}(t_f), t_f] \tag{3.7}$$

The system equation and the constraints on state variables at the terminal are the following.

$$\dot{\boldsymbol{x}} = \boldsymbol{f}(\boldsymbol{x}, \boldsymbol{u}, t) \tag{3.8}$$

$$\boldsymbol{\psi}[\boldsymbol{x}(t_f), t_f] = 0 \tag{3.9}$$

The optimal value of the objective function is expressed below.

$$J_{opt}(\boldsymbol{x}, t) = \min_{\boldsymbol{u}(t), t \in [t,\, t_f]} \left[\int_{t}^{t_f} \mathscr{L}[\boldsymbol{x}(\tau), \boldsymbol{u}(\tau), \tau] d\tau + \phi[x(t_f), t_f] \right] \tag{3.10}$$

On the hypersurface $\psi[x,t]=0$,

$$J_{opt}(\boldsymbol{x},t)=\phi(\boldsymbol{x},t) \tag{3.11}$$

Here, it is assumed that the system has proceeded by the fraction of time Δt by the control $u(t),\ t\in[t,t+\Delta t]$. This control certainly includes non-optimal value. The state $(\boldsymbol{x},t)$ is moved to $(\boldsymbol{x}+\boldsymbol{f}(\boldsymbol{x},\boldsymbol{u},t)\Delta t,\ t+\Delta t)$ by the control. The objective function value at the time t is denoted by Eq. (3.12).

$$J_{opt}\{\boldsymbol{x}+\boldsymbol{f}(\boldsymbol{x},\boldsymbol{u},t)\Delta t,t+\Delta t\}+\mathscr{L}(\boldsymbol{x},\boldsymbol{u},t)\Delta t:=J_1(\boldsymbol{x},t) \tag{3.12}$$

Since the non-optimal control is obviously included in the time Δt, this J_1 is equal to or larger than the optimal value.

$$J_{opt}(\boldsymbol{x},t)\leq J_1(\boldsymbol{x},t) \tag{3.13}$$

The equality is only true when the control $u(t)$ is chosen so as to minimize the right-hand side of Eq. (3.13).

Hence,

$$J_{opt}(\boldsymbol{x},t)=\min_{\boldsymbol{u}(t),t\in[t,\,t+dt]}\left[J_{opt}\{\boldsymbol{x}+\boldsymbol{f}(\boldsymbol{x},\boldsymbol{u},t)\Delta t,t+\Delta t\}+\mathscr{L}(\boldsymbol{x},\boldsymbol{u},t)\Delta t\right] \tag{3.14}$$

The objective function is assumed to be differentiable and continual, thereby, the Taylor expansion can be applied to the term $J_{opt}\{\boldsymbol{x}+\boldsymbol{f}(\boldsymbol{x},\boldsymbol{u},t)\Delta t,t+\Delta t\}$ around the point $(\boldsymbol{x},t)$ ignoring the second and higher-order terms.

$$J_{opt}(\boldsymbol{x},t)=\min_{u}\left[J_{opt}(\boldsymbol{x},t)+\frac{\partial J_{opt}}{\partial x}\boldsymbol{f}(\boldsymbol{x},\boldsymbol{u},t)\Delta t+\frac{\partial J_{opt}}{\partial t}\Delta t+\mathscr{L}(\boldsymbol{x},\boldsymbol{u},t)\Delta t\right] \tag{3.15}$$

Since J_{opt} does not include $\boldsymbol{u}$ explicitly, the limit $\Delta t\to 0$ is taken.

$$\lim_{\Delta t\to 0}\frac{J_{opt}(\boldsymbol{x},t)}{\Delta t}=\lim_{\Delta t\to 0}\min_{\boldsymbol{u}}\left[\frac{J_{opt}}{\Delta t}+\frac{\partial J_{opt}}{\partial \boldsymbol{x}}\boldsymbol{f}(\boldsymbol{x},\boldsymbol{u},t)+\frac{\partial J_{opt}}{\partial t}+\mathscr{L}(\boldsymbol{x},\boldsymbol{u},t)\right] \tag{3.16}$$

$$\frac{\partial J_{opt}(\boldsymbol{x},t)}{\partial t}=\min_{\boldsymbol{u}}\left[\frac{\partial J_{opt}}{\partial t}+\frac{\partial J_{opt}}{\partial \boldsymbol{x}}\boldsymbol{f}(\boldsymbol{x},\boldsymbol{u},t)+\frac{\partial J_{opt}}{\partial t}+\mathscr{L}(\boldsymbol{x},\boldsymbol{u},t)\right] \tag{3.17}$$

$$-\frac{\partial J_{opt}}{\partial t}=\min_{\boldsymbol{u}}\left[\frac{\partial J_{opt}}{\partial \boldsymbol{x}}\boldsymbol{f}(\boldsymbol{x},\boldsymbol{u},t)+\mathscr{L}(\boldsymbol{x},\boldsymbol{u},t)\right] \tag{3.18}$$

The total differentiation of J_{opt} is calculated.

$$dJ_{opt}=\frac{\partial J_{opt}}{\partial \boldsymbol{x}}d\boldsymbol{x}+\frac{\partial J_{opt}}{\partial t}dt \tag{3.19}$$

Substituting Eq. (3.18) into this equation,

$$dJ_{opt}=\frac{\partial J_{opt}}{\partial \boldsymbol{x}}d\boldsymbol{x}-\frac{\partial J_{opt}}{\partial \boldsymbol{x}}\boldsymbol{f}(\boldsymbol{x},\boldsymbol{u},t)dt-\mathscr{L}(\boldsymbol{x},\boldsymbol{u},t)dt \tag{3.20}$$

Now, the Hamiltonian $\mathscr{H}$ defined by the Lagrangian $\mathscr{L}$ and the Lagrangian's multiplier λ are introduced.

$$\mathscr{H}(\boldsymbol{x},\boldsymbol{\lambda},\boldsymbol{u},t)=\mathscr{L}(\boldsymbol{x},\boldsymbol{u},t)+\boldsymbol{\lambda}^{\mathrm{T}}\boldsymbol{f}(\boldsymbol{x},\boldsymbol{u},t) \tag{3.21}$$

The Lagrangian is substituted into Eq. (3.20).

$$\begin{aligned} dJ_{opt} &= \frac{\partial J_{opt}}{\partial \boldsymbol{x}} d\boldsymbol{x} - \frac{\partial J_{opt}}{\partial \boldsymbol{x}} \boldsymbol{f}(\boldsymbol{x},\boldsymbol{u},t)dt - \mathscr{H} dt + \boldsymbol{\lambda}^{\mathrm{T}} \boldsymbol{f}(\boldsymbol{x},\boldsymbol{u},t)dt \\ &= \frac{\partial J_{opt}}{\partial \boldsymbol{x}} d\boldsymbol{x} - \frac{\partial J_{opt}}{\partial \boldsymbol{x}} d\boldsymbol{x} - \mathscr{H} dt + \boldsymbol{\lambda}^{\mathrm{T}} \boldsymbol{f}(\boldsymbol{x},\boldsymbol{u},t)dt \\ &= \boldsymbol{\lambda}^{\mathrm{T}} d\boldsymbol{x} - \mathscr{H} dt \end{aligned} \tag{3.22}$$

Comparing Eq. (3.22) to the original total differentiation of J_{opt},

$$\boldsymbol{\lambda}^{\mathrm{T}} = \frac{\partial J_{opt}}{\partial \boldsymbol{x}} \tag{3.23}$$

$$\mathscr{H} = -\frac{\partial J_{opt}}{\partial t} \tag{3.24}$$

Hence, Eq. (3.18) is expressed as follows using Eq. (3.23) and (3.24).

$$-\frac{\partial J_{opt}}{\partial t} = \min_{\boldsymbol{u}} \left[\mathscr{L}(\boldsymbol{x},\boldsymbol{u},t) + \boldsymbol{\lambda}^{\mathrm{T}} \boldsymbol{f}(\boldsymbol{x},\boldsymbol{u},t) \right] = \min_{\boldsymbol{u}} \mathscr{H}(\boldsymbol{x}, \frac{\partial J_{opt}}{\partial \boldsymbol{x}}, \boldsymbol{u}, t) \tag{3.25}$$

Eq. (3.25) is so-called the Hamilton-Jacobi-Bellman(HJB) equation. This first order partial differential equation with regard to the time and space is true only in case the optimal control $\boldsymbol{u}_{opt}$ which minimizes the objective function (3.7) exists and the optimal return function $J_{opt}(\boldsymbol{x},t)$ is continuous and differentiable.

3.4 Combinatorial optimization calculation

The objective system is defined as following an ordinal differential equation using the state variable vector $\boldsymbol{x}$ and control variable vector $\boldsymbol{u}$. Time t is set as an independent variable that transits monotonously, and the interval is given by the initial time t_0 and final time t_f. Although a physical quantity may be selected as the independent variable in some optimal control problems to decrease the dimension of the state variables, time t is used as the independent variable for the general statement in this thesis.

$$\dot{\boldsymbol{x}} = \boldsymbol{f}(\boldsymbol{x}(t),\boldsymbol{u}(t),t), \qquad \boldsymbol{x} \in \mathbb{R}^n,\ \boldsymbol{u} \in \mathbb{R}^m \tag{3.26}$$

The objective function is expressed as an integration of the Lagrangian added to the terminal constraint.

$$J = \int_{t_0}^{t_f} \mathscr{L}(\boldsymbol{x}(t),\boldsymbol{u}(t),t)dt + \phi(\boldsymbol{x}(t_f),t_f) \tag{3.27}$$

This objective function should be minimized by the optimization process. The initial value of the state variable is given as follows:

$$\boldsymbol{x}(t_0) = \boldsymbol{x}_0 \tag{3.28}$$

r equality constraints are given at the terminal.

$$\psi(\boldsymbol{x}(t_f)) = 0, \qquad \psi \in \mathbb{R}^r \tag{3.29}$$

The calculation algorithm for the $m = n$ case is firstly introduced. In this case, the solution is obtained by solving a combinatorial optimization problem for the quantized grid points of the state variables. The state variables, which are bounded by arbitrary upper and lower values, are divided into an orthogonal isogrid at each stage of the independent variable. Although the interval of the grid points or the shape of grid can be changed to improve the solution accuracy, the simplest version is presented here considering for practical usages; i.e. the kth time t_k is expressed below by dividing time $t \in [t_0, t_f]$ into n_t:

$$t_k = t_0 + (k-1)\frac{t_f - t_0}{n_t}, \qquad k = 1, 2, \cdots, n_t + 1, \qquad t_0 \le t \le t_f \tag{3.30}$$

The ith element of the state variable $x_i(t)$ is divided into $n_i (i = 1, 2, \cdots, n)$. The jth value of x_i is expressed below.

$$\boldsymbol{x}_i(j) = \boldsymbol{x}_{i,\max} + (\boldsymbol{x}_{i,\max} - \boldsymbol{x}_{i,\min})(j-1)/n_i, \qquad j = 1, 2, \cdots, n_i + 1, \qquad \boldsymbol{x}_{i,\min} \le \boldsymbol{x}_i(j) \le \boldsymbol{x}_{i,\max} \tag{3.31}$$

Fig. 3.2 illustrates the grid points of the state variable at two neighboring time stages. The state variable transitions between the grid points are illustrated by solid lines in the two-dimensional state space.

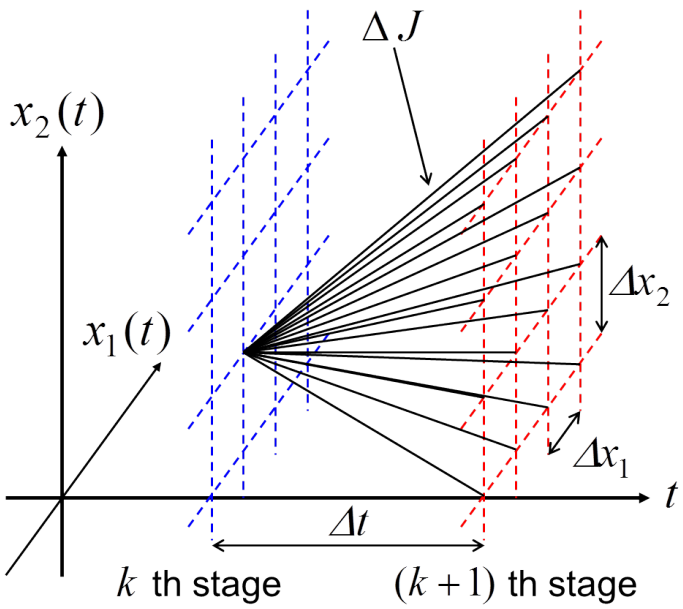

Fig.3.2 Transition between grid points

Here, the ORF value at the kth stage is defined as J_{opt_k} which is derived by minimizing the objective function denoted by Eq. (3.27) through stage k to the terminal stage. The following optimality condition gives J_{opt_k} as a functional of the state variable $\boldsymbol{x}(t_k)$:

$$J_{opt_k}(\boldsymbol{x}_1(j_1), \boldsymbol{x}_2(j_2), \cdots, \boldsymbol{x}_n(j_n)) = \min_{\boldsymbol{u}_1, \boldsymbol{u}_2, \cdots, \boldsymbol{u}_n} \left[\Delta\mathscr{L} + J_{opt_{k+1}}(\boldsymbol{x}_1(j_1'), \boldsymbol{x}_2(j_2'), \cdots, \boldsymbol{x}_n(j_n'))\right] \tag{3.32}$$

$$\Delta\mathscr{L} = \int_{t_k}^{t_{k+1}} \mathscr{L}(\boldsymbol{x}(t), \boldsymbol{u}(t), t)dt \tag{3.33}$$

The state variables at time t_k and t_{k+1} are given as follows.

$$t = t_k \quad : \quad \boldsymbol{x}_1 = \boldsymbol{x}_1(j_1),\ \boldsymbol{x}_2 = \boldsymbol{x}_2(j_2), \cdots, \boldsymbol{x}_n = \boldsymbol{x}_n(j_n) \tag{3.34}$$

$$t = t_{k+1} \quad : \quad \boldsymbol{x}_1 = \boldsymbol{x}_1(j_1'),\ \boldsymbol{x}_2 = \boldsymbol{x}_2(j_2'), \cdots, \boldsymbol{x}_n = \boldsymbol{x}_n(j_n') \tag{3.35}$$

The right-hand side of Eq. (3.32) is obtained by searching for

$$\left[\prod_{i=1}^{n}(n_i+1)\right]^2$$

combinations between the two stages.
At the terminal,

$$J_{opt_{k+1}} = \phi(\boldsymbol{x}_{t_f}, t_f) \tag{3.36}$$

and the terminal constraint $\psi(\boldsymbol{x}(t_f)) = 0$ are satisfied with the terminal state $\boldsymbol{x}(t_f) = [\boldsymbol{x}_1(t_f), \boldsymbol{x}_2(t_f), \cdots, \boldsymbol{x}_n(t_f)]$.

If the control variable is assumed to be constant over the time interval of $t_k \leq t \leq t_{k+1}$, the control variable value between two grid points may be derived from Eq. (3.26) transition condition without any difficulties. This transition cannot be realized if a reachable grid point cannot be obtained by the inequality constraints or the grid point itself does not exist due to the constraints on the state variables. Therefore, the total amount of calculation can be reduced and various constraints may be included because such infeasible paths only have to be eliminated. The ORF value may be obtained from the optimality condition denoted by Eq. (3.32) along the backward time step with the terminal value denoted by Eq. (3.36). The optimal trajectory is also easily derived from an arbitrary stage because the ORF value and optimal path selection information are preserved at each stage. This algorithm can be modified easily even if the initial and terminal values are set on arbitrary points instead of grid points.

3.5 Characteristics in engineering aspects

Dynamic programming has many favorable advantages in engineering aspects. Those advantages cannot be found in other methods. On the other hand, DP has also serious drawbacks which prevent it from being used widely in various practical problems. The engineering characteristics of dynamic programming are listed in the following.

Characteristics of dynamic programming

Advantages

- Global optimality

  DP defines a grid in the search space of the state variables and finds the optimal solution based on the HJB optimality conditions. Consequently, the algorithm provides the global optimum, not a local optimum that satisfies only the necessary conditions.
- Predictable computational time

  The computational process for the DP method is decisive and does not contain any iterative calculations for convergence. Therefore, the computational time may be estimated in advance since it depends only on the number of grid points in the state space.
- Easy to handle inequality constraints on state variables and control variables

  Inequality constraints may easily be included for the state variables themselves and their functions. Rather, inequality constraints are suitable for limiting the search space. Inequality constraints on control variables are also easily implemented.
- Simplicity for coding

  The discrete form of the HJB optimality condition makes the programming code for this method comparatively simple and easy to be understood.

Disadvantages

- Curse of dimensionality

  Computational time and memory increase explosively with the number of state variables and number of their divisions.
- Menace of the expanding grid

  DP finds the optimal solution from the combination of grid points if the number of state variables and control variables are the same. The accuracy of the solution depends on the grid resolution. In case the number of control variables is fewer than that of state variables, the optimal solution cannot be gained by the combinatorial optimization algorithm.

3.6 Overcoming the drawbacks

Due to the above mentioned two bottlenecks, the “Curse of dimensionality” and the “Menace of the expanding grid”, DP’s capability still remains not fully used in the optimal control research field. In the meanwhile, the computational capability of recent miniaturized computers has been rapidly increasing with the high-performance processors and large-scale parallel computation technology. The DP’s scope of application to the practical usage is expected to be enlarged by those trends of modern computers. Therefore, the restrictions of DP should be identified to obtain clarity about its suitability for further applications.

In the aeronautical and astronautical engineering research field, optimal control problems are often stated with many state variables; meanwhile, many practical problems where only the states which mainly influence on the objective function are effectively optimized can be seen. Moreover, it is more common that the number of control variables is fewer than that of state variables. Thereby, it is considered that the following improvements in the dynamic programming algorithm contribute to extend the scope of application of the method.

- Proposing a novel approach which is capable to reduce the computational time or to solve higher-dimensional problem.
- Devising a new calculation algorithm such that enables dynamic programming to be applied to an optimal control problem which has relatively larger number of state variables.

Within the range of author’s previous studies, two promising methods were proposed to overcome those two drawbacks. Moving Search space Dynamic Programming (MS-DP) method where the optimal solution is searched by a gradient based algorithm is introduced in section 5.2. Piecewise Linear Approximation Dynamic Programming (PLA-DP) developed to resolve the “Menace of the expanding grid” is explained with the algorithm in section 6.2.

Chapter. 4

Trajectory Optimization Analysis for Operational Feasibility Study of Supersonic Transport

4.1 Introduction

Japan Aerospace Exploration Agency (JAXA) performs a research project for silent supersonic transport (SST) as one of the most promising air transportations in the near future. Although a bottleneck in economical efficiency as well as environmental concerns has prevented the next generation SST from being realized as a hopeful transportation since the discontinuance of Concorde in 2003, research and development of SST have been continuously carried out in the world. The remarkable improvements of recent elemental technologies in aerodynamics, structures and materials, and propulsion system are expected enough to satisfy various severe requirements for the realization of next generation SST.

The economical efficiency is considered as one of the most significant factors in the SST's revival. All the requisite technologies should be integrated so as to maximize the economical efficiency which may be basically defined by the fuel consumption and flight time. Since early studies, it has been known that the flight performance of an aircraft flying at supersonic speed deteriorates due to aeroelastic issues as represented by the rapid increase of wave drag. Whether the aircraft can efficiently accelerate in the presence of such issues heavily influences on the fuel efficiency and is a typical challenge for enhancing the feasibility of SST. Therefore, the flight trajectory optimization is a key technology for the feasibility study and thus occupies an important role in the system design. Several studies have emphasized the significance of trajectory optimization from an aspect of the economical efficiency [10, 16, 17, 18]. This chapter introduces a flight trajectory optimization analysis which was conducted as a JAXA collaborative research for the next generation Japanese SST. From a perspective of the optimal control, an economically-efficient supersonic flight is revealed by de-

signing an optimal trajectory with an objective function which incorporates the fuel consumption with flight time.

This chapter handles few state variables for a single aircraft in the optimization calculation. Hence, dynamic programming can be applied without computational difficulties caused by the curse of dimensionality. Furthermore, the optimal trajectory can be designed by the general combinatorial optimization algorithm because enough number of control variables does not raise the dimensional difference problem in the transition calculation for the grid points of state variables. A technical advantage of using dynamic programming as an optimization method for this problem is stated that an optimal trajectory can be continuously designed for all flight phases at once. The optimized fuel consumption and flight time are compared to those values obtained from a reference trajectory designed by JAXA. It is statically generated by dividing all flight phases into three parts and simply connecting the trajectories determined from predefined flight conditions in those phases. One of the advantages of using dynamic programming as a trajectory optimization method is that an optimal trajectory can be gained for all flight phases without considering the boundary conditions at the connection points and adjusting the design parameters.

4.2 JAXA supersonic transport model

The research and development for the Japanese next generation supersonic civil transport are being implemented in JAXA. JAXA describes the policy and advantages of future supersonic transport toward its realization as the following [19].

“Current subsonic flight takes more than 12 hours to fly from Japan to Europe or the United States. If it will be possible to fly at twice the speed of sound, the flight time will be reduced approximately by half. By the considerable reduction of flight time, not only the passenger will be able to travel more comfortably but economical effects such as increase of more flexible communication among the countries in both business and tourism are expected. A momentum for the development of business jet class supersonic civil transport has been increasing significantly since 2010. The International Civil Aviation Organization (ICAO) began deliberation of international standards for sonic booms which causes a serious noise problem. To establish a firm footing in the design and production of next generation supersonic civil transport developed through international cooperation, JAXA will demonstrate the high technical potential of aircraft technology owned by Japan through presentation of a unique airframe concept and verification of specialty technologies.”

JAXA proposes the concept image of small supersonic civil transport. The image and the specification are indicated in Fig. 4.1 and Table. 4.1 respectively. Cruise speed is Mach 1.6, number of passengers is 36 to 50, take-off weight is 70 ton, and cruising distance is over 3,500 [NM] (about 6,300 [km]).

Aerodynamic model and engine model under a clean configuration are provided from JAXA. They are given in a tabular data form for altitude and Mach number as follows.

Fig.4.1 An image of JAXA SST

Table.4.1 Specification of JAXA SST

Length	47.8 [m]
Take-off weight	70 [ton]
Wing area	175 [m^2]
Cruise speed	M1.6
Range	$\geq 3,500$ [NM]
Passengers	36 to 50

Aerodynamic model

$$
\begin{aligned}
H_{aero} &= [0\ 10\ 20\ 30\ 40\ 50\ 60] \times 10^3\ [\mathrm{ft}] \\
M_{aero} &= [0\ 0.2\ 0.3\ 0.6\ 0.8\ 0.95\ 1.05\ 1.2\ 1.4\ 1.6\ 1.8\ 2.0\ 2.3] \\
k &= k(M_{aero}) \\
C_{\mathrm{dn}} &= C_{\mathrm{dn}}(M_{aero}) \\
C_{\mathrm{ln}} &= C_{\mathrm{ln}}(M_{aero}) \\
C_{\mathrm{df}} &= C_{\mathrm{df}}(H_{aero}, M_{aero})
\end{aligned}
$$

Drag coefficient is calculated by the following formula.

$$C_D = C_{\mathrm{dn}} + C_{\mathrm{df}} + k(C_L - C_{ln})^2 \tag{4.1}$$

Engine model

$$H_{engine} = [0\ 10\ 20\ 30\ 40\ 45\ 50\ 60] \times 10^3\ [\mathrm{ft}]$$
$$M_{engine} = [0\ 0.3\ 0.6\ 0.9\ 1.2\ 1.4\ 1.6\ 1.8]$$
$$T_{\max} = T_{\max}(H_{engine}, M_{engine})$$
$$c = c(H_{engine}, M_{engine})$$
$$EI = EI(H_{engine}, M_{engine})$$

Flight envelop is defined by the following operational limitations.

Altitude	:	$0 \leq H\ [\mathrm{ft}] \leq 60,000$
Mach number	:	$M \leq 1.8$
Lift coefficient	:	$C_L \leq C_{L_{\max}} = 0.754$
Dynamic pressure	:	$V_{EAS} \leq 200\ [\mathrm{m/s}]$

Altitude and Mach number grids are defined in the aerodynamic model and the engine model respectively. In the aerodynamic model, only C_{df} is dependent on altitude and Mach number and other parameters are only dependent on Mach number. Characteristic parameters of the model are plotted in the flight envelop. Parameters of aerodynamic and engine model provided from JAXA are illustrated in Figs. 4.2 to 4.7. Flight performance variables which are calculated from these parameters are presented in Fig. 4.8 to 4.13. The ranges of lift coefficient and drag coefficient are from 0.2 to 0.7 and from 0.02 to 0.16 respectively. Lift to drag ratio takes maximum value of 12 at the point $(M, H) = (0.8, 20,000\ [\mathrm{ft}])$ in the subsonic region, and takes over 8 in the supersonic region. Energy rate which is the same as excess power has an area where negative value is taken due to insufficient thrust as depicted by deep blue area in Fig. 4.11. This value is calculated by take-off mass; therefore, the negative value area narrows as the mass decreases. Actually, the mass of aircraft is reduced in the climb phase and the aircraft has the maximum thrust enough to cruise from $50,000$ [ft] to $60,000$ [ft] at Mach 1.8. Fig. 4.12 shows the fuel flow required for horizontal steady flight. Fuel flow μ [kg/s] is defined by the product of thrust specific fuel consumption c [kg/N/s] and thrust T [N] denoted by Eq. (4.2).

$$\mu = cT \tag{4.2}$$

Fuel flow takes the value of 1.2 and 2.1 in the subsonic region and supersonic region respectively. Note that thrust is equal to drag by the assumption of horizontal steady flight. Aircraft steady performance is generally expressed by specific range (SR [m/kg]) which is flight distance per unit mass of fuel consumption. SR is calculated by Eq.(4.3).

$$SR = \frac{V_{TAS}}{\mu} = \frac{V_{TAS}}{cT} \tag{4.3}$$

It's obvious from Fig. 4.13 that two points which take the similar maximum values exist in both subsonic and supersonic region. These points are equivalent to the static optimal cruise points. According to the researchers in JAXA, this static characteristic of the model is worth remarking because the design for the aerodynamic model and the engine model is not so strongly connected each other and these two maximum SR values have been obtained by coincidence. Conversely, it can be mentioned that such a characteristic shows an evidence that each model has been appropriately designed so as to satisfy the actual operation requirements such as cruising at a subsonic speed to avoid the noise problem caused by sonic booms above the land.

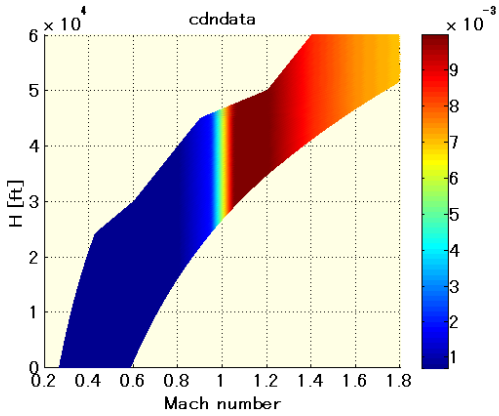

Fig.4.2 C_{dn} data

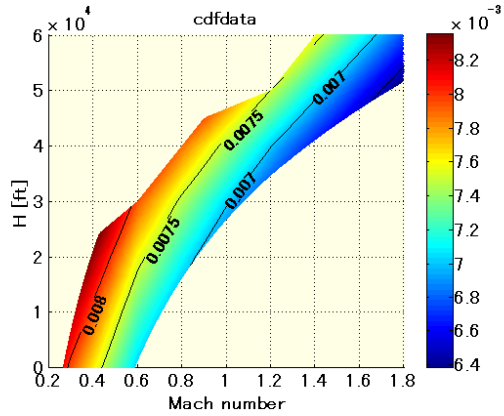

Fig.4.3 C_{df} data

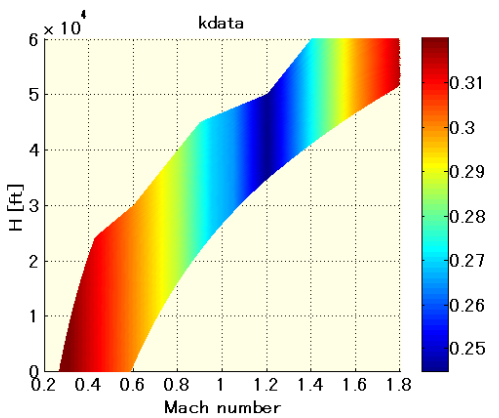

Fig.4.4 k data

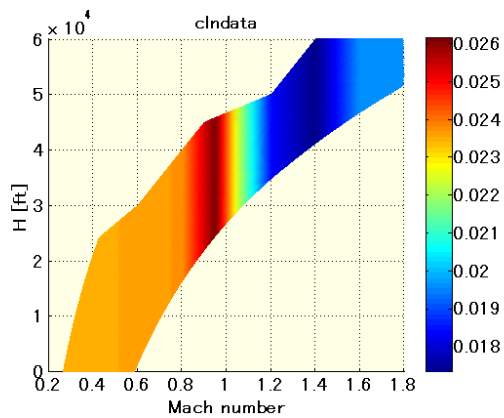

Fig.4.5 C_{ln} data

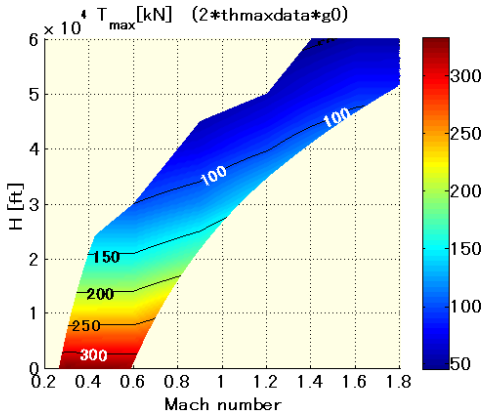

Fig.4.6 Maximum thrust data

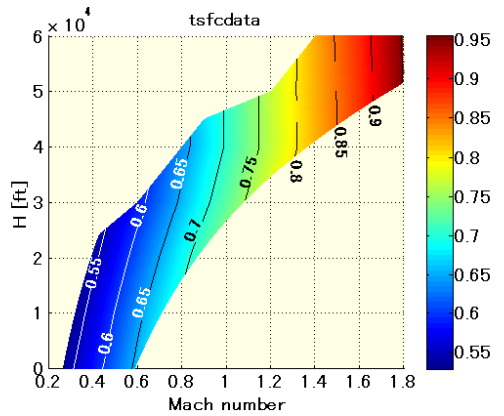

Fig.4.7 Thrust specific fuel consumption data

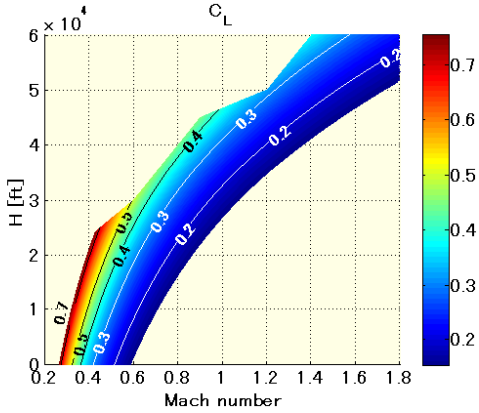

Fig.4.8 Lift coefficient

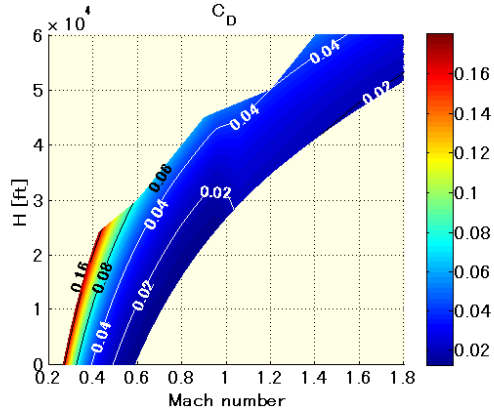

Fig.4.9 Drag coefficient

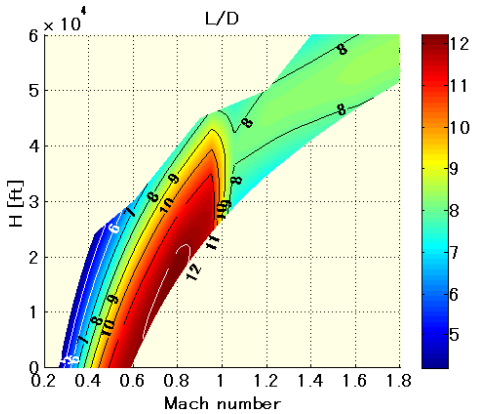

Fig.4.10 Lfit to drag ratio

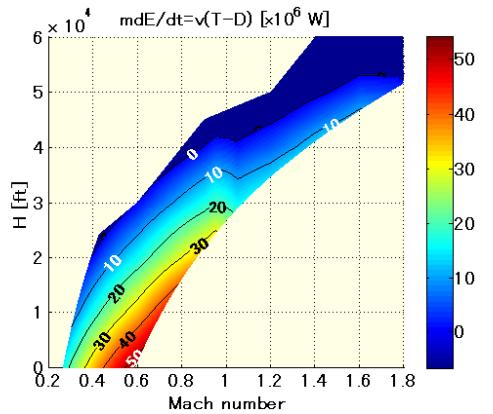

Fig.4.11 Excess power

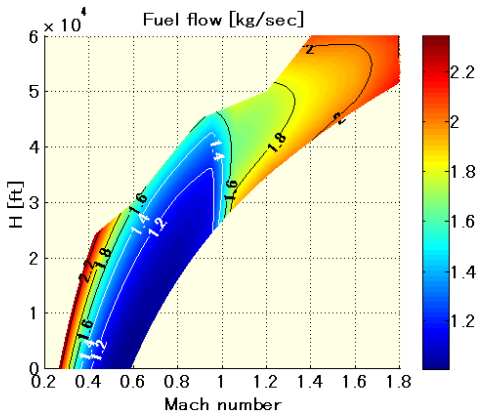

Fig.4.12 Fuel flow

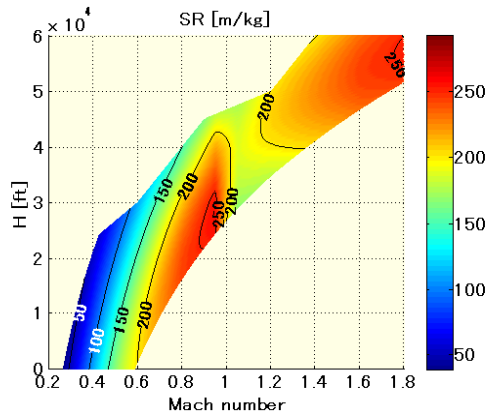

Fig.4.13 Specific range

4.3 Flight trajectory optimization by dynamic programming

The optimal flight trajectory is designed for the JAXA's supersonic transport by using the aerodynamic and engine model introduced in the former section. An objective function defined by fuel consumption and flight time is used to quantify the flight performance and to reveal the economically-efficient flight trajectories.

4.3.1 Statement of trajectory optimization problem

A time based optimal control problem is generally stated as getting a time history of optimal control input which minimizes an objective function.

Optimal control problem

$$\text{Minimize} \quad J = \int_{t_0}^{t_f} \mu(t)dt + \Phi(\boldsymbol{x}(t_f), t_f) \tag{4.4}$$

$$\text{subject to} \quad \psi_0(\boldsymbol{x}(t_0)) = 0 \tag{4.5}$$

$$\psi_f(\boldsymbol{x}(t_f)) = 0 \tag{4.6}$$

$$C_{eq}(\boldsymbol{x}(t), \boldsymbol{u}(t), t) = 0 \tag{4.7}$$

$$C_{ineq}(\boldsymbol{x}(t), \boldsymbol{u}(t), t) \leq 0 \tag{4.8}$$

Objective function

The economical efficiency is considered as the most important factor to realize the next generation supersonic civil transport. For this reason, the objective function is defined as a trade-off between fuel consumption and flight time as following formula.

$$J = \int_{t_0}^{t_f} (\mu + a)\, dt = \int_{t_0}^{t_f} (\mu)\, dt + a \int_{t_0}^{t_f} dt \tag{4.9}$$

The first term presents fuel consumption. The second term presented with a time adjustment parameter a means flight time from an initial point to a terminal point, where the time adjustment parameter has been introduced to evaluate the flight time equivalent to fuel consumption.

Equation of motion and kinematic model

Motion of aircraft is expressed by three degrees of freedom (3 DOF) equation with point mass approximation. Dynamics of velocity vector angle, that are flight path climb angle rate and flight path heading angle

rate, are neglected because they are assumed to give little influence on the objective function.

$$\frac{d\theta}{dt} = \frac{1}{(R_0+H)\cos\phi} V_{TAS}\cos\gamma\sin\psi \tag{4.10}$$

$$\frac{d\phi}{dt} = \frac{1}{R_0+H} V_{TAS}\cos\gamma\cos\psi \tag{4.11}$$

$$\frac{dH}{dt} = V_{TAS}\sin\gamma \tag{4.12}$$

$$m\frac{dV_{TAS}}{dt} = T - D - mg_0\sin\gamma \tag{4.13}$$

Two state variables, latitude ϕ and longitude θ are transformed to downrange angle ξ and lateral deviation angles η by a coordinate transformation. As illustrated in Fig. 4.14, the Earth-Centered-Earth-Fixed (ECEF) coordinate system is defined. Z axis is set to the north pole. X-Y surface indicates the equational plane. X axis and Y axis are set to the first meridian and 90 degrees east longitude respectively. The unit vectors $\boldsymbol{r_0}$ and $\boldsymbol{r_f}$ are defined with regard to the initial point $(\phi_0,\ \theta_0)$ and final point $(\phi_f,\ \theta_f)$.

$$\boldsymbol{r_0} = \begin{pmatrix} \cos\phi_0\cos\theta_0 \\ \cos\phi_0\sin\theta_0 \\ \sin\phi_0 \end{pmatrix}, \quad \boldsymbol{r_f} = \begin{pmatrix} \cos\phi_f\cos\theta_f \\ \cos\phi_f\sin\theta_f \\ \sin\phi_f \end{pmatrix}$$

The angle ξ between vectors $\boldsymbol{r_0}$ and $\boldsymbol{r_f}$, i.e. downrange angle is given as follows.

$$\xi = \cos^{-1}(\boldsymbol{r_0}^T\boldsymbol{r_f}) \tag{4.14}$$

Great-circle route, the shortest path between two arbitrary points on the Earth, is equivalent to this downrange. If the lateral deviation must be considered in the kinematic model, an unit vector $\boldsymbol{r_2}$ which is perpendicular to the great-circle plane determined by $\boldsymbol{r_0}$ and $\boldsymbol{r_f}$ is defined. Additionally, an unit vector $\boldsymbol{r_1}$ is defined on the great-circle route between $\boldsymbol{r_0}$ and $\boldsymbol{r_f}$. These vectors are expressed below.

$$\boldsymbol{r_2} = \frac{\boldsymbol{r_0}\times\boldsymbol{r_f}}{|\boldsymbol{r_0}\times\boldsymbol{r_f}|}, \quad \boldsymbol{r_1} = \frac{\boldsymbol{r_2}\times\boldsymbol{r_0}}{|\boldsymbol{r_2}\times\boldsymbol{r_0}|}$$

The unit vectors $\boldsymbol{r_0}$, $\boldsymbol{r_1}$ and $\boldsymbol{r_2}$ are mutually orthogonal. A series of points which divide the great-circle route into m segments is denoted with a combination of $\boldsymbol{r_0}$ and $\boldsymbol{r_1}$.

$$\boldsymbol{r}_{i0} = \cos\left(\frac{\xi_0 i}{m+1}\right)\boldsymbol{r_0} + \sin\left(\frac{\xi_0 i}{m+1}\right)\boldsymbol{r_1} \tag{4.15}$$

Furthermore, an arbitrary position perpendicular to the great-circle plane is given with the lateral deviation angle η from the great-circle route.

$$\boldsymbol{r_i} = \cos\eta_i\left\{\cos\left(\frac{\xi_0 i}{m+1}\right)\boldsymbol{r_0} + \sin\left(\frac{\xi_0 i}{m+1}\right)\boldsymbol{r_1}\right\} + \sin\eta_i\boldsymbol{r_2} \tag{4.16}$$

An arbitrary waypoint can be described with those angle ξ and η. On the other hand, an arbitrary point on the Earth is presented in the ECEF coordinate system.

$$\boldsymbol{r_i} = \begin{pmatrix} \cos\phi_i \cos\theta_i \\ \cos\phi_i \sin\theta_i \\ \sin\phi_i \end{pmatrix} \tag{4.17}$$

From these formulae, $(\phi,\ \theta)$ and $(\xi,\ \eta)$ can be transformed each other. This chapter only focuses on the longitudinal trajectory; however, the lateral deviation can be considered easily by adding the crossrange angle η if the effect of wind on the lateral flight path must be included in the trajectory optimization calculation.

In the optimal trajectory design by dynamic programming, an independent variable which transits monotonously with time is essential in applying the principle of optimality. In this chapter, flight distance along the great-circle route is set as the independent variable. The flight distance is defined by the distance between an aircraft and the center of the Earth $(R_0 + H)$ and the downrange angle ξ.

$$x = (R_0 + H)\xi \tag{4.18}$$

Two state variables V_{TAS} and H are discretized into grid points; thereafter, the combinatorial optimization can be applied to those grid points along the independent variable x.

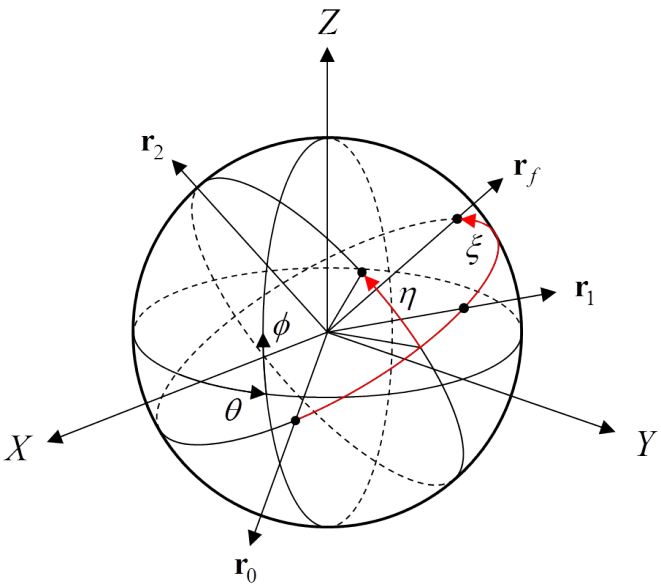

Fig.4.14 Definition of the great-circle route and downrange

Optimal trajectory design condition

Aircraft operational limitations are given by the following inequality constraints on the state variables and control variables.

$$x_{\min} \leq x \leq x_{\max} \tag{4.19}$$

$$H_{\min} \leq H \leq H_{\max} \tag{4.20}$$

$$V_{EAS,\min} \leq V_{EAS} \leq V_{EAS,\max} \tag{4.21}$$

$$M \leq M_{\max} \tag{4.22}$$

$$C_L \leq C_{L,\max} \tag{4.23}$$

$$T_{\min} \leq T \leq T_{\max} \tag{4.24}$$

Dynamic pressure, Mach number and lift coefficient are constrained by each limitation as Eqs. (4.21) to (4.23). Flight envelop is defined by those equations and Eq. (4.20). Here, equivalent airspeed V_{EAS} is expressed by air density ρ and the standard air density ρ_0 at sea level.

$$V_{EAS} = V_{TAS}\sqrt{\frac{\rho}{\rho_0}} \tag{4.25}$$

Initial and final boundary conditions on state variables, altitude and equivalent airspeed are given.

$$H(x_0) = H_0 \tag{4.26}$$

$$V_{EAS}(x_0) = V_{EAS,0} \tag{4.27}$$

$$H(x_f) = H_f \tag{4.28}$$

$$V_{EAS}(x_f) = V_{EAS,f} \tag{4.29}$$

As mentioned above, the optimal control problem is defined to derive optimal control inputs γ and T which minimize the performance index denoted by Eq. (4.9) under equality and inequality constraints and boundary conditions. The solution is obtained by solving the combinatorial optimization problem for the transitions between the quantized grid points. The principle of optimality which is the core concept of DP algorithm is expressed as Eq. (4.30). The optimal value of performance index is given as a function of state variables H, V_{EAS} and independent variable x; thereby, is expressed as $J_{opt}(H, V_{EAS}, x)$. The subscript "EAS" is omitted in the following formula for the simplicity.

$$J_{opt}(H_{i_{k+1}}, V_{j_{k+1}}, x_{k+1}) = \min_{\gamma,\ T}\left\{J_{opt}(H_{i_k}, V_{j_k}, x_k) + \Delta J(H_{i_k} \to H_{i_{k+1}}, V_{j_k} \to V_{j_{k+1}}, x_k \to x_{k+1})\right\} \tag{4.30}$$

$$\Delta J = [a + \mu]_{x_k}^{x_{k+1}}\,\Delta t \tag{4.31}$$

Numerical conditions

Trajectory optimization is implemented by reference to the distance between two cities Tokyo (Haneda) and San Francisco. Table 4.2 shows the numerical conditions used in the optimal trajectory design.

Table.4.2 Numerical design condition

Condition items	Condition settings		
Flight route	Tokyo (Haneda) -San Francisco		
Downrange	$x_{\min} \leq x$ [m] $\leq x_{\max}$		
Altitude	$H_{\min} \leq H$ [m] $\leq H_{\max}$		
Equivalent airspeed	$V_{\min} \leq V_{EAS}$ [m/s] $\leq V_{\max}$		
Downrange resolution	$x_{\min} = 0,$	$x_{\max} = 8,408$ [km],	$\Delta x = 42,000$ [m]
Altitude resolution	$H_{\min} = 0,$	$H_{\max} = 18,000$ [m],	$\Delta H = 200$ [m]
Equivalent airspeed resolution	$V_{\min} = 80,$	$V_{\max} = 200$ [m/s],	$\Delta V = 2$ [m/s]

4.3.2 Purposes of analysis

The application problem is solved by a combinatorial optimization algorithm of DP in this chapter. The main purposes of the trajectory optimization analysis presented in the next section are the following.

(1) To demonstrate the advantages of dynamic programming as a combinatorial optimization method by applying it to a practical application problem.

(2) To investigate a maximum flight performance and to compare it with that of static trajectory designed by JAXA research group. As a result of analysis, the fuel minimum trajectory obtained by setting the time adjustment parameter as zero has become a subsonic flight. By changing the parameter by 0.1, a supersonic flight appeared at $a = 0.2$. Fuel consumption and flight time of the case are compared those values of JAXA reference trajectory.

(3) To investigate the feasibility of JAXA supersonic civil transport model by comparing its maximized flight performance with that of conventional subsonic jet passenger aircraft. Boeing 737-700 which has a similar take-off weight is selected as a conventional aircraft.

4.4 Analysis results

4.4.1 Fuel minimal trajectory of JAXA SST

At first, the flight performance of a fuel minimal trajectory is examined by setting the time adjustment parameter a in the objective function as zero. Figs. 4.15 to 4.20 show a result of the optimal trajectories which give minimum fuel consumption. Horizontal axis indicates flight distance except for Fig. 4.15. Optimal trajectories are shown in blue lines with the JAXA reference trajectories (red lines) designed analytically by a static assumption, which was provided by the JAXA research group. The SR value is shown by colored

contour line in Fig. 4.15. The dotted magenta line represents the flight envelop at the take-off weight. Relationship between Mach number and altitude is plotted on the SR diagram in the same figure. The fuel minimal trajectory shows that the aircraft climbs by maximum dynamic pressure in the subsonic region and cruises from $30,000$ [ft] to $35,000$ [ft] at Mach 0.95 along the contour line of $SR = 250$ [m/kg]. High lift to drag ratio can be maintained as 11 to 12. Available thrust is reached about twice as much as the required thrust due to lower altitude at subsonic speeds. For instance, the maximum thrust takes 120 [kN] at $x = 1000$[NM]. This value corresponds to the maximum thrust at the point of $M = 0.95$ and $H = 31,000$[ft] as can be seen from Fig. 4.6. Results of fuel consumption and flight time are shown in Table 4.3.

Table.4.3 Analysis results for minimization of fuel consumption $(a = 0)$

Flight time	Fuel consumption
8 hour 38 minutes 53 seconds (31,133 seconds)	26,320 [kg]

■ SST fuel minimal trajectory (subsonic cruise)

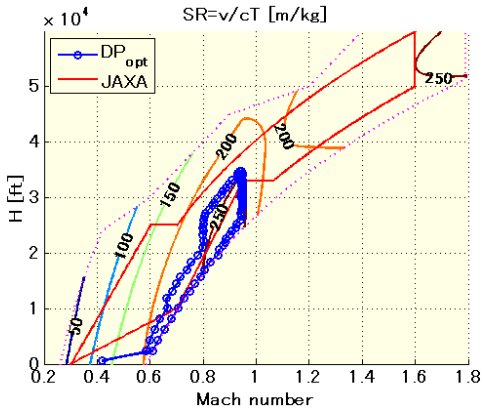

Fig.4.15 Mach number - Altitude,

(SST, $a = 0$)

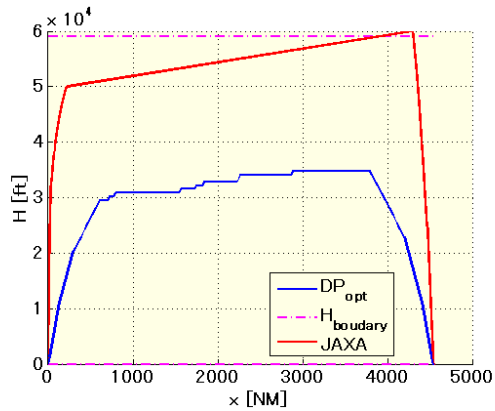

Fig.4.16 Altitude,

(SST, $a = 0$)

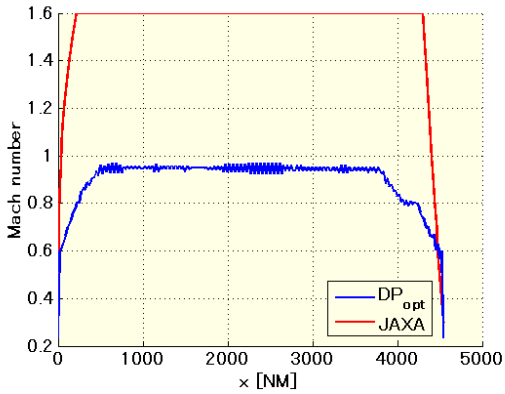

Fig.4.17 Mach number,

(SST, $a = 0$)

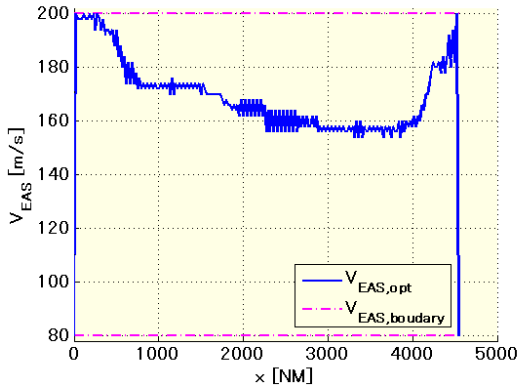

Fig.4.18 Equivalent airspeed,

(SST, $a = 0$)

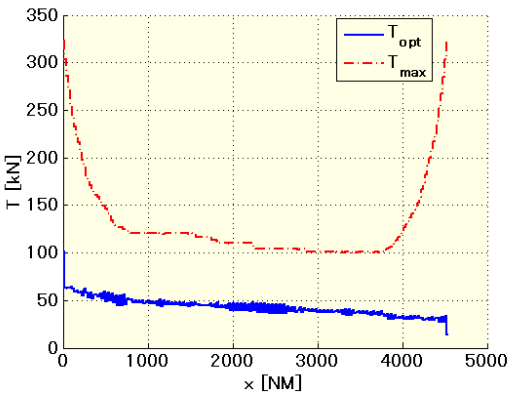

Fig.4.19 Thrust,

(SST, $a = 0$)

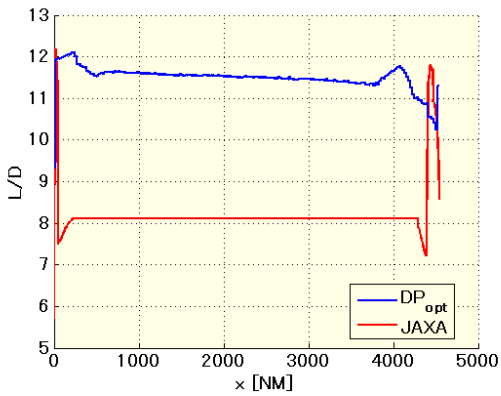

Fig.4.20 Lift to drag ratio,

(SST, $a = 0$)

4.4.2 Trade-off between fuel consumption and flight time

Since the fuel minimum optimization results in subsonic cruise flight, it is necessary to consider flight time in the objective function with the time adjustment parameter a. This is so-called cost index which is often used in making a flight plan of jet passenger aircraft. Optimal trajectories obtained by a trade-off between fuel consumption and flight time are shown in Figs. 4.21 to 4.26. It can be seen from Fig. 4.21 that SST climbs to 13,700 [m] with maximum dynamic pressure $V_{EAS} = 200$ [m/s] after breaking the sound barrier with high SR value in the subsonic region. SST cruises from 16,500 [m] to 18,000 [m] maintaining Mach number as 1.6 with decreasing the dynamic pressure to $V_{EAS} = 150$ [m/s]. Required thrust mostly takes maximum value in the cruise phase. Lift to drag ratio takes about 12 and 8 in the subsonic region and supersonic region respectively. Table 4.4 shows that the optimal trajectory enables the SST to save the fuel consumption by 593 [kg] compared to the reference trajectory designed by the JAXA research group. Fig. 4.27 shows the relationship between fuel consumption and flight time obtained by changing the parameter a from 0 to 1.8 by 0.1. The solutions are separated into two groups. Flight time takes 30,000 [s] in the subsonic cruise group, and takes about 20,000 [s] in the supersonic cruise group; however, significant difference cannot be seen in the fuel consumption. This phenomenon is reasonable because the SR which determines the cruise performance takes similar maximum values in both subsonic and supersonic region.

Table.4.4 Analysis results for trade-off between fuel consumption and flight time ($a = 0.2$)

	Flight time	Fuel consumption
Dynamic programming	5 hour 18 minutes 49 seconds	26,980
JAXA reference trajectory	5 hour 18 minutes 36 seconds	27,573

■ SST fuel-time optimal trajectory (supersonic cruise)

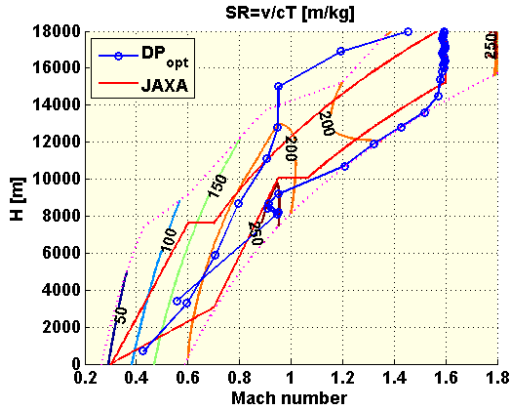

Fig.4.21 Mach number - Altitude,

(SST, $a = 0.2$)

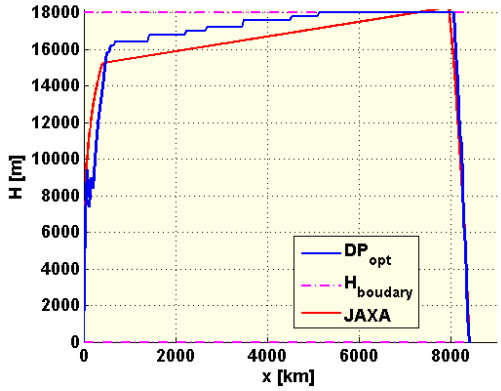

Fig.4.22 Altitude,

(SST, $a = 0.2$)

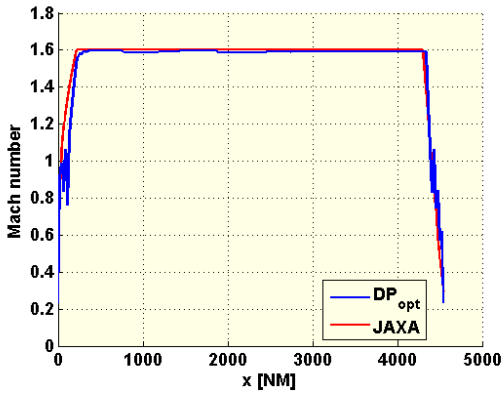

Fig.4.23 Mach number,

(SST, $a = 0.2$)

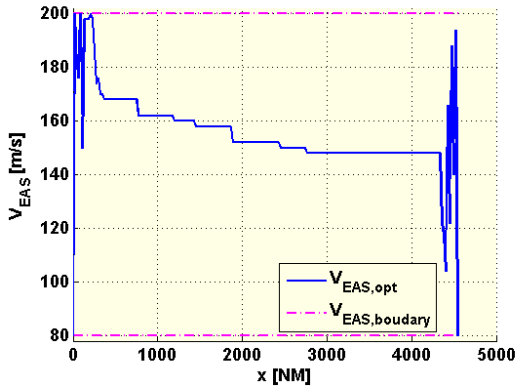

Fig.4.24 Equivalent airspeed,

(SST, $a = 0.2$)

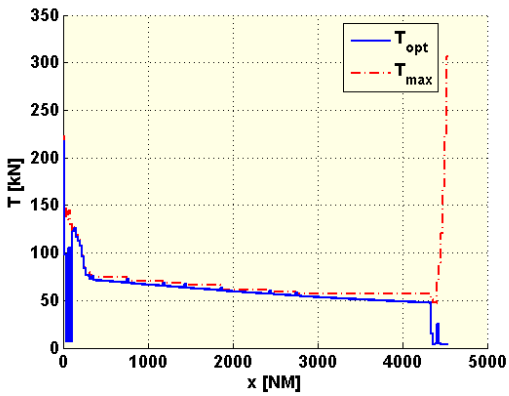

Fig.4.25 Thrust,

(SST, $a = 0.2$)

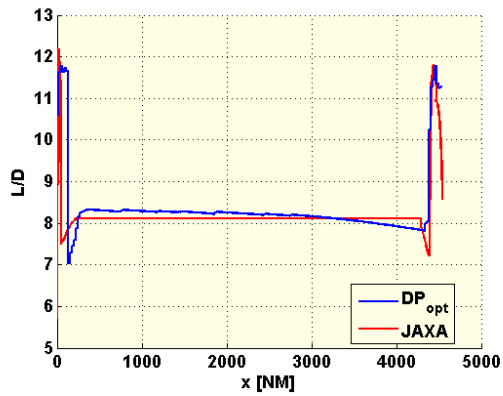

Fig.4.26 Lift to drag ratio,

(SST, $a = 0.2$)

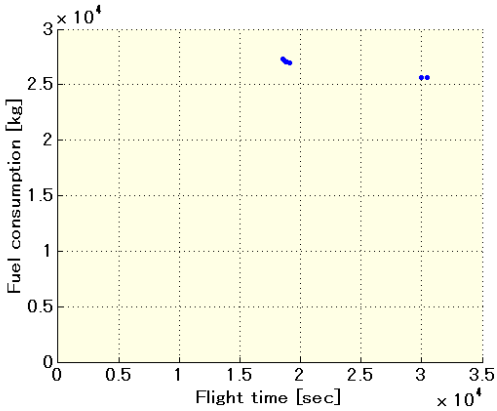

Fig.4.27 Relationship of flight time and fuel consumption for $a = 0,\ 0.1,\ 0.2, \cdots, 1.8$

4.4.3 Comparison to a conventional passenger aircraft

In evaluating the feasibility of SST, comparison of economical efficiency to a conventional passenger aircraft is necessary and is considered to provide worthful findings. This section discusses characteristics of JAXA's SST model by comparing its operational performance with that of a conventional passenger aircraft which has the similar take-off weight as the JAXA's SST airframe. Boeing 737-700 is selected as a typical conventional passenger aircraft. Its take-off weight and wing area are 60×10^3 [kg] and $S = 124.65$ [m^2] respectively. Optimization calculation is implemented for the same range to compare fuel consumption and flight time fairly. Optimal trajectory results of the conventional aircraft are shown in Figs. 4.28 to 4.33. The obtained optimal cruise altitude is 42,650 [ft] which is set as the maximum operating altitude. Optimal CAS decreases in accordance with the change of aircraft mass. This passenger aircraft has comparatively higher performance in the subsonic region. The maximum SR and lift to drag ratio can be reached about 400 [m/kg] and 15.8 respectively. It is worth mentioning that the flight time of JAXA SST can be halved while the fuel consumption is increased by only 50% compared to the conventional passenger aircraft. The numerical result is shown in Table. 4.5.

Table.4.5 Analysis results for conventional passenger aircraft, fuel minimum $(a = 0)$

Flight time	Fuel consumption
10 hour 29 minutes 12 seconds (37,752 seconds)	18,472 [kg]

■ Fuel minimal trajectory of B737-700

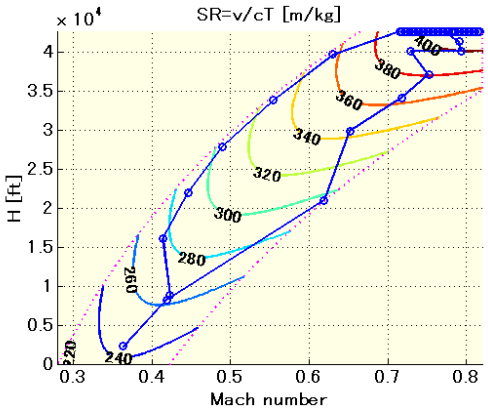

Fig.4.28 Mach number - Altitude,

(B737-700, $a = 0$)

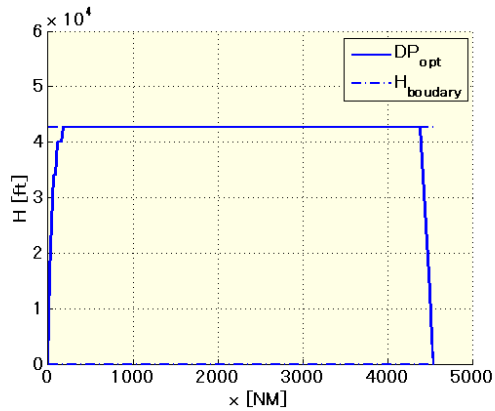

Fig.4.29 Altitude,

(B737-700, $a = 0$)

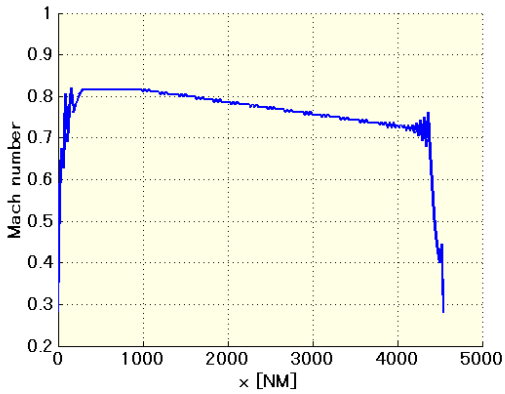

Fig.4.30 Mach number,

(B737-700, $a = 0$)

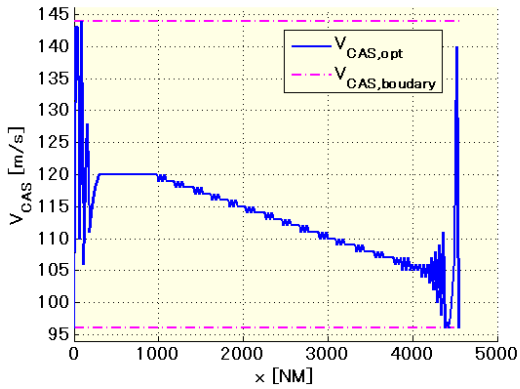

Fig.4.31 Equivalent airspeed,

(B737-700, $a = 0$)

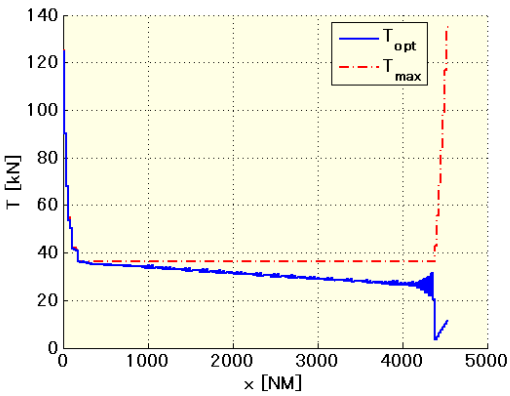

Fig.4.32 Thrust,

(B737-700, $a = 0$)

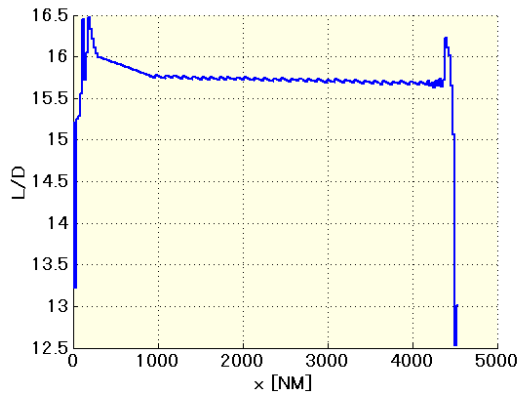

Fig.4.33 Lift to drag ratio,

(B737-700, $a = 0$)

4.5 Summary

Dynamic programming was applied to an optimal trajectory design problem with the aim of revealing the feasibility of JAXA's next generation supersonic civil transport. The developed tool is capable to produce an optimal trajectory for all flight phases from climb to descent continuously and to consider trade-off between fuel consumption and flight time by changing a time adjustment parameter in the objective function. The tool led a result that the flight which includes a supersonic cruise can save flight time by 3 hours 19 minutes with an additional fuel consumption of 680 [kg] by comparing to a subsonic flight. Additionally, usefulness of the developed tool has been demonstrated by getting a result that the aircraft can save the fuel consumption by 570 [kg] compared to a reference trajectory designed by JAXA SST research group. Moreover, it has been suggested that the JAXA's SST concept model has sufficient possibility to be realized as an economical future civil air transport because its operational efficiency has been quantitatively revealed by showing that the flight time can be halved with additional 50 % of fuel consumption in the comparison to a conventional subsonic passenger aircraft. It can be stated that the practical application not only to a SST model but to a subsonic jet aircraft introduced in this chapter is one of the most favorable problems in the point of utilization of dynamic programming because an assumption such that a flight trajectory can be approximated as a series of quantized grid points of state variables is reasonable due to slower motion of passenger aircraft. The performance model is given by a tabular data form not by a simple mathematic model and the various constraints are assigned by considering actual operational limitations; however, an optimal flight trajectory can be easily gained by utilizing many powerful advantages of dynamic programming. If another optimization method were used, it would be impossible to obtain the optimal trajectory by using the same model and constraints. If possible, it would be extremely difficult to complete the required analysis within a short duration because many adjustments or trial-and-error processes would be required to avoid the disadvantages of the method. Additionally, this application problem includes few state variables. The path angle γ and thrust T selected as control variables enable the state transition of two state variables, altitude H and velocity V. The "menace of the expanding grid" does not arise in this case because the number of control variables agrees with that of state variables. Besides, the trajectory optimization calculation was applied not to multiple aircraft problem but to a single aircraft problem. Reduction of computational time is desirable in the case study; though, it is not mandatory in this case. The "curse of dimensionality" is not the critical issue in this application problem. Therefore, it can be stated that dynamic programming trajectory optimization has greatly exerted its advantages without struggling against the difficulties arising from the "curse of dimensionality" or "menace of the expanding grid". It is additionally mentioned that even if one more variable is added respectively to the state variable and the control variable to consider a lateral path change from the great-circle route, the optimization calculation can complete in a realistic time by using the same combinatorial optimization algorithm of dynamic programming.

Chapter. 5

Quantitative Operational Flight Efficiency Analysis of Passenger Aircraft Scheduled Flight

5.1 Introduction

Today's busy air transportation system strongly demands not only safe flight but also greater efficiency. Realization of more efficient operations while increasing capacity is expected to be achieved by introducing new CNS/ATM technologies. Under the NextGen program in the United States and SESAR in Europe, many research projects are exploring innovations and many research papers have been published. In Japan, CARATS (Collaborative Actions for Renovation of Air Traffic Systems) [20] has been defined by the government as a roadmap for developing Japan's future air transportation system, and universities are encouraged to participate in its research. This study is being conducted as one of the collaborative research projects between universities and research institutions to support the program.

In this chapter, current air traffic efficiency is analyzed to evaluate the potential benefits of CARATS. The analysis is based on the flight trajectories of commercial airliners operating in Japan's most heavily congested airspace around Tokyo International Airport. Trajectory information for each flight obtained by an experimental Mode S secondary surveillance radar (SSR Mode S) developed by the Electronic Navigation Research Institute (ENRI) is combined with meteorological data and aircraft performance information to estimate each flight's fuel consumption. The reconstructed flight performance represented by fuel consumption and fight time is then compared with that of an optimal trajectory gained by dynamic programming assuming the same meteorological conditions and aircraft performance data. This analysis estimates the maximum benefit achievable for the flights or the potential benefit which could be realized by an ideal air traffic management system. The conflicts among the objective aircraft or caused by other traffic are not considered in

the optimization calculation; thereby, each flight is optimized individually. To reveal a statistic characteristics of arrival flight efficiency, multiple aircraft should be analyzed. Consequently, a large-scale optimization analysis must be carried out by using dynamic programming. A novel method which greatly contributes to proceed the large-scale analysis efficiently by drastically reducing the amount of calculation is proposed. The main purpose of this chapter is demonstrating that a newly proposed method has a remarkable capability of solving a large-scale optimization problem which plays a significant role to provide worthwhile findings in evaluating current Japanese airspace and in considering more ideal air traffic management system in Japan.

In section 5.2, the algorithm of the method is introduced. Computational capability of the method is demonstrated by comparing a calculation time taken by normal DP algorithm. Section 5.3 explains the analytical method to evaluate the operational flight efficiency. Most of the details can be found in the published references [21, 22, 23, 24]. In section 5.5, the results obtained using one day of SSR data for arrival flights to Tokyo International Airport are discussed. The analysis is limited to arrivals largely by the coverage of the radar, but flight time and fuel efficiency are most influenced by the position of the TOD (Top of Descent) and flight speed during the descent. Although only three types of aircraft are analyzed, these cover about 60 % of all inbound flights. The analysis reveals stochastic characteristics of the air traffic efficiency.

5.2 Gradient based approach for the “Curse of dimensionality”

5.2.1 Moving Search space Dynamic Programming (MS-DP) method

Moving Search space Dynamic Programming method (MS-DP) which was proposed as a fast computation technique by the author’s research group was used in the application of DP to the passenger aircraft’s fuel minimal trajectory design problem [26]. In this method, the optimal solution is renewed to the direction of smaller Optimal Return Function (ORF) value; thereby, the concept of this method is based on gradient based method which is implemented various optimization tools.

The algorithm of MS-DP method is explained in the following.

Algorithm of MS-DP

(1) Partial search space is set around the initial guess as depicted by the space defined by black lines in Fig. 5.1. The full search space used in the normal DP calculation is presented by the blue box.

(2) The optimal solution is searched by the normal DP algorithm, i.e. the combinatorial optimization algorithm, in this partial search space. If the grid is set appropriately, a solution which has a better ORF value than the initial guess is obtained in the space. The improved solution is illustrated by a red line in Fig. 5.2.

(3) The calculation grid is newly set around the obtained solution as illustrated in Fig. 5.3. The name such as “Moving Search space” is originated in this search space shifting. These processes are continued until the ORF value is converged to the same value.

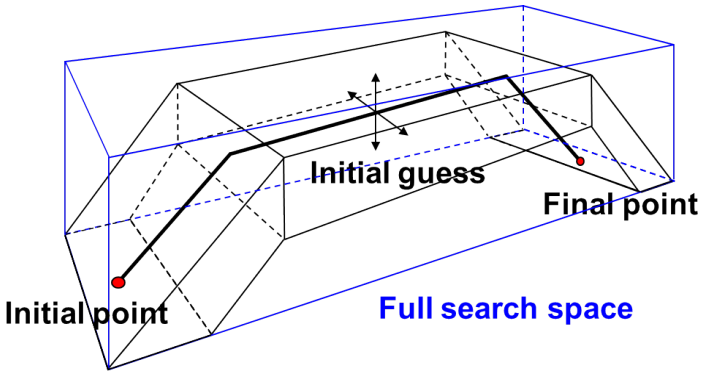

Fig.5.1 Initial guess in the partial search space

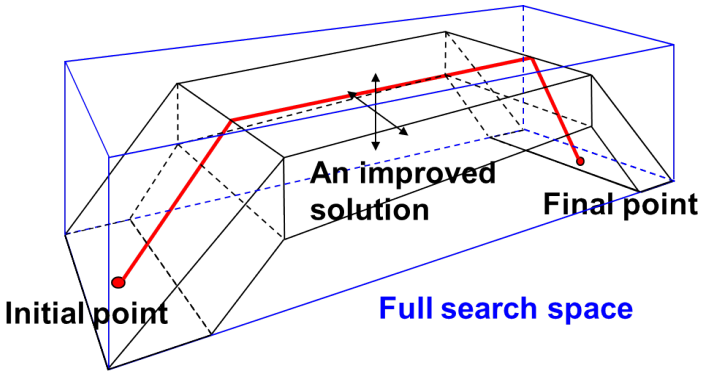

Fig.5.2 An improved solution in the partial search space

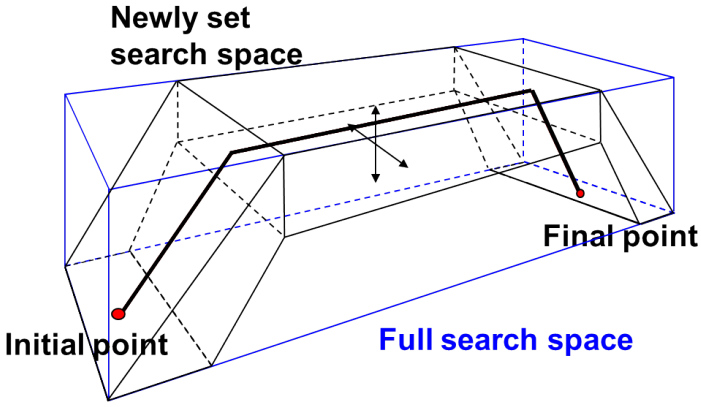

Fig.5.3 Newly set partial search space

5.2.2 Computational capability of MS-DP method

The method was applied to a passenger aircraft's fuel minimal trajectory design problem [27]. In this example, two state variables altitude H and calibrated airspeed V_{CAS} were optimized; consequently, this problem constitutes a longitudinal trajectory optimization problem. Two control variables, flight path climb angle γ

and thrust T were set to realize the transition of those two state variables. The second drawback of DP, the "Menace of the expanding grid" does not arise because the number of control variable is enough to connect two quantized grid points. No wind condition was assumed. The flight distance was set about 900 [km] by reference to the distance between two major cities in Japan, Tokyo (Haneda) and Fukuoka along the great-circle route. The detailed calculation conditions can be found in the conference paper [27].

Fig. 5.4 shows the optimal trajectory of altitude, calibrated airspeed and true airspeed obtained by searching for the full space. Fig. 5.5 is corresponding optimal trajectories obtained by the MS-DP method. An initial guess was set to constant altitude of 3000 [m] and velocity of 120 [m/s] depicted in the blue lines. The number of grid points to be searched is set as 21×11. The optimal trajectory presented with red lines could be obtained by 18 iterations via green trajectories in the convergence process of MS-DP calculation. From this result, it was revealed that exactly the same global optimum as the full search case could be gained by MS-DP method under the no wind condition which introduces the monotonous change of the ORF value.

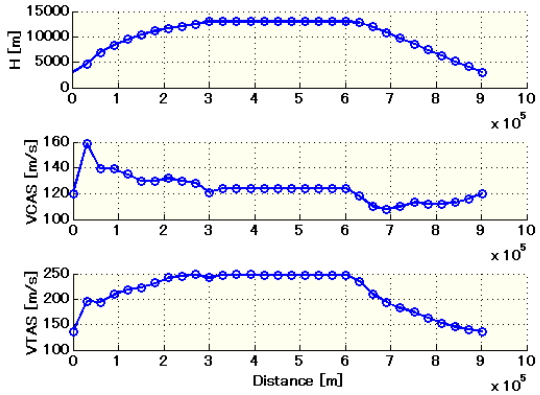

Fig.5.4 Optimal trajectory with no wind (Full search)

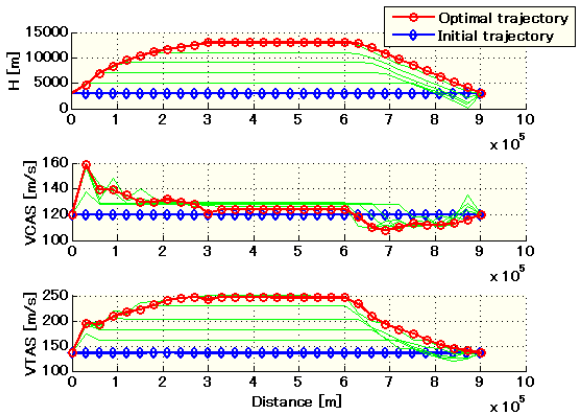

Fig.5.5 Optimal trajectory with no wind (MS-DP)

Since the number of iterations is 18, the reduction rate of total amount of calculation is given as follows.

$$\frac{(21 \times 11)^2 \times 31 \times 18}{(101 \times 61)^2 \times 31} \times 100 = 2.5\% \tag{5.1}$$

On the other hand, the computational time is reduced to 2.7 % as shown in Table 5.1. These almost identical values indicate that the reduction of computational time is reasonable because the reduction of calculation time is proportional to the reduction of amount of computation which is determined by the number of grid points and the number of iteration.

This method only guarantees the local optimum; however, from an application result, it was revealed that the MS-DP method is capable to give a global optimum if the model is simple enough to introduce the monotonous change of the ORF value. This computational technique encouraged the DP's further application not only to a large-scale optimization problem or to a multidimensional problem but to the real time optimal trajectory generation problems.

Table.5.1 Comparison of computational time and total amount of computation

	Full search	MS-DP
Computational time	1,321 [s]	36 [s]
Total amount of computation	$(101 \times 61)^2 \times 31$	$(21 \times 11)^2 \times 31 \times 18$

5.3 Operational flight efficiency evaluation

5.3.1 Flight parameter estimation from actual flight trajectories

The flight efficiency of commercial jet airliners was analyzed in terms of fuel consumption and flight time by using GPS logger data obtained inside an airborne airliner cabin [28]. The process of flight parameter estimation from actual flight trajectories are visually explained in the upside of Fig. 5.6. Flight parameters such as calibrated air speed, true air speed, Mach number, temperature, and wind are estimated from the GPS data and meteorological Grid Point Value (GPV) data released by Japan Meteorological Agency (JMA) [29], and then performance variables such as L/D (lift/drag ratio), thrust, and fuel flow are estimated using the BADA (Base of Aircraft Data) model published by EUROCONTROL[30]. Although each flight is effectively selected randomly because GPS logger data are obtained by a passenger, the analysis gives highly useful information on passenger aircraft operating in an air traffic controlled environment.

The accuracy of the flight parameter estimates depends critically upon the quality of the meteorological GPV data and the aircraft performance information. The comparison of each estimates with flight data obtained from aircraft on-board systems [31, 32] has shown that the errors are at a reasonable level and that flight parameter values estimated from GPS data are of sufficient quality for analyzing flight efficiency [33]. The author contributed to evaluate an accuracy of the aircraft performance model [31]. The results have been of great use in the ATM research field. Similar findings concerning the accuracy of the meteorological GPV data have been obtained by analysis of SSR Mode S DAPs (Downlink Aircraft Parameters) [34] as well as on-board flight data analysis.

In this study, the tool developed for the GPS logger data analysis is applied to SSR data since the data are similar. Utilization of SSR data extends the scope of the study immensely because data can be obtained on the trajectories of almost every aircraft within the surveillance system's coverage area. Data obtained for flights in Japan's most congested air space by ENRI's secondary surveillance radar located in Chofu, Tokyo, are used for the analysis.

5.3.2 Flight trajectory optimization by dynamic programming

Each flight is analyzed by comparing its trajectory (including state parameter estimates) obtained from SSR, meteorological and performance information with an optimal trajectory calculated using the identical meteorological data and performance model as the flight analysis, assuming the same initial and final positions and velocities. The optimization process is presented in the downside of Fig. 5.6. A performance index which incorporates fuel consumption and flight time is minimized by dynamic programming. The combinatorial optimization algorithm, i.e. normal DP algorithm is applied. The trajectory optimization is carried out for three free variables: altitude, velocity, and lateral deviation from the great-circle route between the initial and final points. These three state variables are quantized on a grid and the path which minimizes the performance index is selected for each feasible transition between gridpoints. A four-dimensional grid is defined for the three free parameters and flight distance along the great-circle route. An equidistance grid, the simplest one, is adopted for the calculation.

The performance index J for the optimization is defined as

$$J = \int_{t_0}^{t_f} (\mu(t) + a)\, dt \tag{5.2}$$

where μ [kg/s] is fuel flow and a [kg/s] is a weighting parameter for the flight time. The weighting parameter is equivalent to the so-called "cost index" used in actual flight operations, where the performance index is defined as the cost of flight [dollars],

$$J_{dollars} = \int_{0}^{t_f} \left(\frac{1}{100} C_{fuel} \frac{1}{0.4536} \mu(t) + C_{time} \frac{1}{3600} \right) dt \tag{5.3}$$

C_{fuel} is the fuel cost in [cents/lb] and C_{time} is the time cost in [dollars/hour]. Comparing Eqs. (5.2) and (5.3) gives the following relation, where CI is the cost index.

$$CI = \frac{C_{time}}{C_{fuel}} = \frac{3600}{100 \times 0.4536} a = 79.37a \tag{5.4}$$

The weighting parameter, or cost index, is a free parameter which is set according to aircraft operators' policies, but in general it is selected to generate relatively high speed in the descent phase even though a flight may be later delayed by air traffic control scheduling of the landing sequence.

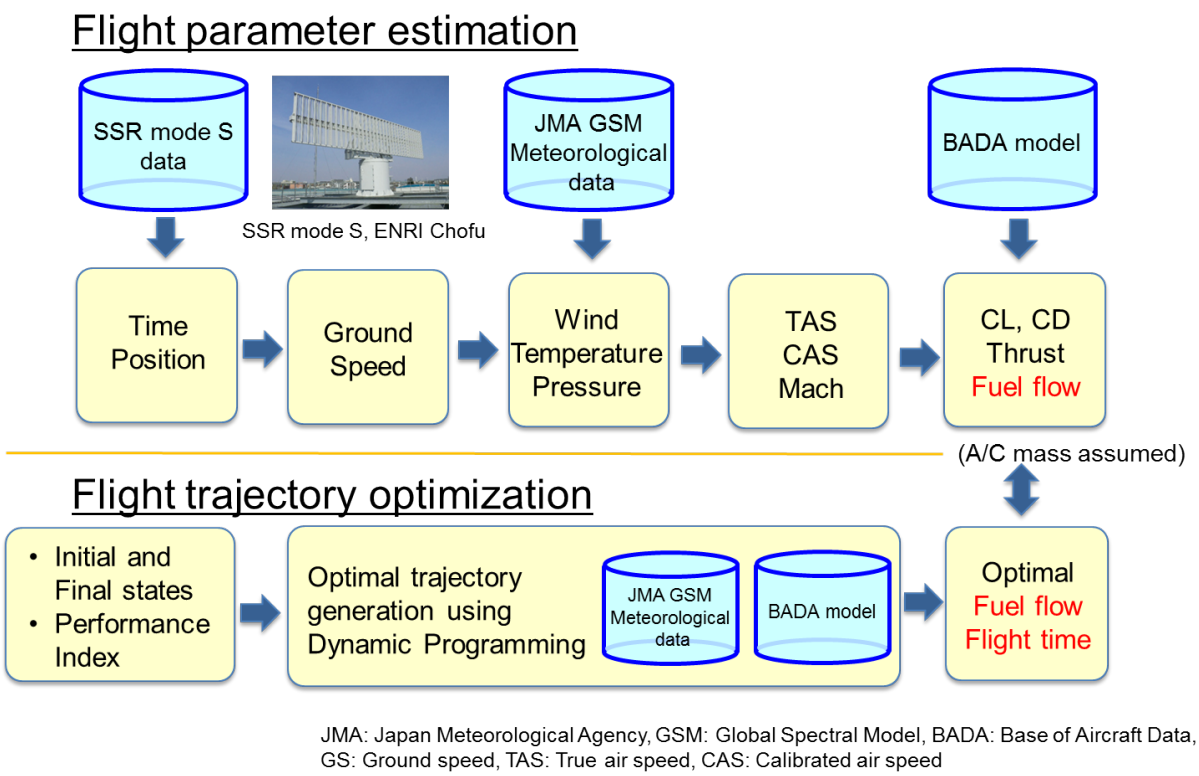

Fig.5.6 A schematic of operational flight efficiency evaluation

5.4 Secondary Surveillance Radar data

5.4.1 A schema of SSR

The Secondary Surveillance Radar (SSR) has been experimentally operated by the Electronic Navigation Research Institute (ENRI) since 2007. This radar corresponds to the Mode-S transponder. Fig. 5.7 shows a photograph of the antenna operated on the top of a building at ENRI. Table. 5.2 lists the major characteristics of the system.

Table.5.2 Characteristics of ENRI's SSR Mode S

	Properties
Radar Site Name	Chofu SSR Mode S Test Ground Station
Position	ENRI (Tokyo, Japan) 35.680118 °N, 139.560962 °E
Rotation cycle	10 [s]
Coverage	250 [NM] at 40,000 [ft]

Fig.5.7 ENRI's experimental SSR

5.4.2 Flight track data recorded by SSR

Fig. 5.8 shows an example of flight trajectories recorded by the SSR. The departure flights and arrival flights from and to Tokyo International Airport are illustrated by blue and red lines respectively and the departure flights and arrival flights from and to Narita International Airport are depicted as cyan and green lines respectively. As can be seen this figure, the arrival flights to Tokyo International Airport are "radar vectored" over the ocean to the south and west of the airport. The operational flight efficiency is analyzed with respect to this arrival flight to Tokyo International Airport.

5.5 Results of potential benefits analysis

5.5.1 Efficiency of arrival flights

Fig. 5.9 and Fig. 5.10 show the number of departure flights and arrival flights per hour from and to Tokyo International Airport. Fig. 5.11 illustrates trajectories of outbound (left) and inbound (right) flights from and to the same airport on an arbitrary day of North Wind Operation in February 2012. Trajectories are plotted below 20,000 [ft], and are color-coded by altitude. It can be recognized from the plots that streams of traffic are merged at three fixes, KAIHO, ARLON and CREAM, on the Tokyo International Airport STARs

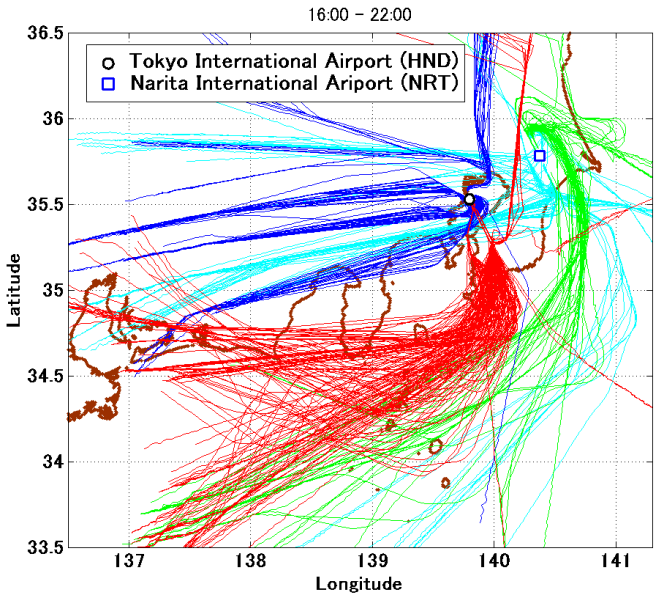

Fig.5.8 Flight trajectories recorded by SSR, (red: HND arrival, blue: HND departure, green: NRT arrival, cyan: NRT departure)

(Standard Instrument Arrival[*1]). Although arrival streams from different directions are merged at KAIHO and ARLON, most aircraft arrived from the west and were "radar vectored" over the ocean to the south and west of the airport in order to adjust their arrival spacing as shown by the wide spread of trajectories in Fig. 5.8. It is clear that the trajectories flown prior to the three merging fixes heavily influences operational efficiency and so should be analyzed in terms of operational performance. On the other hand, the trajectories after the merging three fixes should be considered in terms of capacity and safe separation. Therefore, the final points of the trajectories subject to optimization analysis are defined at the three fixes, and the initial points are defined by the point of first data, i.e. the point of entering SSR coverage. Operational efficiency during climb and most of the cruise phases of flight is excluded from this analysis because of the limited coverage of the single SSR antenna. The trajectory optimization was carried out for three types of aircraft, Type-A, Type-B, and Type-C, the reference masses of which are 208.7 [ton], 154.6 [ton], and 65.3 [ton] respectively. These are three most common types operating at the airport and represent about 60% of all arrivals to the airport.

Although strictly speaking the particular mass of each aircraft is necessary to estimate its flight parameters, the reference mass value of each aircraft type described in BADA model is used in the analysis. Two different values of weighting parameter in the performance index are used for the trajectory optimization: a value of zero, which means "optimize only for fuel consumption" ignoring flight time, and a value of 0.5 [kg/s] which

[*1] STAR was officially the abbreviation of "Standard Terminal Arrival Routes". Its official definition in ICAO changed to "STAndard instrument aRrival" in 2010. It's accepted widely; though, the previous name is still used partially in the United States.

corresponds to Cost Index of about 40. As the latter value is relatively small, it does not have a significant effect on fuel consumption, but it gives some influence on the flight time.

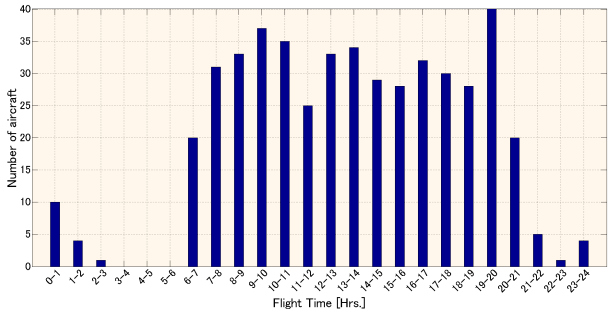

Fig.5.9 Number of departure flights per hour

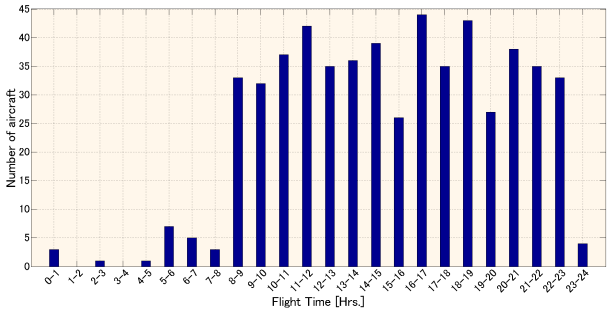

Fig.5.10 Number of arrival flights per hour

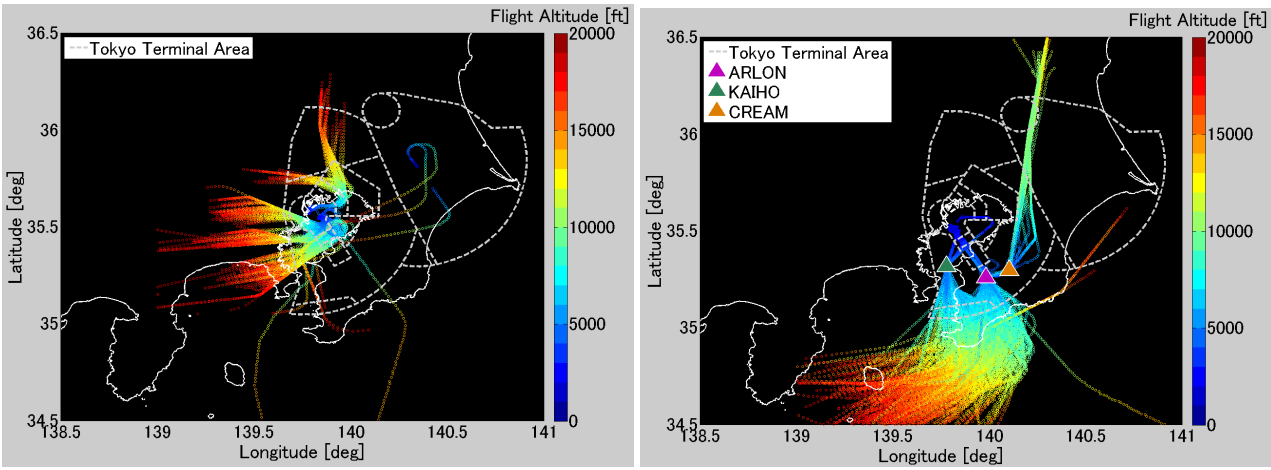

Fig.5.11 Outbound (left) and inbound (right) flights at Tokyo International Airport, on an arbitrary day in February 2012.

5.5.2 A typical example of optimized flight

Figs. 5.12 to 5.17 show a comparison between a sample surveillance trajectory and the optimal trajectory for an aircraft Type-A inbound to Tokyo International Airport. “SSR” denotes time histories of parameters reconstructed from SSR position data, meteorological and performance information, while “Opt” denotes time histories of the optimal trajectory calculated using the same initial and final conditions and the same meteorological and performance information. The flight time weighting parameter is set at $a = 0.5$. Although actual ground tracks generally deviate from the great-circle route due to air traffic control intervention for sequencing and spacing with other traffic before the ARLON fix, the deviation of this case is small. The optimal trajectory’s ground track also slightly deviates from the great-circle route in order to optimize the effect of wind profile. As the altitude shows, the optimal trajectory’s TOD (Top Of Descent) is reached earlier than the actual flight to reduce fuel consumption. The fuel flow plots show a remarkable difference in fuel

consumption. The longer descent flight of the optimal trajectory can be explained by the aircraft's efficiency achieved by flying at a higher L/D ratio which is realized by lower speed. Furthermore, the reconstructed actual flight uses "negative thrust", which corresponds to using speedbrakes. The fuel consumption and flight time of the actual and optimal trajectories are compared in Table 5.3. The optimal trajectory gives a fuel saving of about 497 [kg], which is the benefit achievable by an ideal flight for the conditions. On the other hand, the flight time is greater than the actual flight because of the lower speed during descent.

Table.5.3 Comparison of reconstructed actual flight and the optimal trajectory

	Estimated from SSR data (SSR)	Optimal trajectory (Opt)
Flight time [s]	1464	1647 (+183)
Fuel consumption [kg]	1141	644 (-497)
Flight length [km]	364.6	358.1 (-6.5)

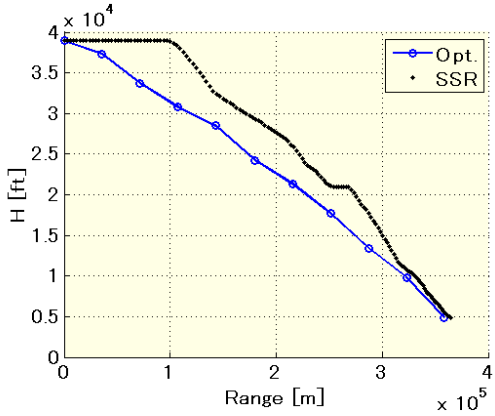

Fig.5.12 Optimal trajectory (Altitude)

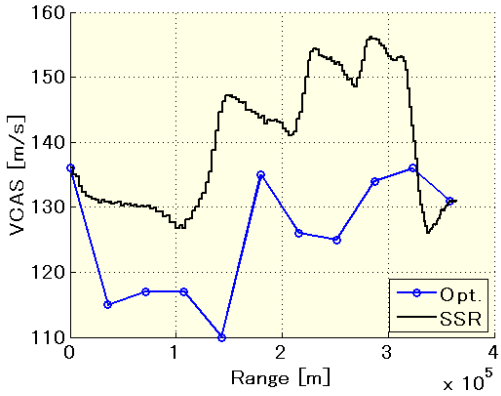

Fig.5.13 Optimal trajectory (CAS)

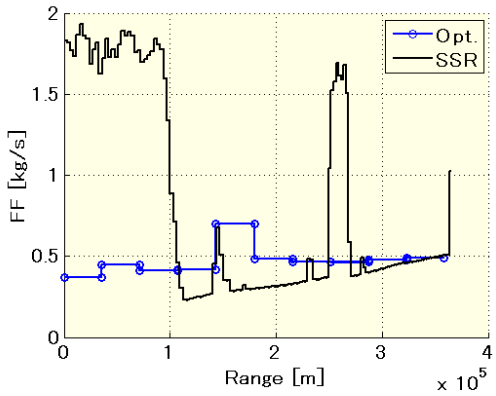

Fig.5.14 Optimal trajectory (Fuel flow)

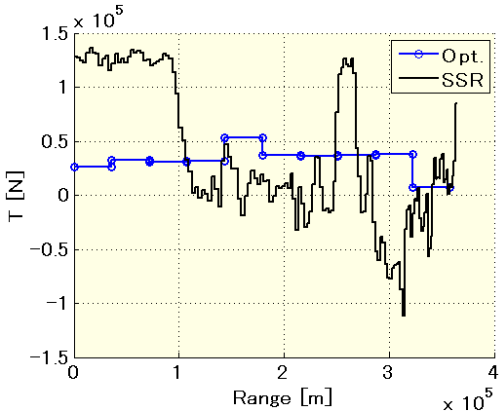

Fig.5.15 Optimal trajectory (Thrust)

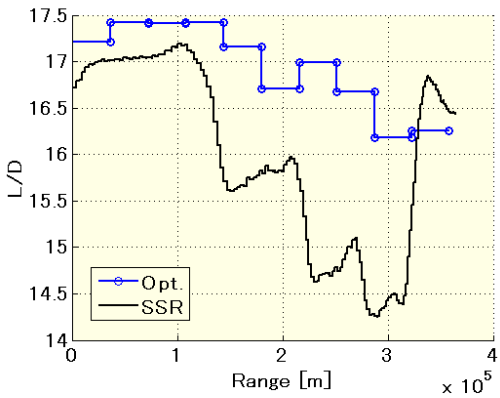

Fig.5.16 Optimal trajectory (Lift to Drag ratio)

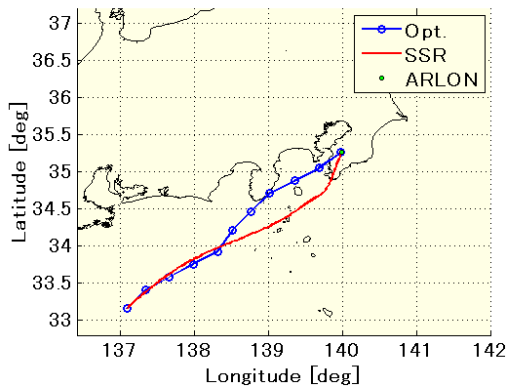

Fig.5.17 Optimal trajectory (Flight path)

5.5.3 Results of statistical characteristics analysis

Data of an arbitrary day in February 2012 were analyzed for the three types of aircraft, three merging fixes, and two values of the performance index weighting parameter. A total of 256 flights were analyzed, which is about 40 % of the number of arrivals on that day. Fig. 5.18 shows differences of fuel consumption, range (flight path length), and flight time for all the analyzed flights. The $a = 0$ cases (i.e. zero weighting on flight time) are shown on the left side and the $a = 0.5$ cases on the right side. The average fuel saving and the average flight time saving for $a = 0.5$ case are derived as 362 [kg] and 202 [s] respectively. Comparing the two weighting parameter values by Table. 5.4 and plots in Fig. 5.18, it is understood that the weighting parameter does not greatly alter fuel consumption but has an influence on flight time. This justifies the claim that setting the weighting parameter to a small value instead of zero gives an operationally practical trajectory with negligible fuel penalty. Fig. 5.19 shows differences of fuel, range, and time relative to the actual flights for the three merging fixes, ARLON, KAIHO and CREAM. The weighting parameter is set as $a = 0.5$. Concerning the range and flight time of actual flights, the KAIHO trajectories are longer than those for ARLON but have similar characteristics. On the other hand, CREAM gives different characteristics; i.e. one group is close to the shortest path, and the other has long range and time. Flights from the north of Japan pass CREAM and land on one of the two runways, 34R and 34L. 34L is mainly used by flights passing ARLON and KAIHO, but 34R is used by flights passing CREAM, which are fewer than that of 34L. Since their descent profile is step-down with a relatively long level flight at a low altitude to avoid interference of the traffic of Narita International Airport, the optimal trajectory can generate fuel and time savings. Some flights passing CREAM arriving from the north-west airspace take flight routes that are originally longer than the great-circle route, which can explain the long range and time cases. Fig. 5.20 shows differences of fuel, range and time for three aircraft types, Type-A, B, C. There are no significant differences between types except for the fuel consumption. These differences are reasonable because fuel consumption is proportional to aircraft mass, and the reference mass of Type-C is about one thirds of that of Type-A. From the stochastic analysis, it can be recognized that there are two dominant sources of fuel saving of the optimal trajectory: a shorter flight path length than the actual flown path due to controller intervention for sequencing and spacing, and a more efficient descent profile realized by setting a smaller cost index than the standard, which is rational for flights to uncongested airports.

Table.5.4 Average differences of the optimal trajectories relative to actual flights, $a = 0$ and $a = 0.5$

	Weighting parameter $a = 0$	Weighting parameter $a = 0.5$
Fuel difference, average [kg]	-386	-362
Range difference, average [m]	-36,228	-36,615
Time difference, average [s]	-66	-202
Number of flights analyzed	256	256

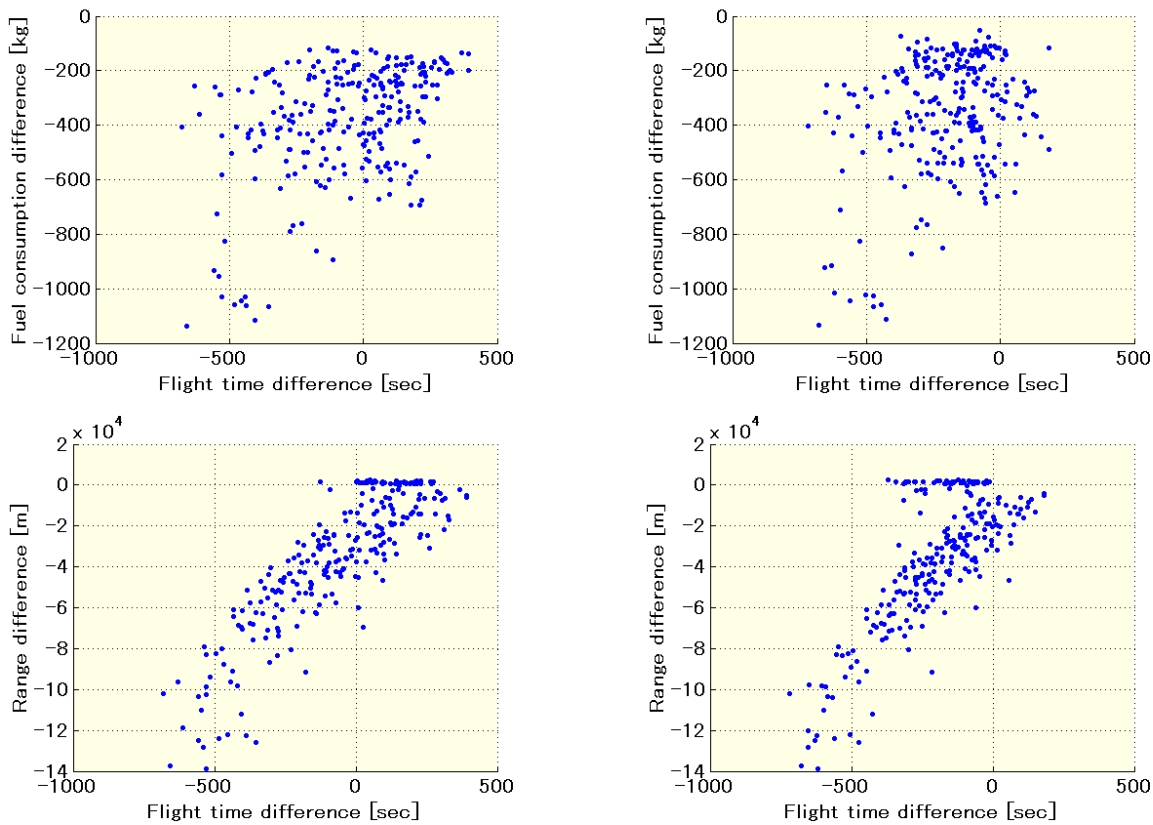

Fig.5.18 Fuel, range and time differences of the optimal trajectories relative to actual flights, $a = 0$ (left) and $a = 0.5$ (right)

Table.5.5 Average differences of the optimal trajectories relative to actual flights, three merging fixes

	Merging Fix, ARLON	Merging Fix, KAIHO	Merging Fix, CREAM
Fuel difference, average [kg]	-327	-381	-396
Range difference, average [m]	-38,305	-54,268	-14,898
Time difference, average [s]	-154	-279	-191
Number of flights analyzed	108	77	71

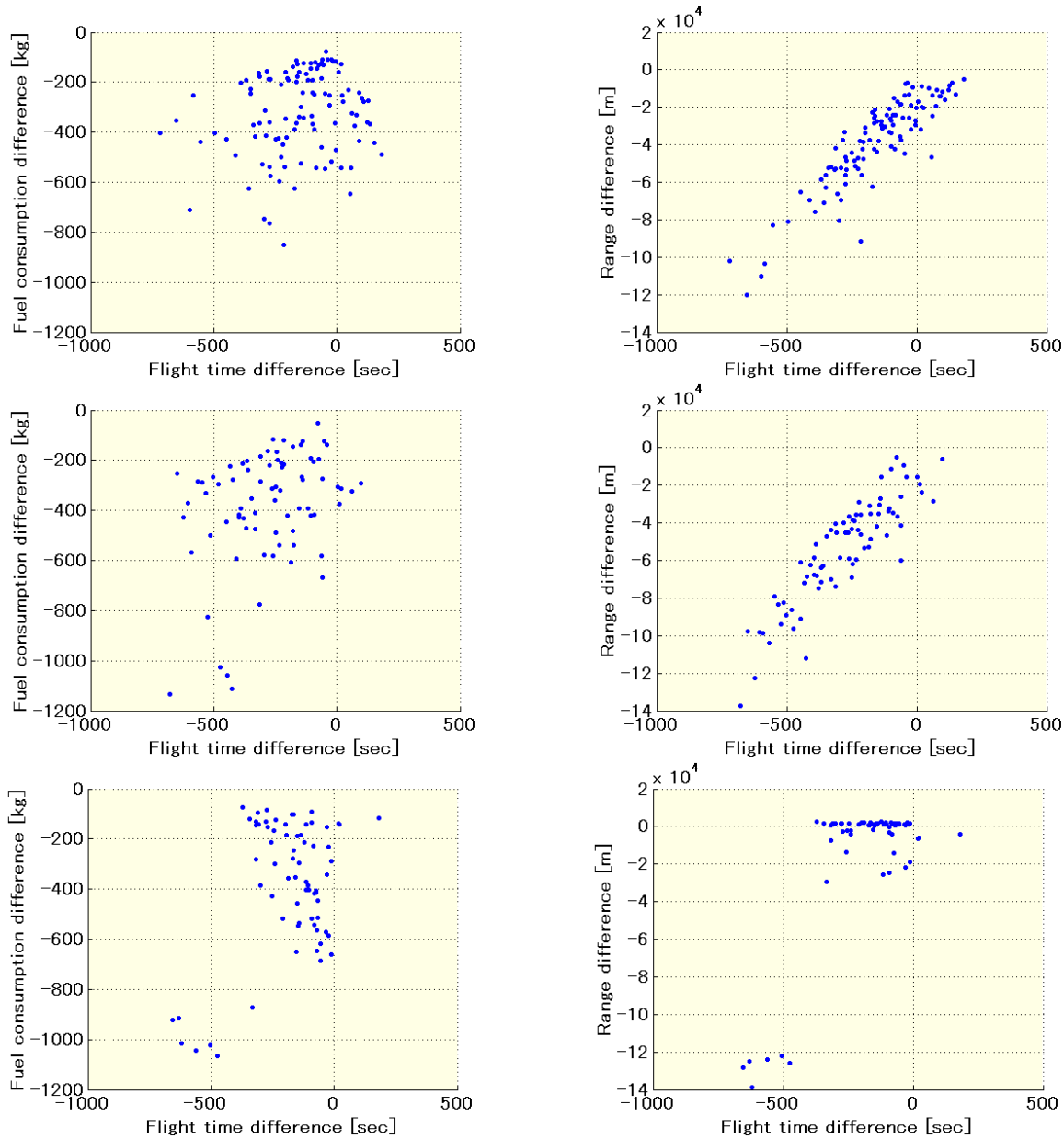

Fig.5.19 Fuel, range and time differences of the optimal trajectories relative to actual flights,three merging fixes

Table.5.6 Average differences of the optimal trajectories relative to actual flights, Type-A, B and C

Aircraft Type (reference mass [ton])	Type-A (208.7)	Type-B (154.6)	Type-C (65.3)
Fuel difference, average [kg]	-541	-410	-180
Range difference, average [m]	-40,063	-37,280	-33,336
Time difference, average [s]	-201	-169	-234
Number of flights analyzed	72	90	94

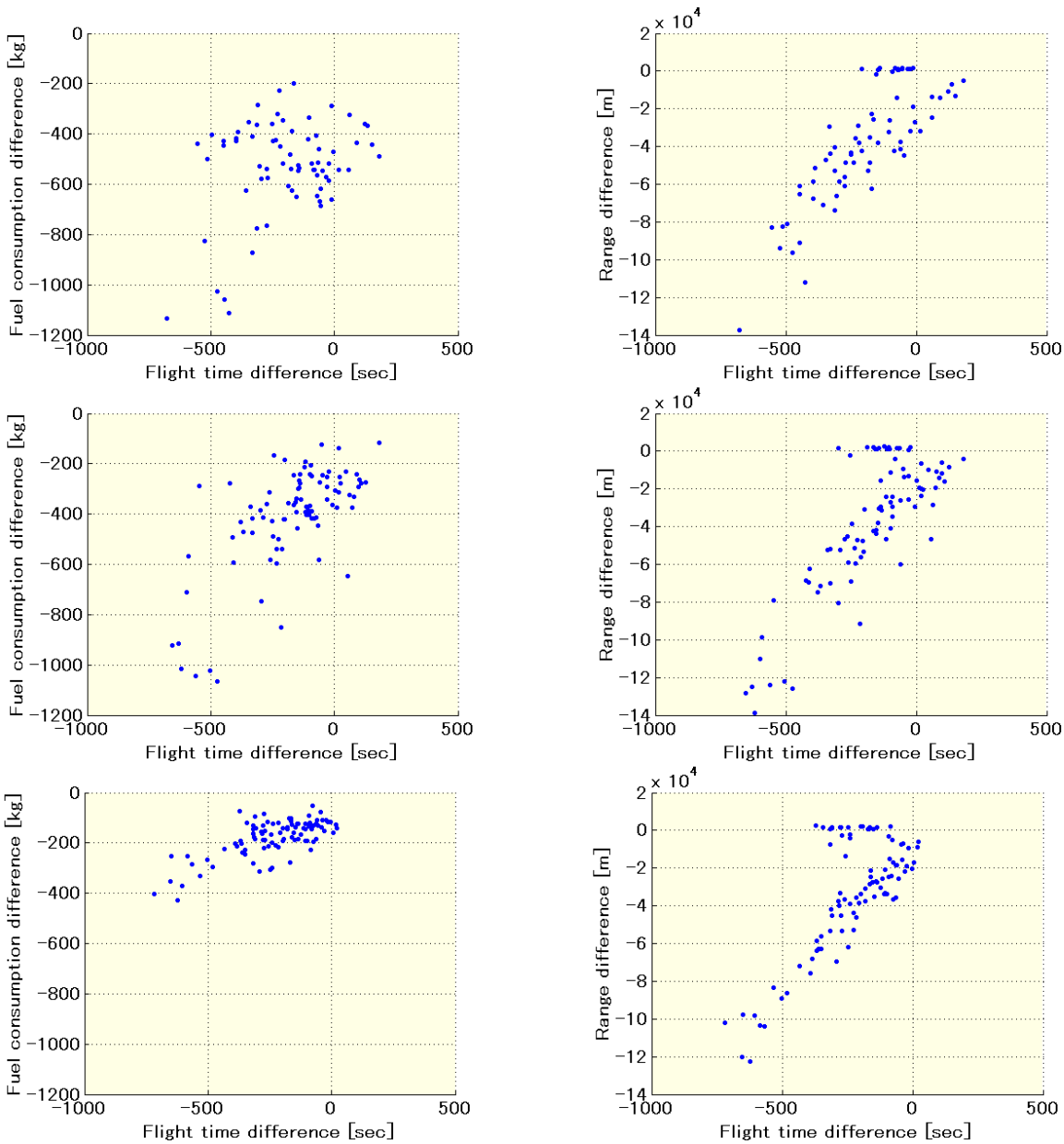

Fig.5.20 Fuel, range and time differences of the optimal trajectories relative to actual flights, Aircraft type-A, B and C

5.6 Summary

Operational efficiency is analyzed for inbound flights to Tokyo International Airport. Surveillance data obtained from an experimental Mode S SSR station operated by ENRI are used for the analysis. The optimal trajectory which minimizes a performance index defined by considering fuel consumption and flight time is calculated for each flight, and is compared with reconstructed parameters of the original flight. A total of 256 flight cases are analyzed. From the analysis, possible savings of fuel and flight time on average are estimated as 362 [kg] and 202 seconds, respectively. These results quantitatively reveal potential benefits which might be obtained by improving the air traffic management system, and encourage further research into the Japanese CARATS CNS/ATM modernization program. Information on the sources of the benefits is useful for prioritizing the research topics and to set research and development goals.

This chapter introduced a quantitative operational flight efficiency analysis where many worthwhile statistical findings have been obtained as a solution of a large-scale optimization problem. Demonstrating the capability of newly proposed MS-DP method which is the main purpose of this chapter has been achieved by solving the large-scale problem for multiple aircraft. The aircraft dynamics is not considered in the governing equation and only three state variables which have stronger impact on the objective function are optimized. Although the number of state variable is limited to only three, it is extremely difficult to optimize one flight even within several hours using a standard personal computer if the normal dynamic programming algorithm is used. The computational time could be drastically reduced to within 15 minutes by the newly proposed MS-DP fast computation algorithm. The practical problem in this chapter could not be solved if MS-DP method would not have been proposed because the “curse of dimensionality” would be a fatal bottleneck in searching for the optimal solution by the normal full search algorithm of DP. MS-DP method substantially contributed to solving a large-scale optimization problem for multiple aircraft in a reasonable computational time.

Chapter. 6

Dynamic Programming Trajectory Optimization by Piecewise Linear Approximation

6.1 Introduction

Real-time trajectory optimization technology for practical use is strongly desired by various research fields. The rapid increases of computational capability due to high-performance processors and parallel processing, as well as continual decreases of hardware costs, are sufficient to achieve this goal. Air Traffic Management (ATM) is one of the most demanding fields where optimal flight trajectory generation leads the realization of Trajectory Based Operations (TBO) which deal the flight route from departure to arrival as one continuous trajectory in the unified airspace. Dynamic programming has been applied in ATM research by several researchers [35, 36]. The paper [35] presents a method based on dynamic programming to generate optimal 4D-trajectories in the presence of multiple time constraints. Soft computing techniques are introduced to improve the DP oriented optimization process in the cruise phase trajectory design. The paper [36] introduces a flight path optimization for minimizing aircraft noise and fuel consumption around airports using a new trajectory generation algorithm based on Hamilton-Jacobi-Bellman considerations. Real-time trajectory generation considering meteorological conditions and conflicts with other aircraft is vital for efficient operations to maximize each aircraft's performance in a crowded airspace [21, 22, 23, 24, 25, 26, 27, 33, 37]. Dynamic programming has been considered unsuitable for trajectory optimization calculations due to its computational load; however, new developments in calculation, such as Moving Search space Dynamic Programming (MS-DP) [8, 24, 27], have enhanced the potential of this method for real-time trajectory optimization.

In the research for future ATM system, developments for Next-Generation Flight Management System (NG-FMS) are recently motivated by integrating 4D-trajectory generation technology with aircraft dynamics,

autonomous flight control technology of Unmanned Aerial Vehicles (UAVs) and digital data link technology [38, 39, 40, 41]. In the current system, the objective altitude, velocity and flight path are transmitted by voice communication between air traffic controllers and pilots. For this reason, only altitude and velocity are calculated in the FMS; therefore, the optimization of altitude and velocity is considered to be sufficient in the current communication based operations. Nevertheless, in the view of realization of the NG-FMS, it is preferable that the aircraft dynamics is explicitly considered in the governing equation. This chapter aims at establishing the trajectory optimization method which can generate the aircraft dynamics-added 4D-trajectory. It is demonstrated that dynamic programming is capable of designing an optimal trajectory with aircraft dynamics. As an application example, longitudinal fuel minimal trajectory is designed by considering pull-up and pull-back motion. The dimensional difference problem occurred by adding flight path angle into the state variable is resolved by newly proposed PLA-DP method. The method is of great value in that it can provide an optimal trajectory as a series of feasible points not only of quantized grid points.

6.2 Practical method to resolve the "Menace of the expanding grid"

At first, a novel approach to resolve the "Menace of the expanding grid" what we call the dimensional difference problem is introduced. A simple two-dimensional system is taken as an example to explain the algorithm of the method.

6.2.1 Dimensional difference problem

As explained in the section 3.4, the DP algorithm experiences no difficulties in providing an optimal solution if the number of control variable is the same as the number of the state variable, i.e. $m = n$.

In the case of $m < n$, the dimensional difference problem inevitably arises. For simplicity, this problem is explained with a two-dimensional system which has two state variables and one control variable indicated by the following system equation.

$$\dot{\boldsymbol{x}}(t) = \boldsymbol{f}(\boldsymbol{x}(t), \boldsymbol{u}(t), t), \qquad \boldsymbol{x} \in \mathbb{R}^2, \quad \boldsymbol{u} \in \mathbb{R}^1 \tag{6.1}$$

$$\boldsymbol{x}(t) = \begin{pmatrix} x_1(t) \\ x_2(t) \end{pmatrix} \tag{6.2}$$

$$\boldsymbol{u}(t) = u_1(t) \tag{6.3}$$

If the control variable is set as a zeroth-order hold over the transition, a solution cannot be derived because the degree of freedom for the control variable are insufficient to connect two quantized grid points of the state variables as illustrated in Fig. 6.1.

This figure shows the state space defined by the independent variable t and the state variables $x_1(t)$ and $x_2(t)$. J_{opt_k} cannot be expressed with the quantized grid points such as Eq. (3.32) because all of the transitions

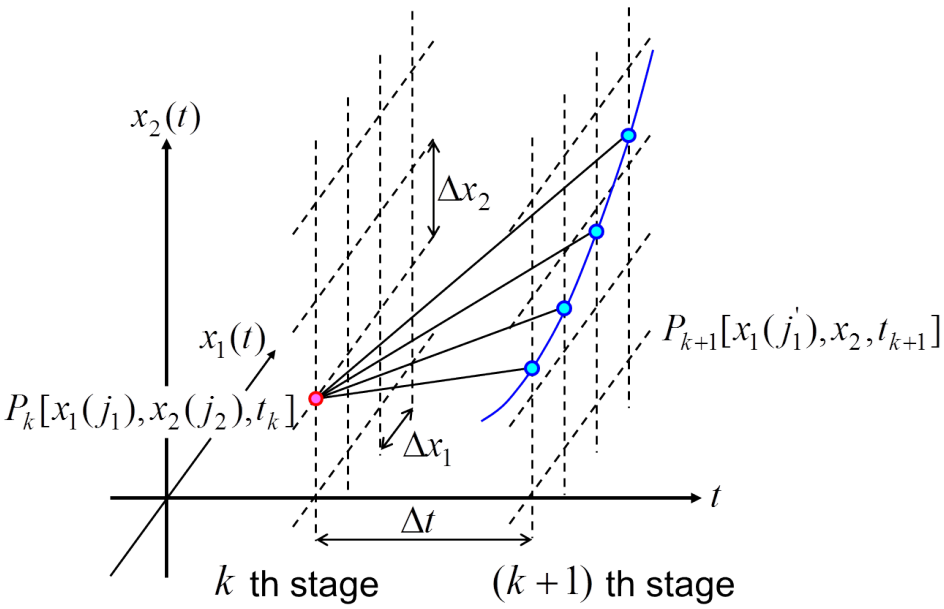

Fig.6.1 Calculation grid and feasible line

between the grid points are not feasible. Even if a finer calculation grid is used, the obtained trajectory and control series are far from optimum. Although the degree of freedom of the control variables might be increased to alleviate the difficulty, some special techniques or complicated adjustments would be needed. This issue has been designated as the dimensional difference problem. To resolve this challenge, a novel approach, Piecewise Linear Approximation Dynamic Programming (PLA-DP) method was proposed by the author's research group [9]. The detailed algorithm is explained in the next subsection.

6.2.2 Piecewise Linear Approximation Dynamic Programming (PLA-DP) method

In the case of one dimensional difference introduced by the above mentioned two-dimensional system, the feasible points are derived between the grid points. In Fig. 6.1, let us consider the transition from a grid point $P_k[x_1(j_1),x_2(j_2),t_k]$ to the stage $k+1$. Considering the destination point from the grid point P_k at the stage k, x_2 may be determined analytically for the given grid point value of $x_1(j_1^{'})$ at the stage $k+1$. Therefore, all the transitions from point P_k to the grid points at the stage $k+1$ are infeasible. The feasible points at the stage $k+1$ are illustrated by the blue points on the blue feasible line in Fig. 6.1.

PLA-DP method uses a piecewise linear function to approximate the ORF value. This method is based on a concept where the genuine optimal solution is derived as a series of feasible points located between the grid points; that is, PLA-DP regards the state variables as continuous physical quantities and departs from the concept of combinatorial optimization problem for the grid points. The PLA-DP algorithm consists of two parts, approximation of the ORF value and the approximation of optimal path selection information. The

algorithm for calculating backward from the terminal to the initial point is introduced below.

■ Algorithm of PLA-DP method

Approximation of the ORF value

(1) The ORF value is assumed to be stored on all grid points at the stage $k+1$.

(2) The feasible points $P_{k+1}[x_1(j_1^{'}), x_2, t_{k+1}]$ at the stage $k+1$ is derived analytically for all grid points of $x_1(j_1^{'})$.

(3) The ORF value at the point P_{k+1} is calculated by linear interpolation using two neighboring grid points along the x_2 axis. The following equation explains the interpolation for the two grid points $x_2(j_2^{'})$ and $x_2(j_2^{'}+1)$.

$$\begin{aligned} J_{opt_{k+1}}(x_1(j_1^{'}), x_2, t_{k+1}) = {} & J_{opt_{k+1}}(x_1(j_1^{'}), x_2(j_2^{'}), t_{k+1}) \\ & + \left[J_{opt_{k+1}}(x_1(j_1^{'}), x_2(j_2^{'}+1), t_{k+1}) - J_{opt_{k+1}}(x_1(j_1^{'}), x_2(j_2^{'}), t_{k+1}) \right] \\ & \times \left[x_2 - x_2(j_2^{'}) \right] / \left[x_2(j_2^{'}+1) - x_2(j_2^{'}) \right] \end{aligned} \tag{6.4}$$

This interpolation for two grid points is illustrated by orange arrows in Fig. 6.2.

(4) The fraction of the objective function $\Delta\mathscr{L}$ denoted by Eq. (3.33) is calculated between P_k and the feasible points P_{k+1}. This value is added to the interpolated ORF value $J_{opt_{k+1}}(x_1(j_1^{'}), x_2, t_{k+1})$ stored at P_{k+1}.

(5) The optimal path that minimizes $\Delta\mathscr{L} + J_{opt_{k+1}}(x_1(j_1^{'}), x_2, t_{k+1})$ is selected from all n_1+1 feasible paths. The optimal destination $x_1(j_1^{'})$ is decided at the stage $k+1$.

(6) The procedures from (2) to (5) are executed for all the grid points at the stage k. The ORF value is stored for each stage recursively.

(7) The optimization calculation completes if the ORF value at the initial point is obtained.

Approximation of optimal path selection information

After the approximation of the ORF value, the optimal destination of $x_1(t)$ is stored on all the grid points. In the paper [9], this optimal destination is designated as the "optimal path selection information". The approximation of optimal path selection information is explained in Fig. 6.3. Since the initial point possesses the optimal path selection information for x_1, the optimal grid point $x_1(1)$ is decided at the first stage. This $x_1(1)$ value determines the feasible point for the $x_2(t)$ axis with the transition condition denoted by Eq. (6.1). This optimal point $P_1[x_1(1), x_2(1)]$ does not possess any optimal path selection information because it is located on an arbitrary point on the $x_2(t)$ axis. Therefore, the optimal path selection information $x_1(2)$ is given by interpolating two neighboring grid points for $x_2(t)$. The optimal point at the second stage $P_2[x_1(2), x_2(2)]$ is determined by the transition condition as well. $x_1(3)$ is obtained by two-dimensional interpolation for four neighboring grid points at the second stage. An optimal trajectory is generated by implementing these processes recursively until the terminal.

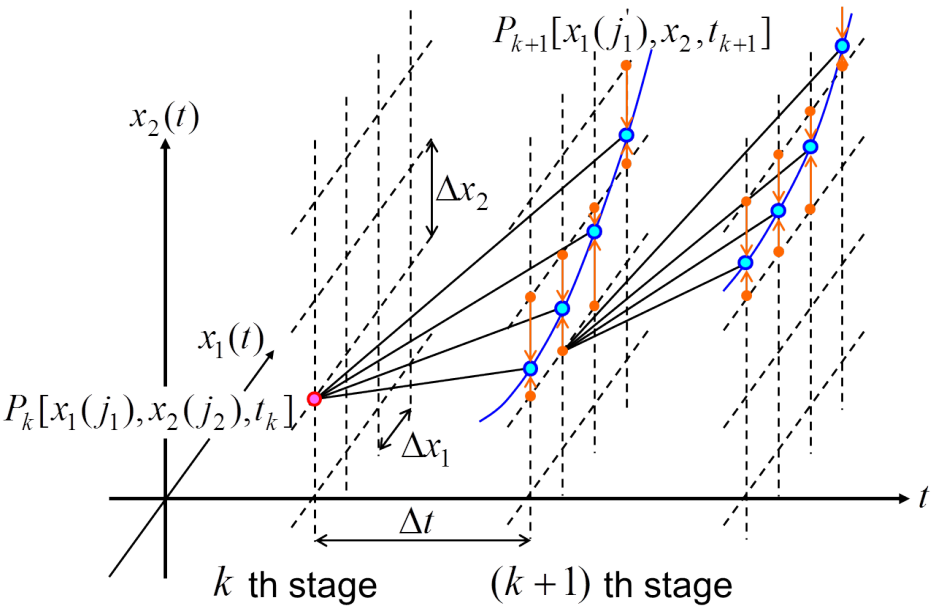

Fig.6.2 Approximation of the ORF value

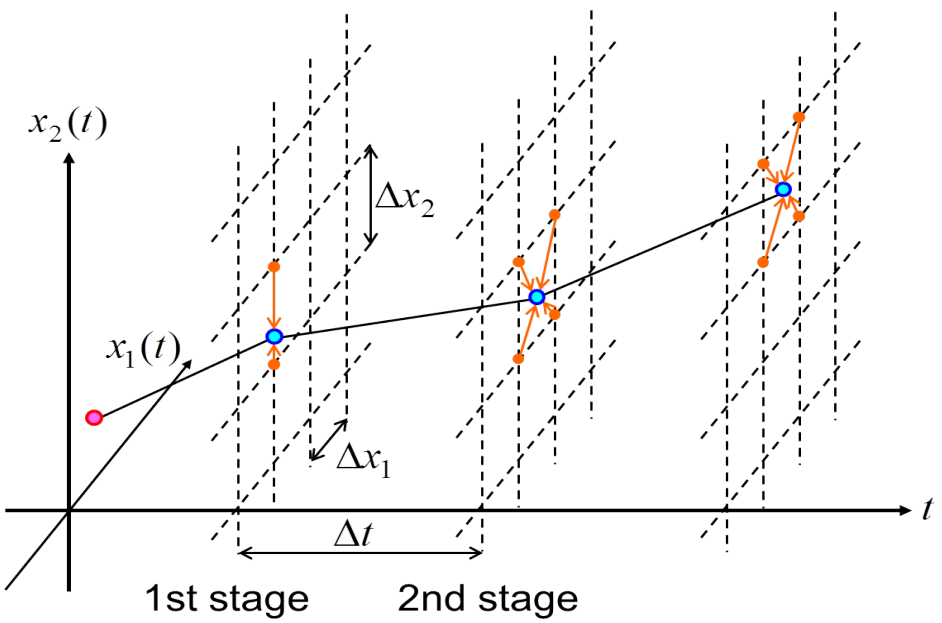

Fig.6.3 Approximation of optimal path selection information

6.3 Validity evaluation of PLA-DP method

A simple LQR is adopted as an example to demonstrate the accuracy of PLA-DP method in comparison to easily obtained continuous-time and discrete-time exact solutions. The state equation for a finite-dimensional, time-invariant linear system and its objective function in quadratic form are defined as follows.

$$\dot{\boldsymbol{x}} = \boldsymbol{A}\boldsymbol{x}(t) + \boldsymbol{B}\boldsymbol{u}(t) \tag{6.5}$$

$$J = \int_0^{t_f} \left[\frac{1}{2}\boldsymbol{x}^{\mathrm{T}}(t)\boldsymbol{Q}\boldsymbol{x}(t) + \frac{1}{2}\boldsymbol{u}^{\mathrm{T}}(t)\boldsymbol{R}\boldsymbol{u}(t) \right] dt + \frac{1}{2}\boldsymbol{x}^{\mathrm{T}}(t_f)\boldsymbol{P}_f\boldsymbol{x}(t_f) \tag{6.6}$$

The state and control variables are defined by $\boldsymbol{x} \in \mathbb{R}^n$ and $\boldsymbol{u} \in \mathbb{R}^m$ respectively. $\boldsymbol{A} \in \mathbb{R}^{n\times n}$ and $\boldsymbol{B} \in \mathbb{R}^{n\times m}$ are constant matrices. The weighting matrices are $\boldsymbol{Q} \in \mathbb{R}^{n\times n}$ and $\boldsymbol{R} \in \mathbb{R}^{m\times m}$, where $\boldsymbol{Q} \geq 0$ (positive semi-definite matrix) and $\boldsymbol{R} > 0$ (positive definite matrix), respectively. When $\boldsymbol{P_f}$ satisfies the following matrix Riccati equation Eq. (6.7), it produces the steady state solution:

$$\boldsymbol{A}^{\mathrm{T}}\boldsymbol{P}_f + \boldsymbol{P}_f\boldsymbol{A} - \boldsymbol{P}_f\boldsymbol{B}\boldsymbol{R}^{-1}\boldsymbol{B}^{\mathrm{T}}\boldsymbol{P}_f + \boldsymbol{Q} = \boldsymbol{0} \tag{6.7}$$

The optimal control $\boldsymbol{u}_{opt}(t)$ and ORF J_{opt} depend only on the state variables, as shown below:

$$\boldsymbol{u}_{opt}(t) = -\boldsymbol{R}^{-1}\boldsymbol{B}^{\mathrm{T}}\boldsymbol{P}_f\boldsymbol{x}(t), \qquad J_{opt} = \frac{1}{2}\boldsymbol{x}^{\mathrm{T}}(t_0)\boldsymbol{P}_f\boldsymbol{x}(t_0) \tag{6.8}$$

When the control input $\boldsymbol{u}$ is assumed to be a zeroth-order hold, that is, to have a constant value of $\boldsymbol{u}_k$ over the interval of $t \in [t_0 + k\Delta t,\ t_0 + (k+1)\Delta t]$, $k = 0, 1, \cdots, N-1$, $\Delta t = (t_f - t_0)/N$, the state equation of the discrete-time system is given by Eq. (6.9), where $\boldsymbol{x}_k$ is a sampled state variable at the kth cycle defined by $\boldsymbol{x}_k = \boldsymbol{x}(k\Delta t)$, $k = 0, 1, \cdots, N$.

$$\boldsymbol{x}_{k+1} = \boldsymbol{A}_d\boldsymbol{x}_k + \boldsymbol{B}_d\boldsymbol{u}_k\boldsymbol{A}_d = \Phi(\Delta t), \quad \boldsymbol{B}_d = \Gamma(\Delta t), \quad \textit{where}\ \ \Phi(t) = e^{\boldsymbol{A}t}, \quad \Gamma(t) = \int_0^t e^{\boldsymbol{A}\tau}d\tau \cdot \boldsymbol{B} \tag{6.9}$$

The objective function is expressed by Eq. (6.10).

$$J = \sum_{k=0}^{N-1} \left[\frac{1}{2}\boldsymbol{x}_k^{\mathrm{T}}\boldsymbol{Q}_d\boldsymbol{x}_k + \frac{1}{2}\boldsymbol{u}_k^{\mathrm{T}}\boldsymbol{R}_d\boldsymbol{u}_k + \boldsymbol{x}_k^{\mathrm{T}}\boldsymbol{N}_d\boldsymbol{u}_k \right] + \frac{1}{2}\boldsymbol{x}_N^{\mathrm{T}}\boldsymbol{P}_{dN}\boldsymbol{x}_N \tag{6.10}$$

where

$$\begin{bmatrix} \boldsymbol{Q}_d & \boldsymbol{N}_d \\ \boldsymbol{N}_d^{\mathrm{T}} & \boldsymbol{R}_d \end{bmatrix} = \int_0^{\Delta t} \begin{bmatrix} \boldsymbol{\Phi}^{\mathrm{T}}(t) & 0 \\ \boldsymbol{\Gamma}^{\mathrm{T}}(t) & \boldsymbol{I} \end{bmatrix} \begin{bmatrix} \boldsymbol{Q} & 0 \\ 0 & \boldsymbol{R} \end{bmatrix} \begin{bmatrix} \boldsymbol{\Phi}(t) & \boldsymbol{\Gamma}(t) \\ 0 & \boldsymbol{I} \end{bmatrix} dt \tag{6.11}$$

When $\boldsymbol{P}_{dN}$ satisfies the following equation Eq. (6.12), it introduces the following steady state solution:

$$\boldsymbol{A}_d^{\mathrm{T}}\boldsymbol{P}_{dN}\boldsymbol{A}_d - \boldsymbol{P}_{dN} + \boldsymbol{Q}_d - (\boldsymbol{A}_d^{\mathrm{T}}\boldsymbol{P}_{dN}\boldsymbol{B}_d + \boldsymbol{N}_d)(\boldsymbol{B}_d^{\mathrm{T}}\boldsymbol{P}_{dN}\boldsymbol{B}_d + \boldsymbol{R}_d)^{-1}(\boldsymbol{A}_d^{\mathrm{T}}\boldsymbol{P}_{dN}\boldsymbol{B}_d + \boldsymbol{N}_d)^{\mathrm{T}} = 0 \tag{6.12}$$

The optimal control $\boldsymbol{u}_{opt_k}$ and ORF J_{opt} depend only on the state variables.

$$\boldsymbol{u}_{opt_k} = (\boldsymbol{B}_d^{\mathrm{T}}\boldsymbol{P}_{dN}\boldsymbol{B}_d + \boldsymbol{R}_d)^{-1}(\boldsymbol{A}_d^{\mathrm{T}}\boldsymbol{P}_{dN}\boldsymbol{B}_d + \boldsymbol{N}_d)^{\mathrm{T}}\boldsymbol{x}_k, \qquad J_{opt_k} = \frac{1}{2}\boldsymbol{x}_k^{\mathrm{T}}\boldsymbol{P}_{dN}\boldsymbol{x}_k \tag{6.13}$$

The following second-order system is taken as an numerical example.

$$\frac{d^2y}{dt^2} = u(t), \qquad y(0) = y_0, \qquad \dot{y}(0) = \dot{y}_0 \tag{6.14}$$

$$\boldsymbol{x}(t) = \begin{pmatrix} y(t) \\ dy/dt \end{pmatrix}, \qquad \boldsymbol{A} = \begin{pmatrix} 0 & 1 \\ 0 & 0 \end{pmatrix}, \qquad \boldsymbol{B} = \begin{pmatrix} 0 \\ 1 \end{pmatrix} \tag{6.15}$$

The state variables y and $\dot{y}$ and the control variable u are scalar. The weight matrix for the objective function is given as follows:

$$\boldsymbol{Q} = \begin{pmatrix} 1 & 0 \\ 0 & 0 \end{pmatrix}, \qquad \boldsymbol{R} = r \tag{6.16}$$

The system matrices of the discrete-time state equation Eq. (6.9) is given.

$$\boldsymbol{A}_d = \begin{pmatrix} 1 & \Delta t \\ 0 & 1 \end{pmatrix}, \qquad \boldsymbol{B}_d = \begin{pmatrix} \Delta t^2/2 \\ \Delta t \end{pmatrix} \tag{6.17}$$

Four cases of different initial conditions, listed in Table 6.1, are examined. The parameters and grid settings for the numerical example are defined in Table 6.2. Table 6.3 shows the obtained minimized objective functions of the continuous-time exact solution, discrete-time exact solution, and PLA-DP for each case. Although the solutions increase from the continuous-time exact solution to the discrete-time exact solution, and from the discrete-time exact solution to the PLA-DP solution, due to the imposed constraints of time discretization and state variable discretization, the differences between the discrete-time exact solution and PLA-DP are less than 0.6%; these differences are dependent on the step size of state variable relative to the range of response. All of the ORF values of the PLA-DP solutions are larger than those of the corresponding discrete-time exact solutions. The analysis result means that the PLA-DP provides accurate solutions, even if its accuracy is affected by state variable discretization. Figs. 6.4 to 6.6 show the time histories of the state variables and the control input of Case 1, in which the discrete-time exact solution and PLA-DP solution are very close. These numerical examples demonstrate the validity of PLA-DP method in a trajectory optimization problem which has the dimensional difference problem.

Table.6.1 Initial value

Case 1	$y_0 = 5$	$\dot{y}_0 = 0$
Case 2	$y_0 = 1$	$\dot{y}_0 = -2$
Case 3	$y_0 = 3$	$\dot{y}_0 = 2$
Case 4	$y_0 = 0$	$\dot{y}_0 = -2$

Table.6.2 Parameters and grid settings

Weight parameter	r	1
Time step	Δt	0.25
Number of independent variable divisions	N	40
Grid resolution of y	Δy	0.05
Grid resolution of $\dot{y}$	$\Delta \dot{y}$	0.05

Table.6.3 Optimum Return Function

	(a) Exact solution (continuous-time system)	(b) Exact solution (discrete-time system)	(c) DP solution
		(b-a)/a, (%)	(c-b)/b, (%)
Case 1	17.6777	17.7467 (0.39)	17.7527 (0.033)
Case 2	1.5355	1.5389 (0.22)	1.5480 (0.59)
Case 3	15.1924	15.2597 (0.44)	15.2692 (0.062)
Case 4	2.8284	2.8395 (0.39)	2.8492 (0.34)

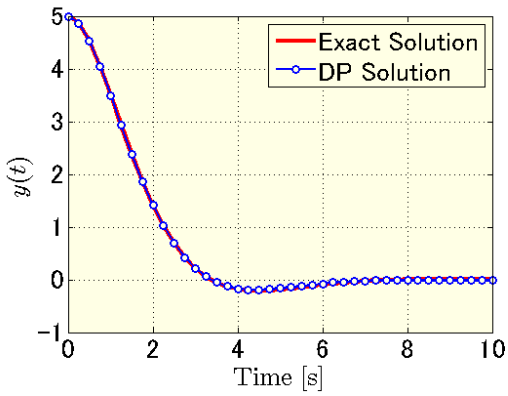

Fig.6.4 Optimal trajectory, state variable y (Case 1)

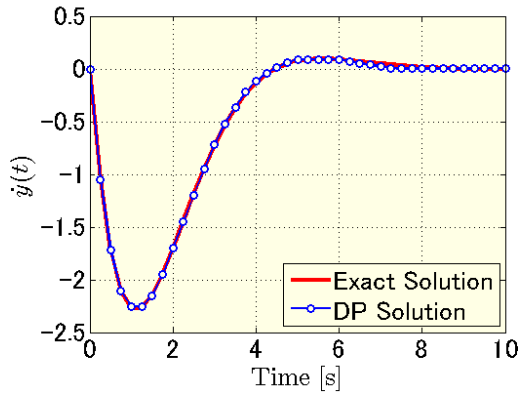

Fig.6.5 Optimal trajectory, state variable $\dot{y}$ (Case 1)

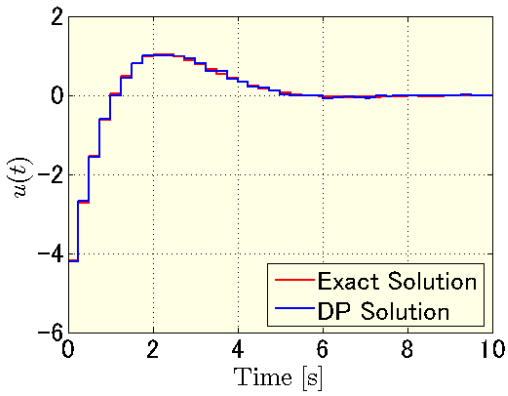

Fig.6.6 Optimal trajectory, control variable u (Case 1)

6.4 Fuel minimal trajectory design by PLA-DP method

The usefulness of PLA-DP method is demonstrated by passenger aircraft's fuel minimal trajectory optimization as an example application. Aircraft operators attempt to ensure maximum operational efficiency to reduce fuel consumption over an adjustable flight time. TBO is regarded as one of the most important concepts for increasing the operational efficiency of current airspace. This advanced model of operations employs 4-D optimal trajectories in which each aircraft flies so as to maximize its performance in consideration of meteorological conditions and conflicts with other aircraft. Such 4-D optimal trajectories, considering tradeoffs between fuel consumption and flight time and the conflict situations, have previously been designed by DP [24]. Operational efficiency analysis has been implemented with a 4-D trajectory optimization tool in the previous research [21, 24, 25, 26, 27, 33, 37]. These studies set the flight path angle as the control variable and provided optimal trajectories while avoiding the dimensional difference problem; therefore, feasible solutions were derived for all transitions between the grid points. However, one major shortcoming of this approach is the longitudinal oscillation occurred on the obtained trajectory. This oscillation has been regarded as one of the barriers limiting the active application of DP to practical trajectory optimization problems. This section introduces a method that optimizes not only altitude and velocity but also path angle, which is set as a state variable, by explicitly considering the aircraft's attitude change in light of NG-FMS. This problem setting enables to consider the aircraft dynamics. Although the dimensional difference problem arises by adding the path angle to the state variables, it can be resolved by the newly proposed PLA-DP method. The effect of considering the path angle is discussed by comparing two optimization analyses. The first case optimizes two state variables: altitude H and true airspeed V_{TAS}. In this conventional case, the path angle is set as a control variable that controls altitude directly. The second case optimizes three state variables: altitude H, true airspeed V_{TAS}, and path angle γ. This settings enable aircraft dynamics to be considered in the optimization calculations. In the previous literatures, few studies have examined DP trajectory optimization in consideration of aircraft dynamics. The optimization problem for H, V_{TAS} and γ aims to provide smooth optimal trajectories that serve as more appropriate reference trajectories for aircraft operators. In the following subsection, by focusing only on aircraft aerodynamics and propulsion performance, a longitudinal optimal trajectory is designed for a passenger aircraft as an example application of PLA-DP method.

6.4.1 Statement of trajectory optimization problem

The objective function is defined as fuel consumption from climb to descent, which is given as the time integral of fuel flow $\mu(t)$. Although flight time is another important concern, only fuel consumption is considered in this numerical example. It's noted that flight time can be easily included in the objective function if needed. The problem settings for this example, such as the terminal free, fixed initial and final states, equality

and inequality constraints on states and controls, define the following optimal control problem.

Optimal control problem

$$\text{Minimize} \quad J = \int_{t_0}^{t_f} \mu(t)dt + \phi(\boldsymbol{x}(t_f), t_f) \tag{6.18}$$

$$\text{subject to} \quad \psi_0(\boldsymbol{x}(t_0)) = 0 \tag{6.19}$$

$$\psi_f(\boldsymbol{x}(t_f)) = 0 \tag{6.20}$$

$$C_{eq}(\boldsymbol{x}(t), \boldsymbol{u}(t), t) = 0 \tag{6.21}$$

$$C_{ineq}(\boldsymbol{x}(t), \boldsymbol{u}(t), t) \leq 0 \tag{6.22}$$

Equation of motion and kinematic model

Generally, the motion of an aircraft is expressed by six-degrees-of-freedom (6DOF) equations of motion, although in the trajectory optimization problems, an aircraft is often approximated as a point mass. The motion of an aircraft (without the wind effect) may be described with three-degrees-of-freedom (3DOF) equations using point mass approximation.

$$\frac{d\theta}{dt} = \frac{1}{(R_0 + H)\cos\phi} V_{TAS} \cos\gamma \tag{6.23}$$

$$\frac{d\phi}{dt} = \frac{1}{R_0 + H} V_{TAS} \cos\gamma \tag{6.24}$$

$$\frac{dH}{dt} = V_{TAS} \sin\gamma \tag{6.25}$$

$$m\frac{dV_{TAS}}{dt} = T - D - mg\sin\gamma \tag{6.26}$$

$$mV\frac{d\gamma}{dt} = L - mg\cos\gamma \tag{6.27}$$

The polar coordinates are transformed from latitude and longitude (ϕ, θ) to down range and cross range (ξ, η) as illustrated in Fig. 6.7.

Furthermore, the independent variable is transformed from time t into flight range x using the equation below.

$$\frac{dx}{dt} = V_{TAS} \cos\gamma \tag{6.28}$$

The governing equation and aerodynamic model used in the optimal control problem are given as follows:

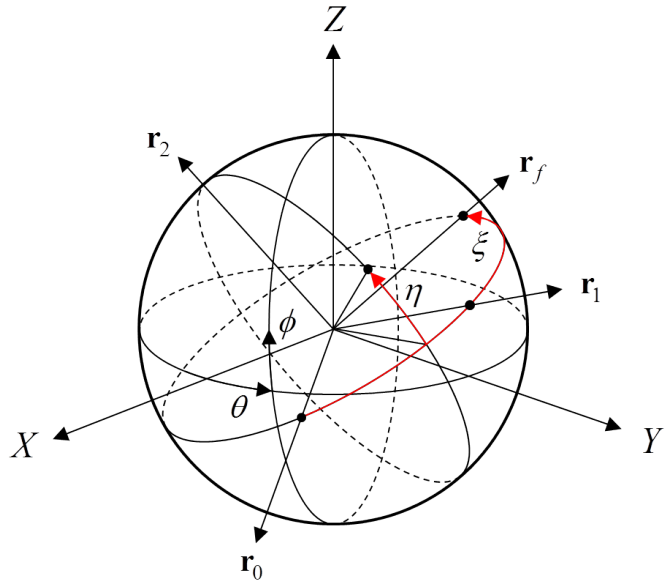

Fig.6.7 Definition of the great-circle route and lateral deviations

Governing equation

$$\frac{dH}{dx} = \tan\gamma \tag{6.29}$$

$$\frac{dV_{TAS}}{dx} = \frac{T - D - mg\sin\gamma}{mV_{TAS}\cos\gamma} \tag{6.30}$$

$$\frac{d\gamma}{dx} = \frac{L - mg\cos\gamma}{mV_{TAS}^2\cos\gamma} \tag{6.31}$$

Aerodynamic model

$$L = \frac{1}{2}\rho V_{TAS}^2 S C_L \tag{6.32}$$

$$D = \frac{1}{2}\rho V_{TAS}^2 S C_D \tag{6.33}$$

$$C_D = C_{D0} + kC_L^2 \tag{6.34}$$

■ OCP1 (Optimization for H and V_{TAS})

The state and control variable vector are defined as follows:

$$\boldsymbol{x} = [\, V_{TAS},\ H \,]^{\mathrm{T}} \tag{6.35}$$

$$\boldsymbol{u} = [\, T,\ \gamma \,]^{\mathrm{T}} \tag{6.36}$$

Altitude and velocity are directly controlled by the path angle and thrust, respectively. In this case, the path angle is assumed to be constant over the transition between two grid points; therefore, discontinuous change

is tolerated at each stage for the independent variable. All grid points can be connected exactly, without any errors caused by the dimensional difference problem, because the number of control variables equals that of state variables in this system.

OCP1 is defined as the minimization of fuel consumption denoted by the following optimality conditions subject to equality constraints, inequality constraints and boundary conditions. Note that the ORF is given as a function of the independent variable x and state variables V_{TAS} and H. The subscript "TAS" is omitted in the following formula for the simplicity.

Optimality conditions

$$J_{opt_k}(V(j_{1_k}),H(j_{2_k}),x(k)) = \min\left[\int_{x_k}^{x_{k+1}} \frac{\mu}{V\cos\gamma}dx + J_{opt_{k+1}}(V(j_{1_{k+1}}),H(j_{2_{k+1}}),x(k+1))\right] \tag{6.37}$$

Independent variable interval

-Down range : $x_0 \le x \le x_f$

Equality constraints

-State equation : $d\boldsymbol{x}/dx = \boldsymbol{f}(\boldsymbol{x},\boldsymbol{u})$

Inequality constraints on state variables

-Altitude : $H_{\min} \le H \le H_{\max}$

-Velocity : $V_{TAS,\ \min} \le V \le V_{TAS,\ \max}$

-Mach number : $M(V_{TAS}) \le M_{\mathrm{MO}}$

Inequality constraints on control variables

-Thrust : $T \le T_{\max}$

Boundary conditions on state variables

-Initial conditions : $H(t_0) = H_0, \quad V_{TAS}(t_0) = V_{TAS,\ 0}$

-Terminal conditions : $H(t_f) = H_f, \quad V_{TAS}(t_f) = V_{TAS,\ f}$

In the transition calculation between the quantized grid points, the state variable value is represented by the average of two grid point values, and the small change of the state variable is approximated by the following difference equations. The control variable value is approximated to be constant by a zeroth-order hold.

$$\begin{aligned}
&\overline{V_{TAS}} = \left\{V_{TAS}(j_{1_k}) + V_{TAS}(j_{1_{k+1}})\right\}/2, && \overline{H} = \left\{H(j_{2_k}) + H(j_{2_{k+1}})\right\}/2 \\
&\Delta V_{TAS} = V_{TAS}(j_{1_{k+1}}) - V_{TAS}(j_{1_k}), && \Delta H = H(j_{2_{k+1}}) - H(j_{2_k}) \\
&T^\circ = T(x),\ x \in [x_k, x_{k+1}], && \gamma^\circ = \gamma(x),\ x \in [x_k, x_{k+1}]
\end{aligned}$$

These assumptions lead the control variables in the transition, which are used to calculate ORF value.

$$T^\circ = D(\overline{V_{TAS}},\overline{H}) + mg\sin\gamma^\circ + m\overline{V_{TAS}}\cos\gamma^\circ\frac{\Delta V_{TAS}}{\Delta x} \tag{6.38}$$

$$\gamma^\circ = \tan^{-1}\frac{\Delta H}{\Delta x} \tag{6.39}$$

Note that,

$$D(\bar{V_{TAS}},\bar{H}) = \frac{1}{2}\rho(\bar{H})\bar{V_{TAS}}^2 S\left[C_{D0} + k\left(\frac{mg\cos\gamma^\circ}{\rho(\bar{H})\bar{V_{TAS}}^2 S/2}\right)^2\right] \tag{6.40}$$

■ **OCP2 (Optimization for H, V_{TAS} and γ)**

The flight path angle γ is added to the state variable vector. The state variable and control variable are defined as follows:

$$\boldsymbol{x} = [\ V_{TAS},\ \gamma,\ H\ ]^{\mathrm{T}} \tag{6.41}$$

$$\boldsymbol{u} = [\ T,\ C_L\ ]^{\mathrm{T}} \tag{6.42}$$

This problem has a one dimensional difference because there are two control variables and three state variables.

OCP2 is defined as the minimization of fuel consumption denoted by the following optimality conditions. The ORF is given as a function of the independent variable x and state variables V_{TAS}, γ and H. Inequality constraints are added to the state variable γ.

Optimality conditions

$$J_{opt_k}(V(j_{1_k}),\gamma(j_{2_k}),H(j_{3_k}),x(k)) = \min\left[\int_{x_k}^{x_{k+1}} \frac{\mu}{V\cos\gamma}dx + J_{opt_{k+1}}(V(j_{1_{k+1}}),\gamma(j_{2_{k+1}}),H,x(k+1))\right] \tag{6.43}$$

Independent variable interval

-Down range : $x_0 \le x \le x_f$

Equality constraints

-State equation : $d\boldsymbol{x}/dx = \boldsymbol{f}(\boldsymbol{x},\boldsymbol{u})$

Inequality constraints on state variables

-Altitude : $H_{\min} \le H \le H_{\max}$

-Velocity : $V_{TAS,\ \min} \le V \le V_{TAS,\ \max}$

-Mach number : $M(V_{TAS}) \le M_{\mathrm{MO}}$

-Path angle : $\gamma_{\min} \le \gamma \le \gamma_{\max}$

Inequality constraints on control variables

-Thrust : $T \le T_{\max}$

Boundary conditions on state variables

-Initial conditions : $H(t_0) = H_0,\quad V_{TAS}(t_0) = V_{TAS,\ 0},\quad \gamma(t_0) = free$

-Terminal conditions : $H(t_f) = H_f,\quad V_{TAS}(t_f) = V_{TAS,\ f},\quad \gamma(t_f) = free$

In the transition calculation, the state and control variables are treated in the same manner as OCP1.

$\bar{V_{TAS}} = \left\{V_{TAS}(j_{1_k}) + V_{TAS}(j_{1_{k+1}})\right\}/2,\quad \bar{\gamma} = \left\{\gamma(j_{2_k}) + \gamma(j_{2_{k+1}})\right\}/2,\quad \bar{H} = \left\{H(j_{3_k}) + H\right\}/2$

$\Delta V_{TAS} = V_{TAS}(j_{1_{k+1}}) - V_{TAS}(j_{1_k}),\quad \Delta\gamma = \gamma(j_{2_{k+1}}) - \gamma(j_{2_k}),\quad \Delta H = H - H(j_{3_k})$

$T^\circ = T(x),\ x \in [x_k, x_{k+1}],\quad C_L^\circ = C_L(x),\ x \in [x_k, x_{k+1}]$

The control variables are

$$T^{\circ} = D(\bar{V_{TAS}}, \bar{H}) + mg\sin\bar{\gamma} + m\bar{V_{TAS}}\cos\bar{\gamma}\frac{\Delta V_{TAS}}{\Delta x} \tag{6.44}$$

$$C_L^{\circ} = \frac{L(\bar{V_{TAS}}, \bar{\gamma})}{\rho(\bar{H})\bar{V_{TAS}}^2 S/2} \tag{6.45}$$

Note that,

$$D(\bar{V_{TAS}}, \bar{H}) = \frac{1}{2}\rho(\bar{H})\bar{V_{TAS}}^2 S\left[C_{D0} + kC_L^{\circ 2}\right] \tag{6.46}$$

$$L(\bar{V_{TAS}}, \bar{\gamma}) = mg\cos\bar{\gamma} + m\bar{V_{TAS}}^2\cos\bar{\gamma}\frac{\Delta\gamma}{\Delta x} \tag{6.47}$$

Although velocity V_{TAS} and flight path angle γ are controlled directly by the two control variables T and C_L, altitude H cannot be controlled directly. Consequently, the feasible solution is distributed on the $V_{TAS} - \gamma$ surface, while the feasible H is not assigned on the grid points. The feasible points are derived analytically along the H axis. ORF value at the point is given by linear interpolation to resolve this dimensional difference problem.

6.4.2 Aircraft performance model

The performance of the aircraft is calculated by the BADA (Base of Aircraft Data) model, which is developed and maintained by the European Organization for the Safety of Air Navigation (EUROCONTROL) [30]. BADA includes parametric models for multiple aircraft, such as an aerodynamic model, C_{D0} and k, maximum thrust model, and fuel flow model, which are used for performance calculations. The maximum operating altitude (HMO), are also provided. The fuel flow calculated by the BADA model has been evaluated with reference to an airliner's on-board flight data, indicating that the model has sufficient accuracy for trajectory optimization calculations [31]. Fig. 6.8 shows the specific range (SR), which represents the flight range per unit mass of fuel consumption, calculated by the BADA model and the reference mass of a passenger aircraft operated in Japanese domestic airspace. The maximum SR, 150 [m/kg], is achieved at the corner of the flight envelope where Mach number and altitude reach maximum values of $M = 0.87$ and $H = 43,100$ [ft].

6.4.3 Numerical example

Trajectory optimization is implemented for the selected aircraft using the BADA aircraft performance model. The International Standard Atmosphere (ISA) is used as the atmospheric model. An isogrid system is defined for the independent variable and state variables. The numerical settings of the grid resolution for the independent variable and state variables, inequality constraints, and boundary conditions are defined.

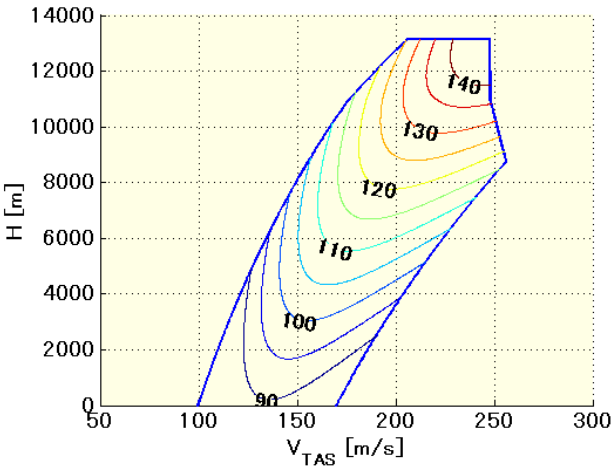

Fig.6.8 Specific range [m/kg]

Independent variable interval

-Down range	:	$x_0 = 0$ [m],	$x_f = 866.3 \times 10^3$ [m],	$\Delta x = 28.88 \times 10^3$ [m]

Inequality constraints on state variables

-Altitude	:	$H_{\min} = 3,000$ [m],	$H_{\max} = 13,000$ [m],	$\Delta H = 100$ [m]
-Velocity	:	$V_{TAS,\ \min} = 140$ [m/s],	$V_{TAS,\ \max} = 260$ [m/s],	$\Delta V_{TAS} = 4$ [m/s]
-Path angle	:	$\gamma_{\min} = -5$ [deg],	$\gamma_{\max} = 5$ [deg],	$\Delta\gamma = 0.2$ [deg]

Inequality constraints on control variables

-Mach number	:	$M_{\mathrm{MO}} = 0.84$

Boundary conditions

-Initial conditions	:	$H_0 = 3,000$ [m],	$V_{TAS,\ 0} = 140$ [m/s]
-Terminal conditions	:	$H_f = 3,000$ [m],	$V_{TAS,\ f} = 140$ [m/s]

The optimal trajectory results for OCP1 and OCP2 are depicted in Figs. 6.9 to 6.14 and Figs. 6.15 to 6.20, respectively. The optimal cruise altitude and true airspeed are 13000 [m] and 244 [m/s] in both results. In OCP1, an unfavorable oscillation occurs in the optimal trajectory of altitude and airspeed. This oscillation which is known as periodic flight is an optimal maneuver for extending the flight range for a given amount of fuel [44]. Periodic optimal flight is related with two major factors: the engine performance model and atmospheric model [8]. As long as these models have the potential to generate periodic flight, a smooth optimal trajectory including steady horizontal flight cannot be obtained, even if a finer calculation grid is used. This optimization does not represent a difficulty caused by the dimensional difference problem in the calculation process; however, the obtained results are inadequate for use as a reference trajectory in actual aircraft operation. In consideration of its usability for aircraft operators, an optimal trajectory should be based on the actual motion represented by aircraft dynamics. The fuel consumption of the OCP1 trajectory is

derived as 6,525 [kg].

Conversely, in OCP2, a smooth trajectory can be obtained for altitude and true airspeed by including path angle as one of the state variables, which can be directly controlled by setting lift coefficient as a control variable. Because the aircraft performance model and atmospheric model used in OCP2 are the same as those used in OCP1, an optimal periodic trajectory is inevitably obtained. However, as illustrated in Figs. 6.15, 6.16 and 6.17, smooth trajectories may by derived by adding a term to suppress the rapid change of path angle into the objective function denoted by Eq. (6.18). The altitude trajectory in the climb phase is connected smoothly to the cruise phase by the rapid increase of airspeed. In the descent phase, the airspeed is decreased moderately from a cruise speed of 244 [m/s] using idle thrust to save on fuel consumption with a high lift to drag ratio. This smooth trajectory is ideal for practical use and may be applied as a reference trajectory. The fuel consumption for the OCP2 is derived as 6,625 [kg].

■ OCP1 (Optimization for H and V_{TAS})

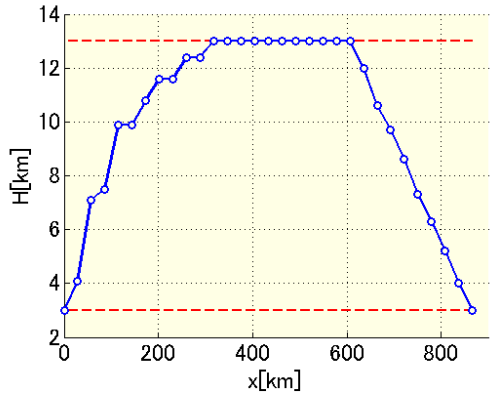

Fig.6.9 Altitude

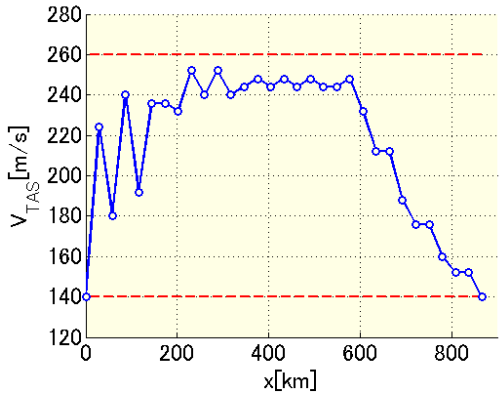

Fig.6.10 True airspeed

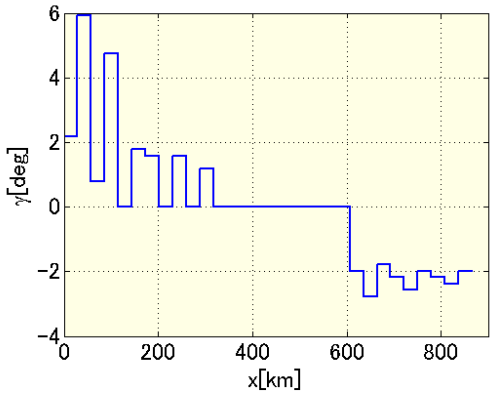

Fig.6.11 Path angle

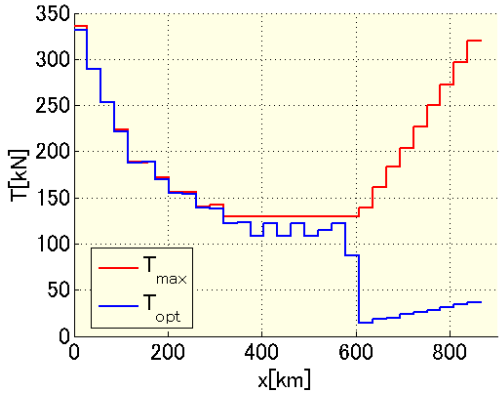

Fig.6.12 Thrust

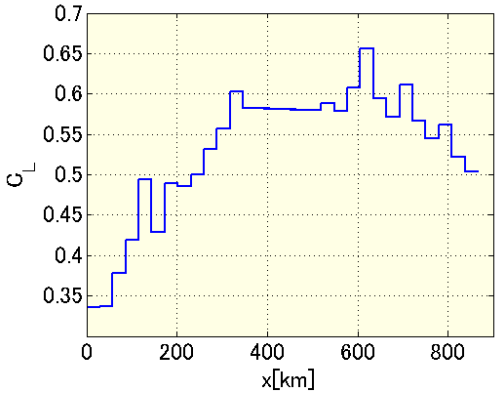

Fig.6.13 Lift coefficient

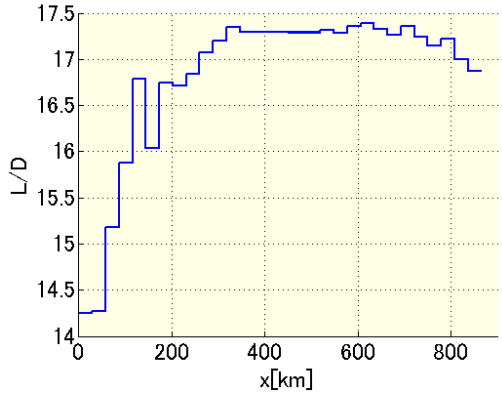

Fig.6.14 Lift to Drag ratio

Fuel consumption : $6,525$ [kg]

Flight time : $4,086$ [s]

■ OCP2 (Optimization for H, V_{TAS} and γ)

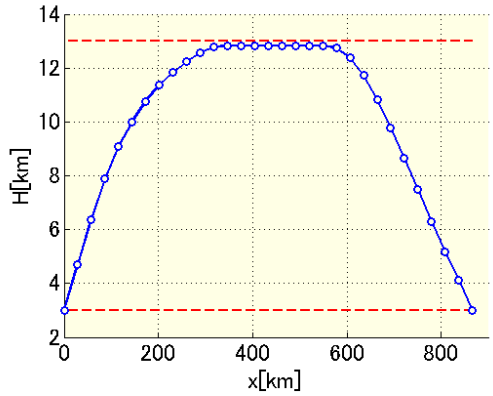

Fig.6.15 Altitude

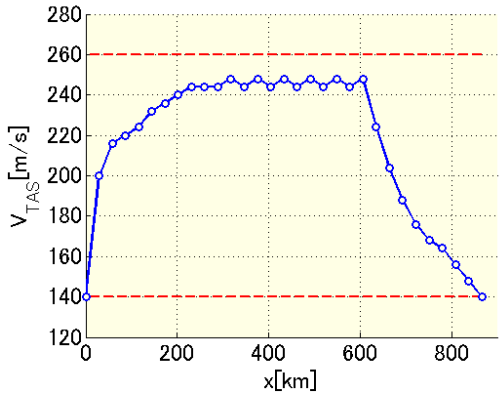

Fig.6.16 True airspeed

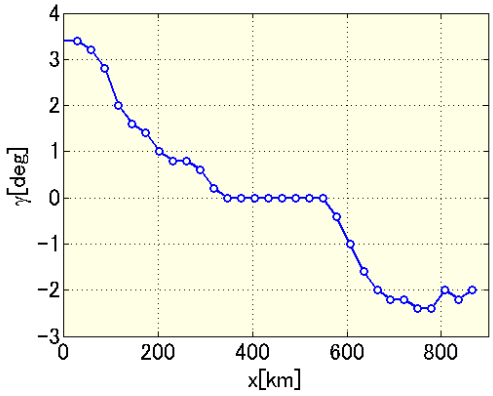

Fig.6.17 Path angle

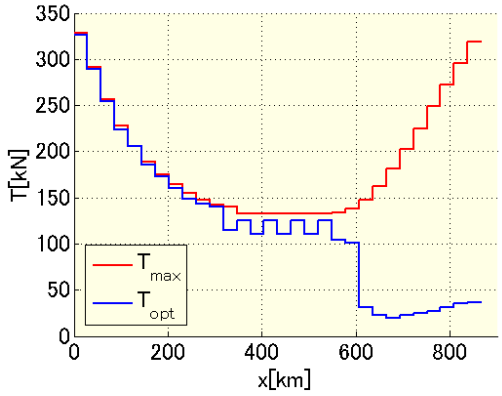

Fig.6.18 Thrust

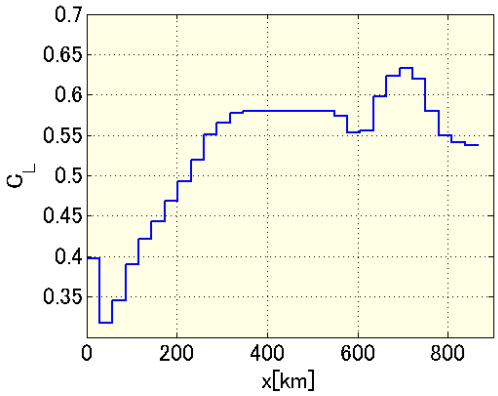

Fig.6.19 Lift coefficient

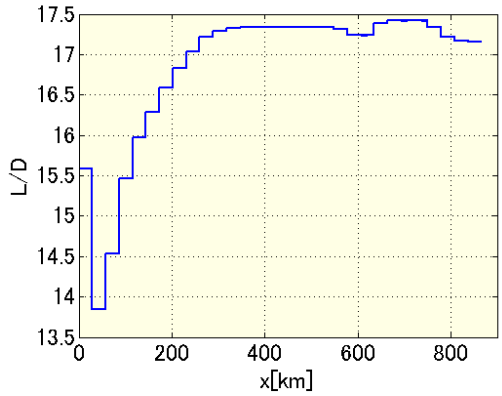

Fig.6.20 Lift to Drag ratio

Fuel consumption : $6,625$ [kg]

Flight time : $4,068$ [s]

6.5 Summary

This chapter has proposed the PLA-DP approach to cope with the dimensional difference problem, which is a major hindrance in the application of DP. This problem occurs in cases where the degrees of freedom for the control variables are insufficient to realize the state transitions between grid points. An error caused by the difference between the feasible point and grid points makes it difficult to obtain accurate optimal trajectories by DP and limits its scope of application. PLA-DP method is capable to resolve this problem departing from the concept of combinatorial optimization, i.e. expressing the genuine optimal solution as a series of feasible points which exist between the quantized grid points.

The applicability of PLA-DP method has been demonstrated by designing a longitudinal fuel minimal trajectory for single passenger aircraft. Although altitude and velocity optimization did not cause quantization error in the transition calculation between quantized grid points, unfavorable vibration occurred on the obtained optimal trajectory. This inconvenience was resolved by optimization in which altitude, velocity, and path angle were set as state variables and by considering aircraft dynamics explicitly. Adding flight path angle into state variables enabled to introduce a term to suppress the unfavorable oscillation in the objective function. The smooth optimal trajectory designed by PLA-DP method will be of use to develop the NG-FMS and will encourage the realization of more efficient and highly developed ATM operations in the foreseeable future. This newly proposed PLA-DP method will also encourage more active utilization of DP in the trajectory optimization research.

Chapter. 7

Conclusion

An easy to handle numerical optimization method has been demanded in the guidance and control system design field. In the research and development, several conditions such as providing an optimal solution accurate enough to be applied to the practical usages with a reasonable computational time, enduring many analyses with the various design conditions, and unnecessity of trial-and-error analyses are required to establish such a versatile optimization method. This thesis focused on dynamic programming as a promising numerical optimization method and demonstrated its feasibility and applicability into the optimal control problems through practical application examples.

The characteristic of dynamic programming in the engineering aspects are listed in the following.

Characteristics of dynamic programming

Advantages

- Global optimality
- No iterative calculations -Computational time may be estimated in advance
- Easy to handle inequality constraints on state variables and control variables
- Easy to adapt for changing design conditions, models and parameters
- Simple programming code

Disadvantages

- Curse of dimensionality
- Menace of the expanding grid

Dynamic programming has many favorable advantages the other methods do not have. These advantages make dynamic programming worthwhile in a point of practical applications to the optimal control problems. Nevertheless, the DP's scope of application still remains unexpanded due to the two major drawbacks, the

"Curse of dimensionality" and the "Menace of the expanding grid." Few researches have been implemented to resolve these drawbacks in recent years in spite that the computational capability of modern computers is rapidly increasing by the high-performance processors and large-scale parallel computation technology. The DP's scope of application to the practical usages is expected to be enlarged by those trends in modern computers. For those reasons, the limit of the scope should be pursued to enhance the possibility of dynamic programming. This thesis clarified the limit of DP's scope of possibility and evaluated its applicability to the practical engineering problems. The applications of two novel methods, MS-DP and PLA-DP, to the practical problems have been proposed.

As the first application, dynamic programming was applied to an optimal trajectory design problem for JAXA's next generation SST to analyze its operational feasibility. Normal DP algorithm could be easily applied to this problem since it does not include any difficulty arising from the drawbacks of DP. As the second application, an usability of flight trajectory optimization tool developed with dynamic programming has been introduced in the Air Traffic Management (ATM) research. The potential benefits of current Japanese airspace were quantitatively evaluated in the application example by using the optimization tool and the passenger aircraft's actual position data recorded by Secondary Surveillance Radar (SSR). Multiple aircraft must be analyzed in terms of operational efficiency; therefore, it was necessary to devise the DP algorithm to reduce the computational time. The proposed MS-DP method worked quite effectively to save the computational time in the application problem. The third example is passenger aircraft's reference trajectory design problem. To design a smooth optimal trajectory, the second drawback of DP, "Menace of the expanding grid" arises in the defined optimal control problem. The difficulty has been resolved by the proposed PLA-DP method and its validity and availability were demonstrated. The accuracy of an aircraft performance model which is essential to derive the fuel consumption was evaluated using airliner flight data to present the feasibility of the trajectory optimization analysis. The analysis result shows that dynamic programming is capable of designing a smooth optimal trajectory which may be beneficial for research and developments for the next-generation FMS.

The obtained findings are listed in each chapter below.

Chapter. 4:

Trajectory Optimization Analysis for Operational Feasibility Study of Supersonic Transport

- A trajectory optimization tool was developed for the purpose of analyzing a feasibility of JAXA's next generation supersonic civil transport.
- The developed tool led a result that the supersonic flight can save flight time by 3 hours 19 minutes with an additional fuel consumption of 680 [kg] by comparing to a subsonic flight gained by the same SST model.
- It has been suggested that the JAXA's SST model has sufficient possibility to be realized as an economical future air transport by showing that the flight time can be halved with additional 50 % of fuel

consumption in the comparison to a conventional subsonic passenger aircraft.

- An optimal trajectory has been easily obtained by utilizing the advantages of dynamic programming in the problem where the “curse of dimensionality” nor “menace of the expanding grid” does not arise.
- It can be stated that the practical application not only to a SST model but to a subsonic jet aircraft introduced in this chapter is one of the most favorable applications in the point of utilization of dynamic programming.

Chapter. 5:

Quantitative Operational Flight Efficiency Analysis of Passenger Aircraft Scheduled Flight

- Demonstrating the capability of newly proposed MS-DP method which is the main purpose of this chapter has been achieved by solving a large-scale problem for multiple aircraft.
- As a result of analyzing 256 flight cases, possible savings of fuel and flight time are estimated as 362 [kg] and 202 [s] respectively.
- These results have quantitatively revealed potential benefits which might be obtained by improving the current air traffic management system, and have encouraged further research into the Japanese CARATS CNS/ATM modernization program.
- The MS-DP method substantially contributed to solving a large-scale optimization problem for multiple aircraft in a reasonable computational time using a standard personal computer.

Chapter. 6:

Dynamic Programming Trajectory Optimization by Piecewise Linear Approximation

- The PLA-DP method which was proposed to alleviate the “Menace of the expanding grid” has a capability of providing a feasible solution close to a genuine optimal solution.
- The PLA-DP method provides accurate solutions even if its accuracy is affected by state variables’ quantization.
- Unfavorable oscillation occurs in the optimization of altitude and velocity. This oscillation has been resolved by applying the newly proposed PLA-DP method to the optimization problem where altitude, velocity and path angle were set as state variables and aircraft dynamics were explicitly considered.
- The method is of great value in that it can provide an optimal trajectory as a series of feasible points not only of quantized grid points.

Appendix. A:

Accuracy Evaluation for an Aircraft Performance Model with Airliner Flight Data

- The results of comparison have shown that the error between the BADA model and flight data is within plus or minus 5 [%].
- Although the accuracy deteriorates relatively in the climb and descent phases, the influence on the

error for whole flight time is not very significant because the cruise phase, which has high accuracy, constitutes a large part of the flight.

- The BADA model has sufficient accuracy to calculate the fuel consumption for general flight trajectory and it is of great use to various analyses for the research of air traffic management systems.

At the end of this thesis, the main contributions of this research are described.

This research focused on dynamic programming as an easy to handle and promising numerical optimization method in the engineering optimal control research field. Its versatility and applicability have been demonstrated by the three practical application examples. The combinatorial optimization algorithm which is a normal algorithm of DP has been applied to the optimal trajectory design problem of JAXA supersonic civil transport. It has been shown that the optimal flight trajectory can be easily obtained as a series of quantized grid points by using many powerful advantages of dynamic programming. The developed optimization tool has contributed to evaluate the operational feasibility of JAXA SST concept model.

Two novel methods, “Moving Search space Dynamic Programming (MS-DP)” and “Piecewise Linear Approximation Dynamic Programming (PLA-DP)”, have been proposed to resolve the “curse of dimensionality” and the “menace of the expanding grid” which are the two major drawbacks of DP. Their capability has been presented by applying them to the two practical engineering problems.

The MS-DP method has made a remarkable contribution to reduce computational burden in a large-scale optimization problem. Many worthwhile findings could be gained in the quantitative operational flight efficiency analysis where the large-scale optimization problem must be solved efficiently for multiple aircraft. Those findings are of great use to reveal potential benefits of current Japanese airspace and to encourage further research into the CARATS CNS/ATM modernization program.

The PLA-DP method has discovered the possibility of resolving the “menace of the expanding grid”. A trajectory optimization problem where one dimensional difference is caused by three state variables and two control variables has been successfully solved by the method. The optimal trajectory has been introduced as a series of feasible points which exactly satisfy the governing equation. The results have shown that the PLA-DP method has a capability to design an aircraft dynamics-added optimal trajectory which can be used in the developments for the next-generation FMS.

The utilization of dynamic programming has been limited by the technical challenges for a long period regardless of many favorable advantages the other methods do not have. This research has proposed two promising and powerful methods which may resolve those challenges, and has made a great contribution to enlarge DP’s scope of application by solving practical trajectory optimization problems which include actual model, data and constraints given by the various design requirements. The great potential of dynamic programming utilization has been indicated by the proposed methods and valuable new findings in the practical application examples.

Appendix A

Accuracy Evaluation for an Aircraft Performance Model with Airliner Flight Data

In the flight trajectory optimization of passenger aircraft, the performance model must have sufficient accuracy to make the analysis meaningful. The BADA model developed and maintained by a research group of EUROCONTROL is widely used in the research community of air traffic management. [21, 22, 46, 47, 48, 49, 50, 51, 52, 53] The accuracy of the BADA model is investigated in some papers, [51, 52, 53] and one of them suggests that fuel consumption derived with the BADA model has high accuracy in the cruise phase. [53] This paper evaluates the accuracy of the aircraft performance model by comparing calculated fuel flow with the actual flight data recorded by airliner's quick access recorder (QAR). Total fuel consumption (TFC), which is a time integral of the fuel flow, is also compared.

A.1 Airliner flight data and BADA model

A.1.1 Flight data

As shown in Table A.1, 18 cases of flight data were analyzed. The flight data consist of the same type of modern large passenger aircraft, for three domestic routes and one international route. HND, FUK, CTS, OKA, SFO indicate each airport name under the International Air Transport Association (IATA) code and correspond to Haneda (Tokyo), Fukuoka, New Chitose (Sapporo), Naha (Okinawa) and San Francisco, respectively. The 18 flight cases consist of: eight cases between Haneda and Fukuoka, four cases between Haneda and Sapporo, four cases between Haneda and Okinawa and two cases between Haneda and San Francisco.

Table.A.1 The 18 flight cases of flight data

	Year/Month	Departure/Destination	Data recorded time (UTC)	
			Initial time	Terminal time
1	2011/8	HND / FUK	5:07	6:17
2	2011/8	FUK / HND	7:28	8:37
3	2011/10	HND / FUK	8:23	9:45
4	2011/10	FUK / HND	10:57	12:08
5	2011/12	HND / FUK	1:32	3:03
6	2011/12	FUK / HND	4:12	5:07
7	2011/12	HND / FUK	9:37	11:08
8	2011/12	FUK / HND	12:12	13:13
9	2011/8	HND / CTS	8:01	9:07
10	2011/8	CTS / HND	5:21	6:26
11	2011/10	HND / CTS	6:57	7:53
12	2011/10	CTS / HND	9:16	10:27
13	2011/8	HND / OKA	4:37	11:11
14	2011/8	OKA / HND	8:05	10:00
15	2011/10	HND / OKA	4:40	7:05
16	2011/10	OKA / HND	8:17	10:04
17	2011/10	HND / SFO	15:23	23:28
18	2011/10	SFO / HND	1:59	12:24

Initial and terminal times are determined to limit the scope of evaluation to a clean configuration; that is, take-off and landing configurations are excluded from the analysis. Each flight data consist of 13 items such as time, calculated gross weight of the aircraft, longitude, latitude, wind direction and speed, true air speed V_{TAS}, indicated air speed V_{IAS}, vertical velocity V_V, Mach number, QNE pressure altitude, static air temperature and fuel flow. Each recorded variable is used for the calculation every second.

A.1.2 BADA model

The BADA model is an aircraft performance model developed and maintained by the European Organization for the Safety of Air Navigation (EUROCONTROL) through active cooperation with aircraft manufacturers and operating airlines. The information and data contained in BADA is designed for use in aircraft trajectory simulations and predictions.

BADA consists of two components:[30]

(1) Model specifications:

Theoretical fundamentals are provided in form of generic polynomial expressions to calculate aircraft performance parameters. The motion model which is used within BADA is a so-called total energy model (TEM). It can be considered as a reduced point-mass model.

(2) Datasets:

A dataset for a given aircraft contains specific values of the coefficients in the model specification, which particularize the BADA model for a specific aircraft type.

A.2 Fuel flow calculation

Fuel flow is calculated using the aerodynamic model and fuel flow model defined in BADA 3.9. Thrust is calculated by substituting flight data variables into equations of the aircraft motion.

A.2.1 Thrust

Thrust is estimated from the acceleration along the wind axis. Only the velocity changes which are directly related to energy are considered, but the velocity direction change is assumed to be negligible. The equation of motion with point mass approximations is given as follows.

$$m\frac{dV_{ES}}{dt}\cos(\gamma_a-\gamma)\cos(\psi_a-\psi)=F-D-mg\sin\gamma_a \tag{A.1}$$

Two kinds of velocity V_{TAS} and V_{ES} are used in this equation. V_{ES} represents an internal velocity considered in the Earth-centered Earth-fixed (ECEF) coordinate system. This inertial velocity is required to derive the acceleration of aircraft which excludes the influence of wind changes. The direction of each velocity is given by the path angle γ and γ_a, and azimuth angle ψ and ψ_a as shown in Fig. A.1.

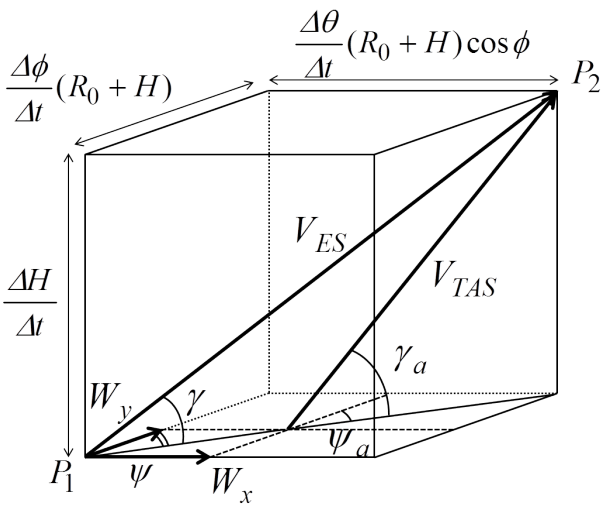

Fig.A.1 Relationship of γ, ψ and V

Although an aircraft has the acceleration along the direction of V_{ES}, the thrust force is in the direction of V_{TAS}. Therefore, the left-hand side of Eq. (A.1) includes cosines of $(\gamma_a - \gamma)$ and $(\psi_a - \psi)$. Path angle γ, γ_a and the inertial velocity V_{ES} can be calculated from vertical velocity V_V, V_{GS} and V_{TAS} included in the flight data.

$$\gamma = \tan^{-1} \frac{V_V}{V_{GS}} \tag{A.2}$$

$$\gamma_a = \tan^{-1} \frac{V_V}{V_{TAS}} \tag{A.3}$$

$$V_{ES} = \frac{V_{GS}}{\cos\gamma} \tag{A.4}$$

A central difference approximation is applied to gain the inertial acceleration dV_{ES}/dt.

$$\frac{dV_{ES}}{dt}(t_i) = \frac{\Delta V_{ES}}{\Delta t} = \frac{V_{ES}(t_{i+1}) - V_{ES}(t_{i-1})}{2\Delta t} \tag{A.5}$$

A.2.2 Atmospheric model

Atmospheric pressure is obtained from the QNE pressure altitude H in the flight data using the following equation defined in the International Standard Atmosphere (ISA) model.

$H > H_1$:

$$p = p_1 \exp\left[-\frac{g}{RT}\left(H - \frac{R_0 H_1}{R_0 + H_1}\right)\right] \tag{A.6}$$

$$T = T_1 \tag{A.7}$$

$H \leq H_1$:

$$p = p_0 \left(\frac{T}{T_0}\right)^{-g/Rb} \tag{A.8}$$

$$T = T_0 + bH \tag{A.9}$$

Air density is gained by substituting this atmospheric pressure and static air temperature T_s of the flight data into the following equation.

$$\rho = \frac{p}{RT_S} \tag{A.10}$$

A.2.3 BADA aerodynamic model

The lift and drag forces which act on the body are expressed with the coefficients C_L and C_D as follows.

$$L = \frac{1}{2}\rho V^2 S C_L \tag{A.11}$$

$$D = \frac{1}{2}\rho V^2 S C_D \tag{A.12}$$

The lift coefficient is derived by assuming the aircraft in steady flight with small bank angle.

$$C_L = \frac{2mg\cos\gamma_a}{\rho V^2 S} \tag{A.13}$$

The relationshipbetween C_L and C_D is defined with two coefficients as a mathematical model.

$$C_D = C_{D0} + C_{D2}C_L^2 \tag{A.14}$$

C_{D0} and C_{D2} are parasite drag and induced drag coefficients. These coefficients are modeled independent from Mach number or angle of attack.

Thrust of the aircraft can be calculated by substituting drag into Eq. (A.1).

A.2.4 BADA fuel flow model

Nominal fuel flow:

The fuel flow for nominal flight conditions f_{nom} is defined as the product of the thrust F and coefficient of thrust specific fuel consumption η as in Eq. (A.15).

$$f_{nom} = \eta \times F \tag{A.15}$$

η is a function of true airspeed, V_{TAS}.

$$\eta = C_{f1} \times \left(1 + \frac{V_{TAS}}{C_{f2}}\right) \tag{A.16}$$

Cruise fuel flow:

Cruise fuel flow f_{cr} is given with a cruise fuel flow factor, C_{fcr}.

$$f_{cr} = \eta \times F \times C_{fcr} \tag{A.17}$$

Minimum fuel flow:

Minimum fuel flow f_{min}, corresponding to idle thrust descent conditions, is specified as a function of altitude above sea level, H.

$$f_{\min} = C_{f3}\left(1 - \frac{H}{C_{f4}}\right) \tag{A.18}$$

The constant parameters for the type of aircraft are given in the operations performance files (OPF). Fuel flow in the climb and cruise is obtained from Eqs. (A.15) and (A.17), respectively. For the descent phase, including idle thrust conditions, the larger value of Eqs. (A.15) and (A.18) is selected.

A.2.5 Filtering

Since ground speed V_{GS} in the flight data contains measurement noise, the fuel flow calculated by time derivative of the velocity amplifies high frequency noise. Fig. A.2 is an example of calculated fuel flow and

flight data comparison for flight case 1. It can be seen that the calculated fuel flow contains high frequency noise due to time derivative of V_{GS}.

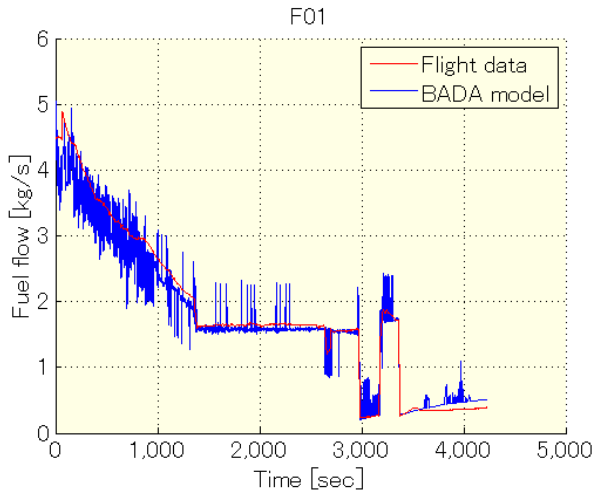

Fig.A.2 Calculated fuel flow without eliminating the noise

A zero phase finite impulse response (FIR) low pass filter is applied to eliminate the high frequency noise of V_{GS}, where the cutoff frequency is set to 0.025 [Hz]. The gain and phase frequency characteristics of the filter are shown in Fig. A.3. The higher frequency signal is reduced by one-thousandth and the lower signal passes through as it is. The x-axis is normalized by the Nyquist frequency defined as half of sampling frequency. The flight data are recorded every second, hence the Nyquist frequency is 0.5 [Hz]. Therefore, the normalized cutoff frequency is 0.05.

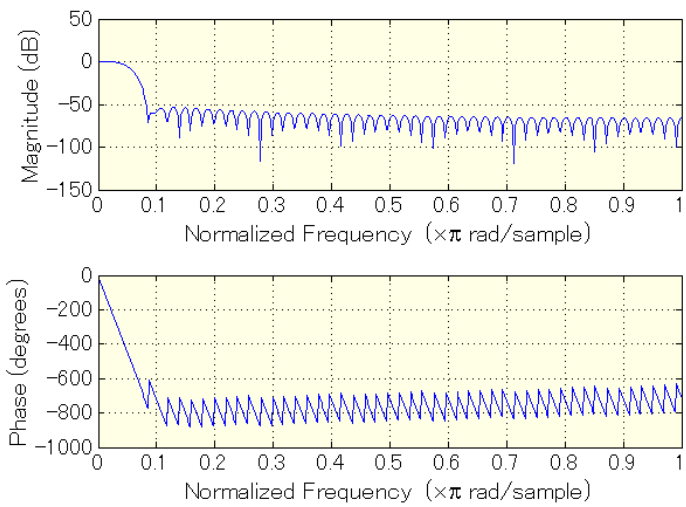

Fig.A.3 Frequency characteristics of a zero phase FIR filter

A.3 Evaluation of model error

A.3.1 Calculated fuel flow and flight data

The fuel flow calculated using the BADA model is compared with the flight data. Figs. A.4 to A.21 show time histories of the fuel flow for each flight case. Calculated fuel flow is in close accordance with the flight data in the cruise phase for all flight cases. On the other hand, the flight data fuel flow tends to be larger than that in the climb phase, and some biased error remains in the descent phase.

A.3.2 Analysis of fuel flow error

The error between calculated fuel flow and flight data is evaluated by the mean value and standard deviation. If the error of fuel flow is defined as follows, the mean value and standard deviation are expressed as Eqs. (A.20) and (A.21), respectively. The statistical values are derived from every second of data for each phase; i.e. climb, cruise and descent in all flight cases.

$$\Delta f(t) = f_{BADA}(t) - f(t) \tag{A.19}$$

$$\Delta \bar{f} = \frac{1}{n}\sum_{t=1}^{t_f} \Delta f(t) \tag{A.20}$$

$$\sigma = \sqrt{\frac{1}{n-1}\sum \left\{\Delta f(t) - \Delta \bar{f}\right\}^2} \tag{A.21}$$

These statistical variables are plotted in Figs. A.22 to A.25, where the standard deviation and the mean value of fuel flow error are shown. The mean value of fuel flow error takes a large negative value in Fig. A.23, because calculated fuel flow is smaller than the flight data in the climb phase in most cases. In contrast, since the calculated fuel flow varies around the flight data in the cruise phase, the mean value is close to zero as shown in Fig. A.24. Furthermore, the mean value takes a positive value in the descent phase as shown in Fig. A.25. In this phase, the standard deviation is smaller than that of other phases because the calculated fuel flow takes the minimum value which is independent from the time derivative of velocity; i.e. the main cause of high frequency noise.

A.3.3 Fuel consumption error

The TFC is obtained by integrating the fuel flow with time. The following numerical approximation for every second is applied to the integration.

$$TFC = \sum_{t=0}^{t_f} f(t)\Delta t \tag{A.22}$$

Each TFC obtained from calculated fuel flow and flight data is compared for the whole flight time and three phases. Figs. A.26 to A.43 show the comparison of TFC obtained from calculated fuel flow with the BADA model and the real fuel flow in the flight data. They are in good agreement with the cruise phase. TFC calculated from the BADA model is smaller than that from flight data for the whole flight time in many cases because of large error in the climb phase. On the other hand, calculated TFC is larger than flight data in the international route in case 17. This is because the calculated fuel flow in the cruise phase which occupies a major part of the international flight is slightly larger than the flight data as shown in Fig. A.20.

Table A.2 shows the error of calculated TFC from flight data. The error value is defined in Eq. (A.2), and proportion of the error to the flight data is calculated by Eq. (A.24), where TFC means the actual value obtained from flight data in the equations.

$$\Delta TFC = TFC_{BADA} - TFC \tag{A.23}$$

$$\frac{\Delta TFC}{TFC} = \frac{TFC_{BADA} - TFC}{TFC} \tag{A.24}$$

Although the calculated TFC fits in well with the TFC obtained from flight data in the cruise phase as the percentage of the error shows from -4.7 [%] to +4.2 [%], the accuracy reduces in the climb and descent phase as the percentage is -12.8 [%] to +1.5 [%] and -4.6 [%] to +21.2 [%], respectively. However, if the cruise phase occupies a large part of the flight as in these 18 cases, the error for whole flight time falls within plus or minus 5 [%]. It can be said that sufficient accuracy is obtained overall.

A.4 Summary

The accuracy of the BADA model was evaluated by comparing calculated fuel flow and TFC with the flight data stored in the QAR. The results of comparison show that the error between the BADA model and flight data is within plus or minus 5 [%]. Although the accuracy reduces relatively in the climb and descent phases, the influence on the error for whole flight time is not very significant because the cruise phase, which has high accuracy, constitutes a large part of the flight. In conclusion, this chapter revealed that the BADA model has sufficient accuracy to calculate the fuel consumption for general flight trajectory and it is of great use to various analyses for the future ATM research.

Fuel flow comparison (Flight case 1 to 6)

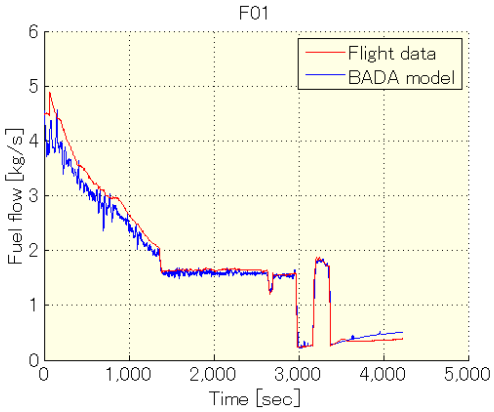

Fig.A.4 Fuel flow for HND→FUK (2011/8)

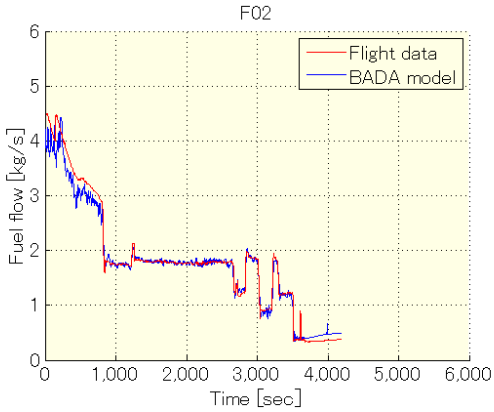

Fig.A.5 Fuel flow for FUK→HND (2011/8)

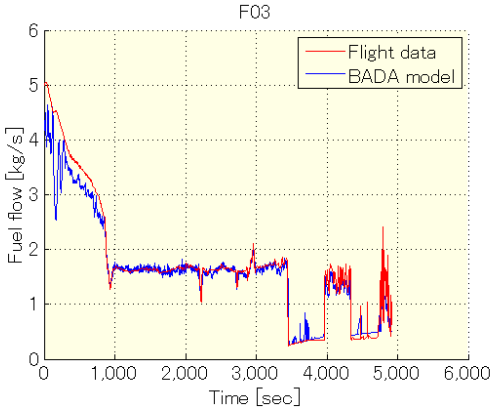

Fig.A.6 Fuel flow for HND→FUK (2011/10)

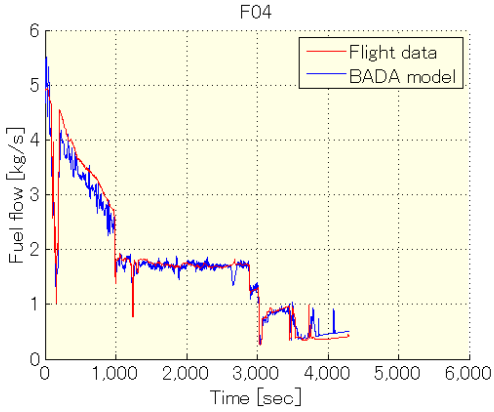

Fig.A.7 Fuel flow for FUK→HND (2011/10)

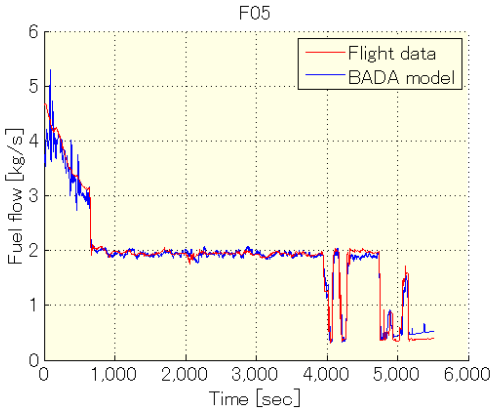

Fig.A.8 Fuel flow for HND→FUK (2011/12)

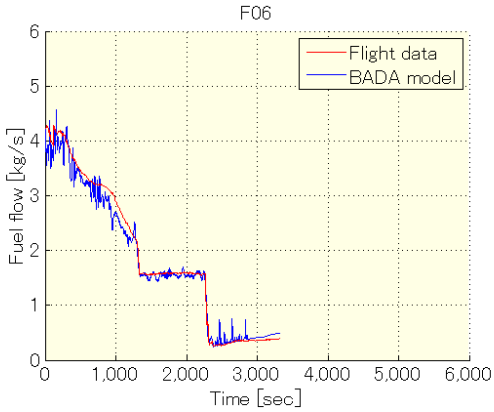

Fig.A.9 Fuel flow for FUK→HND (2011/12)

Fuel flow comparison (Flight case 7 to 12)

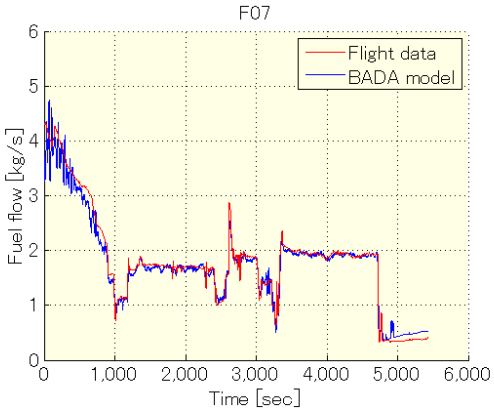

Fig.A.10 Fuel flow for HND→FUK (2011/12)

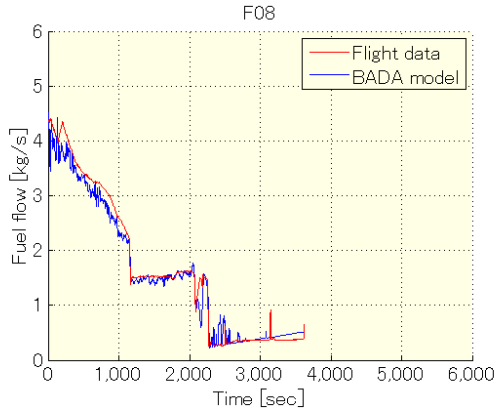

Fig.A.11 Fuel flow for FUK→HND (2011/12)

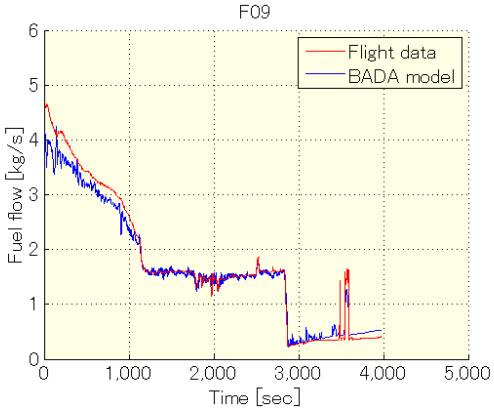

Fig.A.12 Fuel flow for HND→CTS (2011/8)

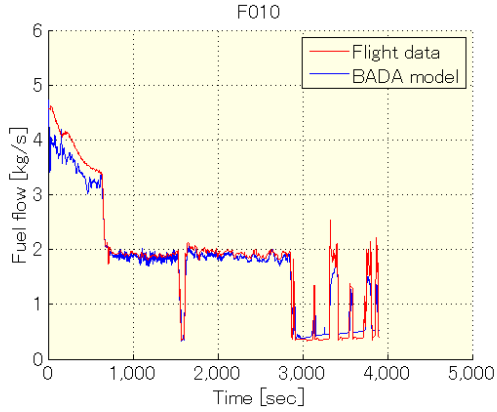

Fig.A.13 Fuel flow for CTS→HND (2011/8)

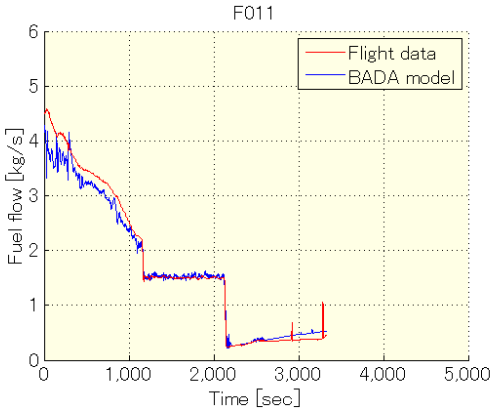

Fig.A.14 Fuel flow for HND→CTS (2011/10)

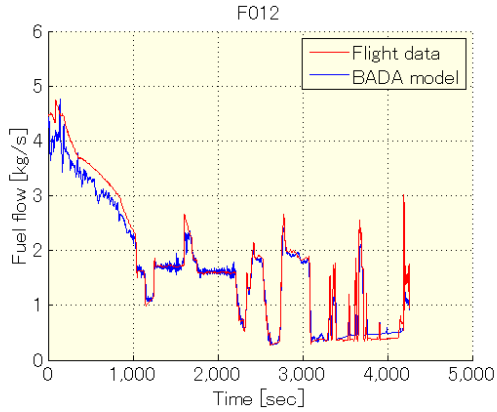

Fig.A.15 Fuel flow for CTS→HND (2011/10)

Fuel flow comparison (Flight case 13 to 18)

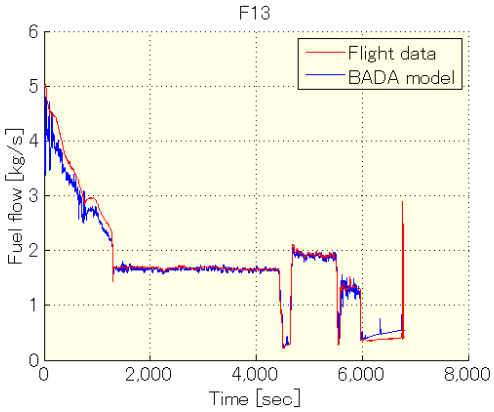

Fig.A.16 Fuel flow for HND→OKA (2011/8)

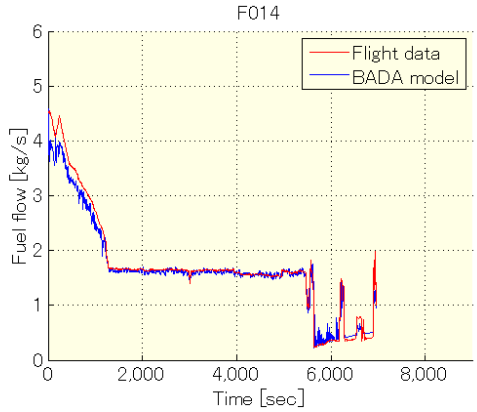

Fig.A.17 Fuel flow for OKA→HND (2011/8)

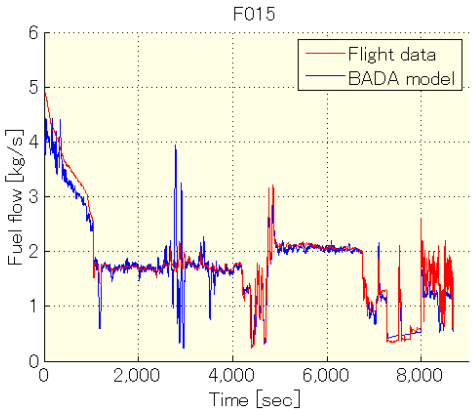

Fig.A.18 Fuel flow for HND→OKA (2011/10)

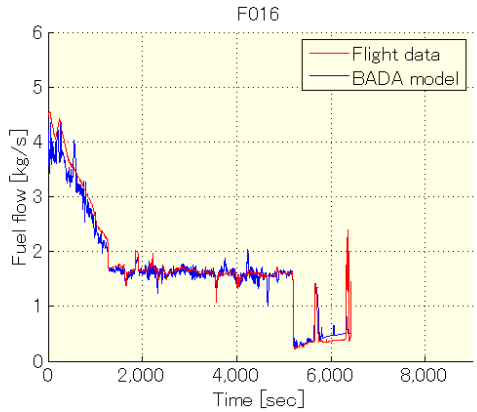

Fig.A.19 Fuel flow for OKA→HND (2011/10)

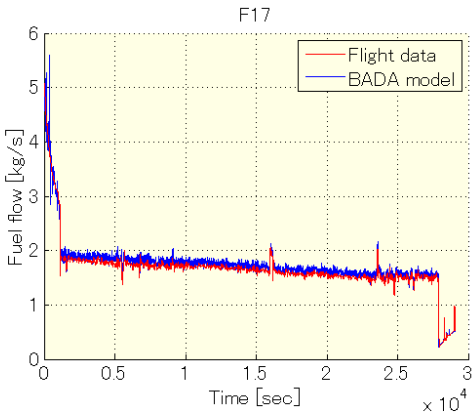

Fig.A.20 Fuel flow for HND→SFO (2011/10)

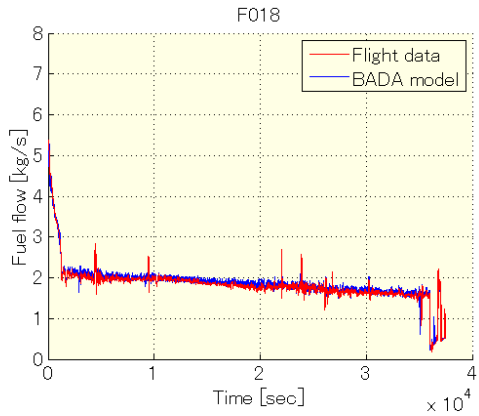

Fig.A.21 Fuel flow for SFO→HND (2011/10)

Statistical evaluation for the fuel flow error

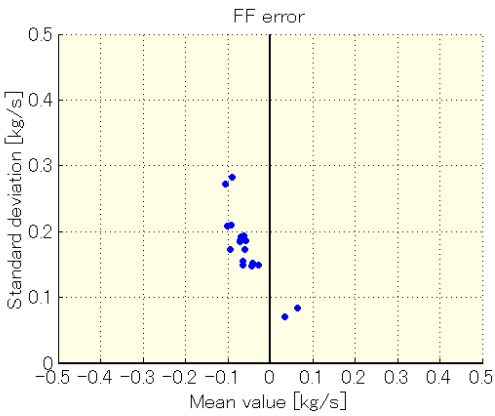

Fig.A.22 Fuel flow error for whole flight time

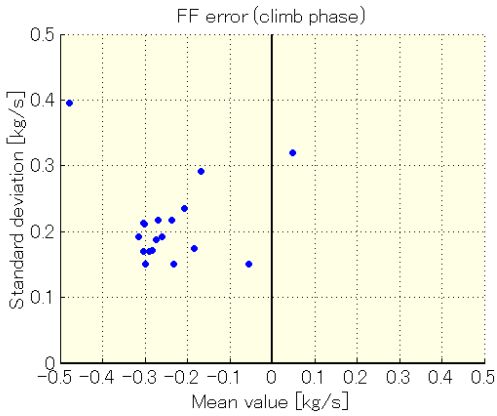

Fig.A.23 Fuel flow error for climb phase

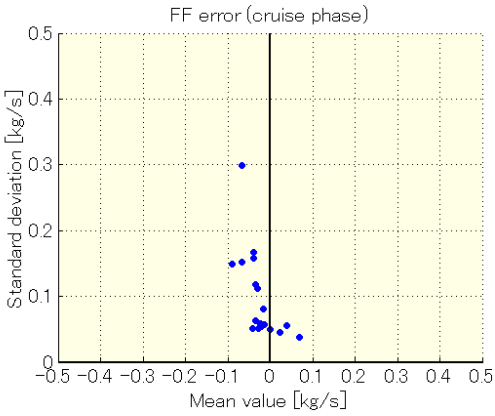

Fig.A.24 Fuel flow error for cruise phase

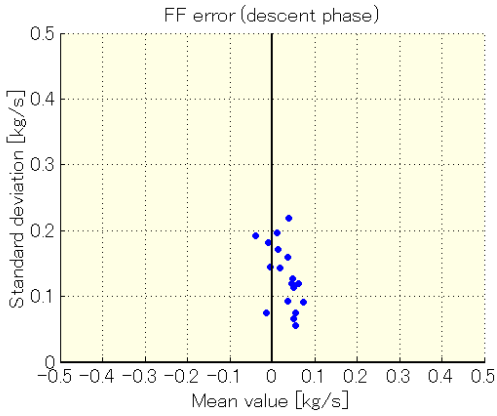

Fig.A.25 Fuel flow error for descent phase

Total fuel consumption comparison (Flight case 1 to 6)

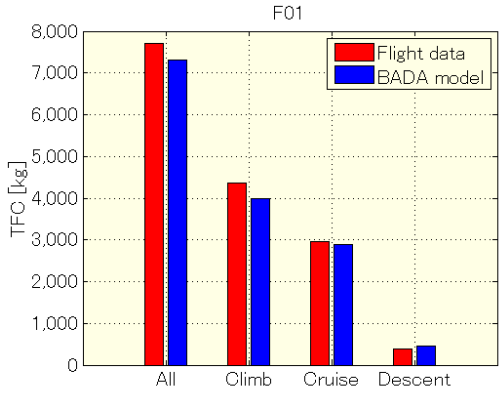

Fig.A.26 TFC for HND→FUK (2011/8)

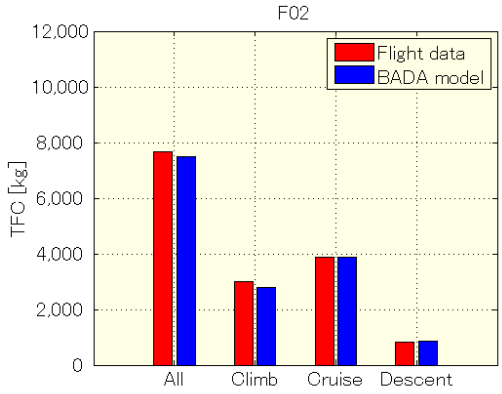

Fig.A.27 TFC for FUK→HND (2011/8)

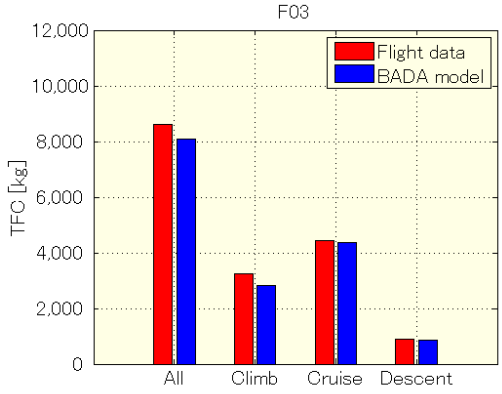

Fig.A.28 TFC for HND→FUK (2011/10)

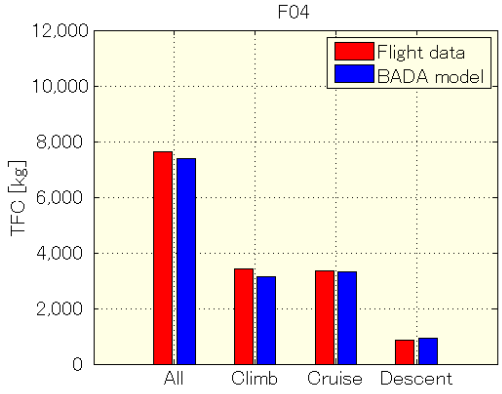

Fig.A.29 TFC for FUK→HND (2011/10)

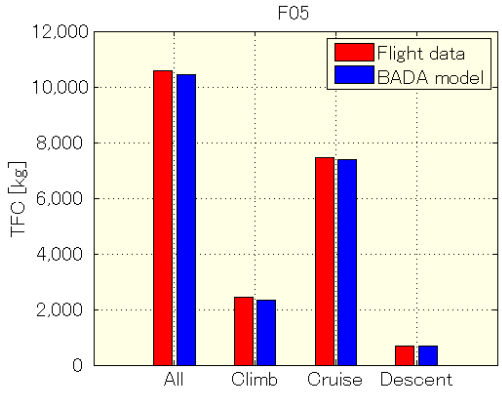

Fig.A.30 TFC for HND→FUK (2011/12)

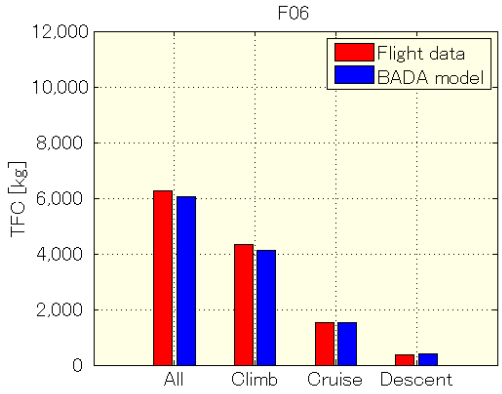

Fig.A.31 TFC for FUK→HND (2011/12)

Total fuel consumption comparison (Flight case 7 to 12)

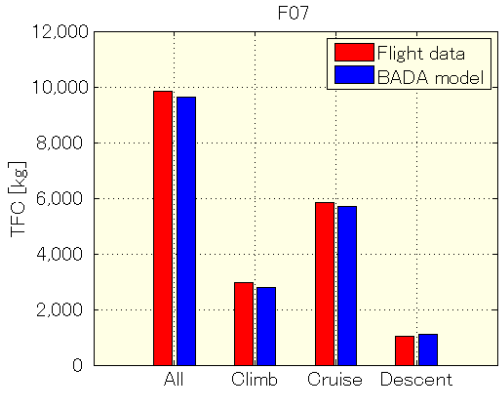

Fig.A.32 TFC for HND→FUK (2011/12)

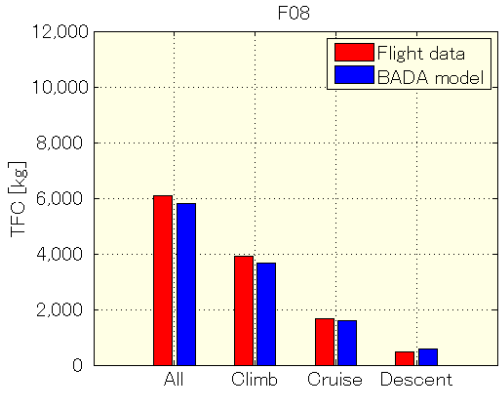

Fig.A.33 TFC for FUK→HND (2011/12)

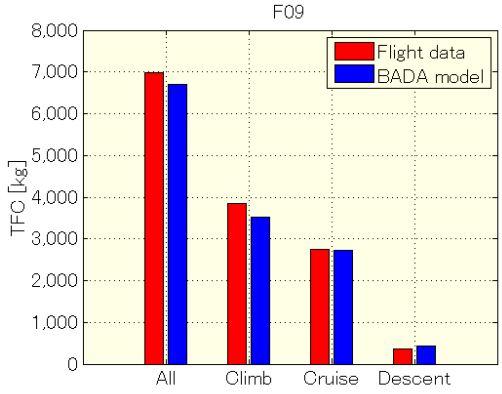

Fig.A.34 TFC for HND→CTS (2011/8)

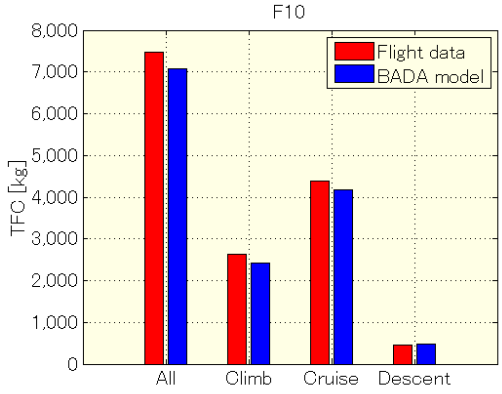

Fig.A.35 TFC for CTS→HND (2011/8)

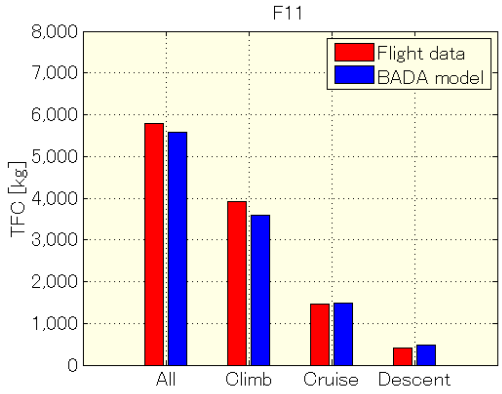

Fig.A.36 TFC for HND→CTS (2011/10)

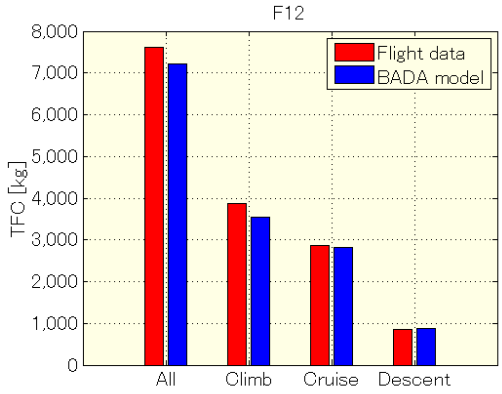

Fig.A.37 TFC for CTS→HND (2011/10)

Total fuel consumption comparison (Flight case 13 to 18)

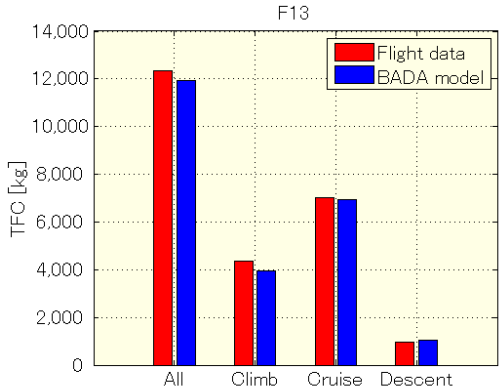

Fig.A.38 TFC for HND→OKA (2011/8)

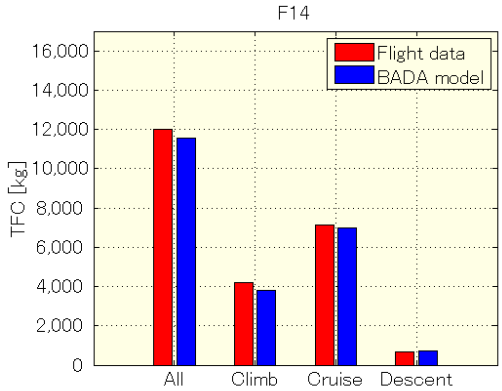

Fig.A.39 TFC for OKA→HND (2011/8)

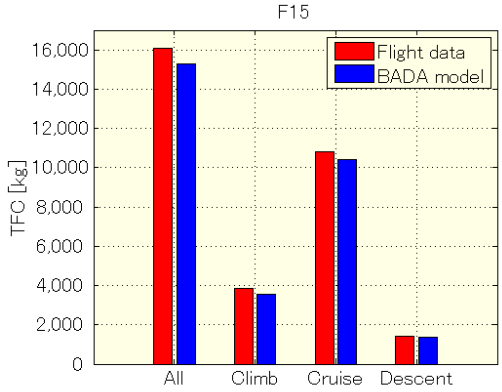

Fig.A.40 TFC for HND→OKA (2011/10)

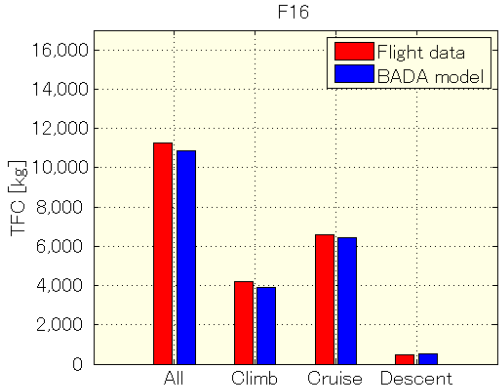

Fig.A.41 TFC for OKA→HND (2011/10)

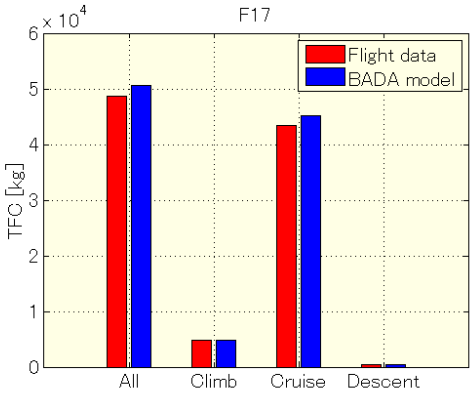

Fig.A.42 TFC for HND→SFO (2011/10)

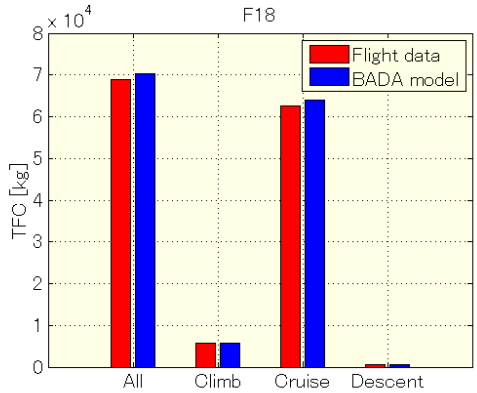

Fig.A.43 TFC for SFO→HND (2011/10)

Table.A.2 Error of calculated TFC from flight data

	F01		F02		F03	
Climb	-382[kg]	-8.76[%]	-217[kg]	-7.25[%]	-415[kg]	-12.76[%]
Cruise	-77[kg]	-2.59[%]	1[kg]	0.03[%]	-94[kg]	-2.10[%]
Descent	58[kg]	14.94[%]	43[kg]	5.35[%]	-13[kg]	-1.50[%]
All	-401[kg]	-5.20[%]	-173[kg]	-2.26[%]	-522[kg]	-6.07[%]

	F04		F05		F06	
Climb	-256[kg]	-7.51[%]	-111[kg]	-4.52[%]	-240[kg]	-5.52[%]
Cruise	-58[kg]	-1.71[%]	-54[kg]	-0.72[%]	-27[kg]	-1.74[%]
Descent	63[kg]	7.39[%]	12[kg]	1.76[%]	51[kg]	14.15[%]
All	-251[kg]	-3.29[%]	-153[kg]	-1.44[%]	-216[kg]	-3.45[%]

	F07		F08		F09	
Climb	-185[kg]	-6.23[%]	-270[kg]	-6.87[%]	-329[kg]	-8.53[%]
Cruise	-110[kg]	-1.89[%]	-75[kg]	-4.47[%]	-31[kg]	-1.11[%]
Descent	64[kg]	6.08[%]	84[kg]	17.32[%]	76[kg]	21.18[%]
All	-232[kg]	-2.36[%]	-260[kg]	-4.28[%]	-283[kg]	-4.06[%]

	F10		F11		F12	
Climb	-221[kg]	-8.39[%]	-317[kg]	-8.12[%]	-341[kg]	-8.78[%]
Cruise	-206[kg]	-4.71[%]	22[kg]	1.49[%]	-67[kg]	-2.34[%]
Descent	33[kg]	7.38[%]	65[kg]	15.47[%]	20[kg]	2.32[%]
All	-394[kg]	-5.27[%]	-231[kg]	-3.98[%]	-388[kg]	-5.10[%]

	F13		F14		F15	
Climb	-383[kg]	-8.82[%]	-366[kg]	-8.75[%]	-323[kg]	-8.37[%]
Cruise	-82[kg]	-1.17[%]	-105[kg]	-1.48[%]	-389[kg]	-3.61[%]
Descent	54[kg]	5.55[%]	25[kg]	3.65[%]	-66[kg]	-4.64[%]
All	-411[kg]	-3.33[%]	-446[kg]	-3.72[%]	-778[kg]	-4.84[%]

	F16		F17		F18	
Climb	-293[kg]	-6.96[%]	73[kg]	1.53[%]	-93[kg]	-1.62[%]
Cruise	-157[kg]	-2.38[%]	1827[kg]	4.22[%]	1386[kg]	2.21[%]
Descent	54[kg]	11.64[%]	-15[kg]	-2.97[%]	-4[kg]	-0.77[%]
All	-396[kg]	-3.51[%]	1885[kg]	3.87[%]	1289[kg]	1.87[%]

References

[1] Bellman, R.: *Dynamic Programming*, Princeton Univ. Press, 1957.

[2] Luus, R.: *Iterative Dynamic Programming*, Chapman & Hall/CRC, London, UK, 2000.

[3] Jaroslaw, S.S.: "Overcoming the Bellman's Curse of Dimensionality in Large Optimization Problems," *NASA Technical Memorandum 102662*, 1990.

[4] Alekseev, O.G. and Volodos, I.F.: "Combined use of dynamic programming and branch-and-bound methods in discrete programming problem," *Automation and Remote Control*, Vol. 37, pp. 557-565, 1976.

[5] Morin, T.L. and Masten, R.E.: "Branch-and-bound strategies for dynamic programming," *Operations Research*, Vol. 24, pp. 611-627, 1976.

[6] Mayne, D.Q.: "A Second-order Gradient Method for Determining Optimal Trajectories of Non-linear Discrete-time Systems," *International Journal of Control*, Vol. 3, No. 1, pp. 85-95, 1966.

[7] Jacobson, D.H. and Mayne, D.Q.: *Differrential Dynamic Programming*, American Elsevier, 1970.

[8] Miyazawa, Y., Harada, A., Wickramasinghe, N.K. and Miyamoto, Y.: "Effect of Jet Passenger Aircraft Performance Model on the Optimal Periodic Cruise Maneuver," in Japanese, *JSASS Kouku-Uchu Gijutsu (Aerospace Technology)*, Vol. 12, pp. 99-105, 2013.

[9] Matsuda, H., Harada, A. and Miyazawa, Y.: "Trajectory Optimization using Piecewise Linear Approximation Dynamic Programming," in Japanese, *JSASS Kouku-Uchu Gijutsu (Aerospace Technology)*, Vol. 14, pp. 33-41, 2015.

[10] Miyazawa, Y., Harada, A., Kawaguchi, J., Ninomiya, T., Suzuki, H. and Tomita, H.: "Dynamic Programming Trajectory Optimization and its Application to D-SEND #2 Low Sonic-boom Research Project," AIAA-2012-4827, *AIAA Guidance, Navigation and Control Conference*, Minneapolis, August, 2012.

[11] Harada, A. and Miyazawa, Y.: "Optimal Trajectory Design for Reentry Flight with Dynamic Programming," Paper No. 8.1.2, *Asia-Pacific International Symposium on Aerospace Technology*, Jeju, November, 2012.

[12] Harada, A. and Miyazawa, Y.: "Dynamic Programming Applications to Flight Trajectory Optimization," *19th IFAC Symposium on Automatic Control in Aerospace*, Würzburg, September, 2013.

[13] Lapidus, L. and Luus, R.: *Optimal Control of Engineering Processes*, Blaisdel, Waltham, Mas-

sachusetts, pp. 84-86, 1967.

[14] Kato, K.: *Kougakuteki Saitekiseigyo*, in Japanese, University of Tokyo Press, 1988.

[15] Kato, K.: *Space Plane*, in Japanese, University of Tokyo Press, pp. 37-42, 1989.

[16] Windhorst, R., Ardema, M. and Kinney, D.: "Fixed-Range Optimal Trajectories of Supersonic Aircraft by First-Order Expansions," *Journal of Guidance, Control and Dynamics*, Vol. 24, No. 4, pp. 700-709, 2001.

[17] Windhorst, R. and Ardema, M.: "Some Characteristics of Supersonic Transport Trajectories," *Journal of Aircraft*, Vol. 42, No. 4, pp. 1079-1081, 2005.

[18] Pierson, B.L. and Ong, S.Y.: "Minimum-Fuel Aircraft Transition Trajectories," *Mathematical and Computer Modelling*, Vol. 12, No. 8, pp. 925-934, 1989.

[19] Japan Aerospace Exploration Agency, Aeronautical Technology Directorate website, URL: http://www.aero.jaxa.jp/

[20] Study Group for the Future Air Traffic Systems: *Collaborative Actions for Renovation of Air Traffic Systems, CARATS*, Long Term Vision for the Future Air Traffic Systems, URL: http://www.mlit.go.jp/common/000128185.pdf, 2010.

[21] Wickramasinghe, N.K., Harada, A. and Miyazawa, Y.: "Flight Trajectory Optimization for an Efficient Air Transportation System," ICAS2012-5.8.3, *28th International Conference of the Aeronautical Sciences*, Brisbane, September, 2012.

[22] Wickramasinghe, N.K., Totoki, H., Harada, A., Miyamoto, Y., Kozuka, T. and Miyazawa, Y.: "Flight Trajectory Optimization for Jet Passenger Aircraft using Dynamic Programming," Paper No. 8.1.4, *Asia-Pacific International Symposium on Aerospace Technology*, Jeju, November, 2012.

[23] Wickramasinghe, N.K., Totoki, H., Harada, A. and Miyamoto, Y.: "A Study on Benefits Gained by Flight Trajectory Optimization for Modern Jet Passenger Aircraft," EN-41, *ENRI International Workshop on CNS/ATM*, Tokyo, February, 2013.

[24] Miyazawa, Y., Wickramasinghe, N.K., Harada, A. and Miyamoto, Y.: "Dynamic Programming Application to Airliner Four Dimensional Optimal Flight Trajectory," AIAA-2013-4969, *AIAA Guidance, Navigation and Control Conference*, Boston, August, 2013.

[25] Wickramasinghe, N.K., Miyamoto, Y., Harada, A., Kozuka, T., Shigetomi, S., Miyazawa, Y., Brown, M. and Fukuda, Y.: "Flight Trajectory Optimization for Operational Performance Analysis of Jet Passenger Aircraft," *Asia-Pacific International Symposium on Aerospace Technology*, Takamatsu, November, 2013.

[26] Miyazawa, Y., Wickramasinghe, N.K., Harada, A. and Miyamoto, Y.: "Passenger Aircraft Optimal Trajectory with an Arrival Time Constraint," in Japanese, *JSASS Kouku-Uchu Gijutsu (Aerospace Technology)*, Vol. 12, pp. 31-38, 2013.

[27] Harada, A., Wickramasinghe, N.K., Miyamoto, Y. and Miyazawa, Y.: "Flight Trajectory Optimization Tool with Dynamic Programming Developed for Future Air Transportation System," *2nd International*

Conference on Interdisciplinary Science for Innovative Air Traffic Management, Toulouse, July, 2013.

[28] Totoki, H., Wickramasinghe, N.K., Hamada, T. and Miyazawa, Y.: "Estimation of Flight Trajectories by Using GPS Data Measured in Airliner Cabin," in Japanese, *JSASS Kouku-Uchu Gijutu (Aerospace Technology)*, Vol. 11, pp. 43-50, 2012.

[29] Japan Meteorological Business Support Center Online Data Service,
URL: http://www.jmbsc.or.jp/hp/online/f-online0.html

[30] Eurocontrol Experimental Center, User Manual for the Base of Aircraft Data (BADA) Revision 3.9: EEC Technical/Scientific Report No. 11/03/08-08, April, 2011.

[31] Harada, A., Miyazawa, Y. and Funabiki, K.: "Accuracy Evaluation of an Aircraft Performance Model with Airliner Flight Data," *Transactions of JSASS Aerospace Technology Japan*, Vol. 11, pp. 79-85, 2013.

[32] Totoki, H., Kozuka, T., Miyazawa, Y. and Funabiki, K.: "Comparison of JMA Numerical Prediction GPV Meteorological Data and Airliner Flight Data," in Japanese, *JSASS Kouku-Uchu Gijutu (Aerospace Technology)*, Vol. 12, pp. 57-63, 2013.

[33] Miyamoto, Y., Wickramasinghe, N.K., Harada, A., Miyazawa, Y. and Funabiki, K.: "Analysis of Fuel Efficient Airliner Flight via Dynamic Programming Trajectory Optimization," *Transactions of JSASS Aerospace Technology Japan*, Vol. 11, pp. 93-98, 2013.

[34] Shigetomi, S., Kozuka, T., Totoki, H., Miyazwa, Y., Brown, M. and Fukuda, Y.: "Evaluation Analysis of Seasonal GPV Meteorological Data with SSR Mode S Surveillance Data," Paper No. 592, *6th International Conference on Research in Air Transportation*, Istanbul, May, 2014.

[35] Hagelauer, P. and Mora-Camino, F.: "A Soft Dynamic Programming Approach for On-line Aircraft 4D-trajectory Optimization," *European Journal of Operational Research*, No. 107, pp. 87-95, 1998.

[36] Khardi, S.: "Aircraft Shortest and Fastest Continuous Descent Approach Development," *Journal of Aircraft* Vol. 49, No. 6, pp. 1931-1939, 2012.

[37] Harada, A., Kozuka, T., Miyazawa, Y., Wickramasinghe, N.K., Brown, M. and Fukuda, Y.: "Analysis of Air Traffic Efficiency using Dynamic Programming Trajectory Optimization," *29th International Congress of the Aeronautical Sciences*, St. Petersburg, September, 2014.

[38] Sabatini, R., Gardi, A., Ramasamy, S., Liu, Y., Zammit-Mangion, D. and Quaglia, D.: "Novel Avionics and Air Traffic Management Systems for Intent Based Operations," *10th USA/Europe Air Traffic Management Research and Development Seminar*, Chicago, USA, 2013.

[39] Gardi, A., Sabatini, R., Ramasamy, S. and Kistan, T.: "Real-Time Trajectory Optimisation Models for Next Generation Air Traffic Management Systems," *Applied Mechanics and Materials*, Vol. 629, pp. 327-332, 2014.

[40] Ramasamy, S., Sabatini, R., Gardi, A. and Kistan, T.: "Next Generation Flight Management System for Real-Time Trajectory Based Operations," *Applied Mechanics and Materials*, Vol. 629, pp. 344-349, 2014.

[41] Gardi, A., Sabatini, R., Kistan, T., Lim, Y. and Ramasamy, S.: "4 Dimensional Trajectory Functionalities for Air Traffic Management Systems," *Integrated Communication, Navigation and Surveillance Conference*, Herndon, USA, 2015.

[42] Betts, J.T.: "Survey of Numerical Methods for Trajectory Optimization," *Journal of Guidance, Control and Dynamics*, Vol. 21, No. 2, pp. 193-206, 1998.

[43] Fahroo, F. and Ross, I.M.: "Direct Trajectory Optimization by a Chebyshev Pseudospectral Method," *Journal of Guidance, Control and Dynamics*, Vol. 25, No. 1, pp. 160-166, 2002.

[44] Menon, P.K. and Sweriduk, G.D.: "Study of Near-Optimal Endurance-Maximizing Periodic Cruise Trajectories," *Journal of Aircraft*, Vol. 44, No. 2, pp. 393-398, 2007.

[45] Nolan, M.S.: "Fundamentals of Air Traffic Control 5th edition," Delmar, New York, 2011.

[46] Fukuda, Y., Shirakawa, M. and Senoguchi, A.: "Development and Evaluation of Trajectory Prediction Model," *Proceedings of the 27th International Congress of the Aeronautical Sciences*, Nice, September, 2010.

[47] Rodriguez, J.M.C., Deniz, L.G., Herrero, J.G., Portas, J.B. and Corredera, J.R.C.: "A Model to 4D Descent Trajectory Guidance," *26th Digital Avionics Systems Conference*, Dallas, October, 2007.

[48] Turgut, E.T.: "Estimating Aircraft Fuel Flow for a Three-Degree Flight-Path-Angle Descent," *Journal of Aircraft*, Vol. 48, pp. 1099-1106, 2011.

[49] Sridhar, B., Ng, H.K. and Chen, N.Y.: "Aircraft Trajectory Optimization and Contrails Avoidance in the Presence of Winds," *Journal of Guidance, Control and Dynamics*, Vol. 34, pp. 1577-1583, 2011.

[50] Gallo, E., Leones, J.L., Vilaplana, M.A., Navarro, F.A. and Nuic, A.: "Trajectory Computation Infrastructure Based on BADA Aircraft Performance Model," *26th Digital Avionics Systems Conference*, Dallas, October, 2007.

[51] Nuic, A., Poinsat, C., Iagaru, M.G., Gallo, E., Navarro, F.A. and Querejeta, C.: "Advanced Aircraft Performance Modeling for ATM Enhancements to the BADA Model," *24th Digital Avionics System Conference*, Washington D.C., October-November, 2005.

[52] Nuic, A., Poles, D. and Mouillet, V.: "BADA An Advanced Aircraft Performance Model for Present and Future ATM Systems," *International Journal of Adaptive Control and Signal Processing*, Vol. 24,pp. 850-866, 2010.

[53] Senzig, D.A., Fleming, G.G. and Iovinelli, R.J.: "Fuel Consumption Modeling in Support of ATM Environmental Decision-Making," *8th USA/Europe Air Traffic Management Research and Development Seminar* , Napa, USA, 2009.